ASSESSMENT OF FREQUENCY DOMAIN FORCE IDENTIFICATION PROCEDURES

by

THOMAS EDWIN SLAUGHTER KRIEL

Submitted in partial fulfillment of
the requirements for the degree
Masters in Engineering in the
Faculty of Engineering
University of Pretoria

Pretoria

February 2000

ASSESSMENT OF FREQUENCY DOMAIN FORCE IDENTIFICATION PROCEDURES

by

Thomas Edwin Slaughter Kriel

Supervisor : Prof. P. S. Heyns
Department : Mechanical and Aeronautical Engineering
Degree : Masters of Engineering

ABSTRACT

The location and magnitude of self-generated or input forces on a structure may prove to be very important for the proper evaluation at the design and modification phases, as well as in the case of control and fatigue life predictions. The identification of the input forces has also attracted a great deal of interest in machine health monitoring and troubleshooting.

Instead of being able to directly measure the force inputs, some other quantity is usually measured, e.g. the response, from which the forces can be determined indirectly. In essence the structure becomes the force transducer. Theoretically, it is possible to determine the forces by simply reversing the process of calculating the responses of a system subjected to known forces, but this procedure was shown to be ill-posed and sensitive to noise, and might contribute to meaningless results. Various matrix decomposition and regularisation methods were presented in dealing with the inverse problem.

Two frequency domain force identification procedures were evaluated in this work, i.e. the frequency response function and the modal coordinate transformation method. Both numerical and experimental studies have been presented to assess the advantages and disadvantages associated with each method.

The ultimate objective of this research was to implement these methods in an experimental investigation on a simple well-behaved structure, given the lack of experimental work pertaining to especially the modal coordinate transformation method. A single harmonic force was determined on an aluminium beam subjected to different boundary conditions. The work was then extended to predict two point sinusoidal forces from measured acceleration signals. Strain measurements have also been employed and the results noted.

Based on the results presented it was concluded that the frequency response function method was superior to the modal coordinate transformation method for the structure used in the investigations.

EVALUASIE VAN FREKWENSIEDOMEIN KRAGTE-IDENTIFIKASIE PROSEDURES

deur

Thomas Edwin Slaughter Kriel

Studieleier : Prof. P. S. Heyns
Departement : Meganiese en Lugvaartkundige Ingenieurswese
Graad : Magister in Ingenieurswese

SAMEVATTING

Die posisie en grootte van self-gegenereerde of eksterne insette wat op 'n struktuur inwerk, blyk 'n belangrike aspek van die ontwerp- en modifikasiefases te wees. Die indirekte kragte identifikasie wek ook belangsteling in beheerstelsels, die voorspelling van vermoeidheidleeftyd en die veld van toestandsmonitering.

In plaas daarvan om die kraginsette direk te meet word byvoorbeeld die responsie gemeet, waardeur die kragte indirek bepaal kan word. In essensie word die struktuur die kragomsetter. Dit is teoreties moontlik om die proses vir die bepaling van die responsie van 'n struktuur wat onderhewig is aan bekende kragte, slegs om te keer; hierdie proses is egter numeries sleggeaard en sensitief vir geraas. Dit kan nuttelose resultate oplewer. Verskillende matriksontbindings strategië word voorgestel om inverse probleme aan te spreek.

Die frekwensie responsie funksie metode en modal koördinaattransformasie metode word beskou in hierdie werk. Numeriese en eksperimentele studies word ondersoek om die voor- en nadele van elke metode te bepaal.

Die doelwit van hierdie ondersoek was om bogenoemde metodes eksperimenteel te ondersoek aan die hand van 'n eenvoudige struktuur, gegewe die gebrek aan eksperimentele werk met spesiale verwysing na die modale koördinaattransformasie metode. 'n Aluminium balk is onderwerp aan verskillende randvoorwaardes, terwyl 'n enkele harmoniese krag geïdentifiseer is. Die studie is uitgebrei na die bepaling van twee sinusvormige kragte vanuit gemete versnelling- en vervormingseine.

Gebaseer op die eksperimentele ondersoeke wat geloods is skyn die frekwensie responsie funksie metode beter kwantifisering van die kragte op te lewer as die modale koördinaattransformasie metode.

"Most inverse problems of mathematical physics are ill-posed under the three conditions of Hadamard. In a humorous vein Stakgold pointed out that there would likely be a sharp drop in the employment of mathematicians if this were not the case"

(Sarkar *et al.*, 1981)

ACKNOWLEDGEMENTS

Gloria in excelsis Deo.

The author wishes to express his gratitude firstly to his supervisor, Prof. P. S. Heyns, who initiated this research and has provided his sustained interest and guidance throughout the duration of this work. Also thanks are due to the many lecturers in the Department of Mechanical and Aeronautical Engineering and the author's mentor at Sasol, Mr. P Vermeulen, for their advice and encouragement.

Special thanks are due to the colleagues at the Gold Fields Dynamic Laboratory, for their keen interest, cooperation and discussions throughout this work.

For their technical assistance and cooperation, the author thanks the staff members of the Sasol Laboratory.

Finally, the author wishes to express his gratitude to Sasol Limited for their financial support during the course of this study.

NOMENCLATURE

$A_i(t)$	i-th measured acceleration time signal
$A_{ij}(\omega)$	Inertance frequency response function for excitation at point j and the response measured at i
$[A(\omega)]$	Inertance frequency response function matrix
$[b]$	Input shape matrix
$[c]$	Output shape matrix
$[C]$	Damping matrix
$[\overline{C}]$	Modal damping matrix
$\{e(\omega)\}$	Fourier transform of the strain response vector.
$E(\omega)$	Absolute error
$[E]$	High frequency residual
$\{f(t)\}$	Force vector as a function of time
$F_j(\omega)$	Fourier transform of force input at point j
$[F]$	Low frequency residual
$\{F(\omega)\}$	Actual force vector
$\{\hat{F}(\omega)\}$	Estimated force vector
$\{F_m(\omega)\}$	Modal force vector
G_{xx}	Auto spectrum of the time function $x(t)$
G_{xy}	Cross spectrum of the time functions $x(t)$ and $y(t)$
$[h(t)]$	Impulse response function matrix
$H_{ij}(\omega)$	Frequency response function for excitation at point j and the response measured at i
$[H(\omega)]$	Frequency response function matrix
$[H(\omega)]^+$	Pseudo-inverse of the rectangular matrix $[H(\omega)]$
$[I]$	Identity matrix
j,k	Integer
$[\hat{L}]$	Linear operator in Tikhonov Regularisation
$[K]$	Stiffness matrix
$[\overline{K}]$	Modal stiffness matrix
m	Number of forces
M_i	i-th equivalent mass
$[M]$	Mass matrix
$[\overline{M}]$	Modal mass matrix
n	Number of response locations
n_a	Number of acceleration measurements
n_d	Number of averages used in the measurements
N	Degrees of freedom / number of modes
$N(\omega)$	Fourier transform of the noise contaminating the response

p	Number of participating modes
$\{p\}$	Principal/modal coordinates as a function of time
$\{P(\omega)\}$	Modal coordinates as a function of frequency
Q_r	Modal scaling factor of the r-th mode
$[Q]$	$(n \times m)$ orthogonal matrix
$[R]$	$(m \times m)$ upper triangular matrix with the diagonal elements in descending order
$s = i\omega$	Laplace variable
$[T]_r$	Residue matrix of the r-th mode
$\{u\}$	Input vector to the system
$[U]$	$(n \times n)$ matrix, columns comprise the normalized eigenvectors of $[H][H]^T$
$[V]$	$(m \times m)$ matrix, columns are composed of the eigenvectors of $[H]^T[H]$
$\{y\}$	Output vector of the system
$\{\ddot{x}(t)\}$	Acceleration vector as a function of time
$\{\dot{x}(t)\}$	Velocity vector as a function of time
$\{x(t)\}$	Displacement vector as a function of time
$x(k)$	Discrete series of a sampled time function $x(t)$
$X(n)$	Fourier series coefficients
$\{X(\omega)\}$	Fourier transform of the physical displacement vector
$\{\ddot{X}(\omega)\}$	Fourier transform of the physical acceleration vector
$[Y(\omega)]$	Strain frequency response function matrix
$\alpha_{ij}(\omega)$	Receptance frequency response function for excitation at point j and the response measured at i
$[\alpha(\omega)]$	Receptance frequency response function
$[\beta]$	Mass-normalised modal damping matrix
δ_{ij}	Kronecker delta function
$\varepsilon_f(\omega)$	Force error norm
$\{\phi\}_r$	r-th independent eigenvector (normal modes)/mode shape corresponding to the measurement point
$\{\hat{\phi}\}$	r-th independent eigenvector (normal modes)/mode shape corresponding to the excitation point
$[\Phi]$	Modal matrix
γ^2	Coherence function
κ_2	Condition number
λ_r	r-th complex eigenvalue
$[\Lambda]$	Diagonal modal stiffness matrix (normal mode frequencies squared)
μ	Lagrange multiplier
$\sigma_1, \sigma_2, \ldots, \sigma_m$	Singular values in the matrix $[\Sigma]$

$[\Sigma]$	$(n \times m)$ matrix with singular values of $[H]$ on its leading diagonal
ω_r	Natural circular frequencies of r-th mode $[rad/s]$
ω_r^2	r-th independent eigenvalues (natural frequencies squared)
$\{\psi\}_r$	Reciprocal modal vector, corresponding to the r-th mode
ζ_r	Modal damping factor for r-th mode

DFT	Discrete Fourier Transform
DOF	Degrees-Of-Freedom
FEA	Finite Element Analysis
FEM	Finite Element Model
FEN	Force Error Norm
FFT	Fast Fourier Transform
IDFT	Inverse Discrete Fourier Transform
IRF	Impulse Response Function
MIMO	Multiple Input Multiple Output
MMIF	Multivariable Mode Indicator Function
RBM	Rigid Body Modes
RMV	Reciprocal Modal Vector
SFRF	Strain Frequency Response Function
SVD	Singular Value Decomposition

$(\tilde{\cdot})$	Denotes contaminated values
$[\cdot]^T$	Transpose of the indicated matrix
$[\cdot]^*$	Complex conjugate (Hermitian) transpose of the indicated matrix
$[\cdot]^{-1}$	Inverse of a square matrix
$\|\cdot\|_2$	Vector 2-norm

TABLE OF CONTENTS

CHAPTER 1

Introduction

1. INTRODUCTION

1.1 PREAMBLE

The location and magnitude of self-generated or input forces on a structure, or for that matter any piece of equipment, may prove to be very important for the proper evaluation at the design and modification phases, as well as in the case of control and fatigue life predictions. The identification of the input forces has also attracted a great deal of interest in machine health monitoring and troubleshooting (Shih *et al.*, 1989). The location of the excitation forces can reveal the possible causes of vibration, while the force amplitude determines the severity of the vibration condition.

In cases where the direct measurement of these forces is possible, it is usually accompanied by structural changes to accommodate the attachment of force sensing equipment, and may as a result change the dynamic characteristics of the system.

However, there are many situations where the direct measurement of the excitation forces is not possible or feasible. For example:

- Shock/impact loads on ship hulls (Dubowski and Dobson, 1985).
- Engine torque pulses and shaking forces are difficult to measure, since these forces are distributed throughout the engine (Starkey and Merrill, 1989).
- Forces transmitted from machinery, such as compressors, to the foundations.
- Stress analysis on a finite element model of a structure can be performed by applying prescribed displacements. In the case of structural modifications, the stress analysis would require knowledge of the excitation forces.
- Propellor-induced pressure fluctuations on a ship hull (Stevens, 1987).
- Determining of acoustic loads where the environment does not permit the use of microphones to measure the acoustic field (Elliott *et al.*, 1988).
- Explosive loading or force input within hostile environments (Dubowski and Dobson, 1985)
- The indirect computation of the flow-induced forces in a piping system or petrochemical reactor.

Instead of being able to measure the force inputs directly, some other quantity, e.g. the response, is usually measured from which the forces can be determined indirectly. The aim of the present work is to show that it is possible to estimate dynamic forces by measuring the responses, be they acceleration, displacement or strain, of a linear structure subjected to those forces. In essence the structure becomes the force transducer.

Theoretically, it is possible to determine the forces by simply reversing the process of calculating the responses of a system subjected to known forces, but this procedure is known to be ill-posed and sensitive to noise, and may contribute to meaningless results.

1.2 FORMULATION OF DIRECT AND INVERSE PROBLEM

In this section the classification of the force identification as an inverse process and an ill-posed problem is motivated and the principal difficulties in such a procedure are discussed.

The direct problem (also referred to as the forward problem) is to find the response of the structure from knowledge of the excitation force through the use of a transfer function, which gives the relationship between the measured response and the excitation forces:

$$\{F(\omega)\} \Rightarrow \{X(\omega)\} \tag{1.1}$$

Conversely, the force identification problem is to accurately infer the excitation force from knowledge of the vibration responses via some transfer function:

$$\{X(\omega)\} \Rightarrow \{F(\omega)\} \tag{1.2}$$

The latter problem involves the recovery of the force (cause) given the incomplete and noise-contaminated response (effect) and system matrix, whence the name inverse problem.

Two important observations regarding the differences between the direct and inverse problem can be made (Karlsson, 1996):

Firstly, the excitation force in the direct problem is known all over the structure. These forces are usually concentrated on limited portions of the structure, while the rest of the structure can be regarded as non-loaded. This is typically the procedure followed in the finite element analysis of a structure in order to obtain its dynamic response as a result of the applied forces/loads.

However, in the inverse problem, a non-zero vibration response is in most cases present all over the structure. Furthermore, the responses can usually be measured only at a finite number of discrete points, and there is no information available regarding the responses between these points. Thus, the entire response can be solved for the direct problem, whereas the full excitation forces cannot be determined in the

inverse problem. As a result, the solution to the direct problem is straightforward while the inverse problem is left without a unique solution.

The second observation to note is that even if the responses could be measured at closely spaced positions, the force identification problem is ill-posed and ill-conditioned. A well-posed problem can be stated as a problem that satisfies the three conditions of Hadamard. These are the existence, uniqueness and stability of the solution (Hashemi and Hammond, 1996). If any of these conditions are violated, the problem is said to be ill-posed. On the other hand, ill-conditioning refers to the phenomena where small measurement errors (noise) are mapped onto unboundedly large errors in the force estimates. For an in-depth discussion of ill-posed problems, as well as ways to regularise these problems to be well-behaved, refer to Sarkar *et al.* (1981).

As a result it is impossible to calculate the entire force distribution on a structure, simply from response measurements. To make the force identification solvable, additional information regarding the force distribution is needed *a priori*. The force identification problem can be regularised to a well-posed problem by limiting the excitation forces to a finite number of discrete points on the structure. An $(n \times m)$ frequency response function, $[H]$, is deduced consisting of both response and force identification points. With this *a priori* information the force identification problem is reduced to the determination of only the unknown force amplitudes at the discrete points.

This approach can be justified, since in many applications the exact forcing locations are known, for instance at an engine mount or bearing support. In the case of, for example, distributed acoustic loads the vicinity of the excitation forces needs to be known, since the force identification procedure will determine the pseudo- or equivalent forces that will result in the same response of the structure, but with quite a different spatial distribution than the actual applied forces.

1.3 LITERATURE SURVEY

Three commonly used 'domains' are employed in the indirect force identification process, i.e. the frequency, time and modal domains. The frequency domain models utilise the frequency response function, which gives the linear relationship between the measured response and the excitation force. As for the time domain models, these methods produce force estimates as a function of time. The modal models are defined as a set of natural frequencies with corresponding mode shapes and modal damping factors and can be used for either frequency or time domain models.

Stevens (1987) has given an overview of the general problems involved in the force identification process, while Dobson and Rider, (1990) reviewed some of the different techniques and applications reported in the literature.

1.3.1 Frequency Response Function Method

The frequency response function can be defined as the linear relationship between the measured response and the excitation forces and gives rise to a set of linear equations normally formulated in the frequency domain as

$$\{X(\omega)\}=[H(\omega)]\{F(\omega)\} \tag{1.3}$$

where

$\{X(\omega)\}$ is the $(n\times 1)$ response vector,

$[H(\omega)]$ is the $(n\times n)$ frequency response function matrix, and

$\{F(\omega)\}$ is the $(n\times 1)$ force vector.

The frequency response function matrix can be measured experimentally, reconstructed from an experimental modal analysis, or obtained from a finite element model.

The unknown forces can be reconstituted by taking the inverse of equation (1.3) as follows

$$\{F(\omega)\}=[H(\omega)]^{-1}\{X(\omega)\} \tag{1.4}$$

However, the frequency response function matrix proves to be singular and ill-conditioned at frequencies close to and at resonance (Desanghere, 1983).

In an attempt to improve the condition of the inverse problem, the formulation of an over-determined problem is proposed, which allows the use of more equations than unknowns. The advantage of using redundant information minimises the consequences of measurement errors (Hillary, 1983). If the number of responses, n,

exceeds the number of force estimates, m, the frequency response function becomes rectangular. Adopting a least-squares solution of the force estimates are given by:

$$\{F(\omega)\}=[H(\omega)]^{+}\{X(\omega)\} \tag{1.5}$$

where

$[H(\omega)]^{+}$ is known as the pseudo-inverse of the $(n\times m)$ rectangular matrix $[H(\omega)]$.

The added effect of noise, as encountered in experimental measurements, will further degrade the inversion process. Hillary (1983) and Okubo *et al.* (1985) both investigated the influence of noise contaminating the response and frequency response functions on the accuracy of the force identification. The results show that noise in the frequency response function, and more specifically in the modal matrix, lead to gross errors in the force estimates. The noise contaminating the frequency response function matrix also reduces the number of significant figures in the matrix and, consequently reduces the rank of the matrix (Fregolent and Sestieri, 1990). This in turn reduces the number of forces that can be correctly estimated (Fabunmi, 1986). The quality of the frequency response function matrix can be improved by measuring the frequency response functions by means of a shaker excitation, rather than with an impact hammer (Hendricx, 1994). Even when taking great care hitting the test object in a perpendicular way, the impact hammer may exert in-plane forces. This in turn results in unreliable pseudo-driving point frequency response functions, which are detrimental to force estimates.

Mas *et al.* (1994) published an excellent article in which other causes for unreliable force estimates are explored, other than the poor conditioning of the frequency response function matrix usually associated with indirect force identification. It is shown that the error propagation in the inversion process is proportional to the condition number of the frequency response function matrix to be inverted. Over-determination can improve the condition number and as a result reduce the errors of the force estimates. The damping in the system can have an influence on the force identification, since the condition number varies with damping. Starkey and Merrill (1989) have suggested that the condition number of the frequency response function matrix should be used as an 'indication' of the expected accuracy of indirectly measured force amplitudes at a given frequency.

Hillary and Ewins (1984) have employed both accelerometers and strain gauges to determine two simultaneous sinusoidal forces on a uniform cantilever beam. The strain responses gave more accurate force estimates than the accelerations. This is because the strain responses are influenced more by the higher modes at low frequencies, and therefore the frequency response functions are more complex in

shape and hence obtain better force predictions. Han and Wicks (1990) also studied the application of displacement, slope and strain measurements. From both these studies it is evident that proper selection of the measurement type can improve the condition of the frequency response function matrix.

Another paper by O'Callahan and Piergentili (1996) have noted that regardless of the number of response locations chosen, the force prediction result is excellent if the response locations coincide with actual force locations. For the case where the actual force locations are excluded from the response locations the forces are distributed to all response locations in the set. The amount of distribution to each of the surrounding response locations depends on the direction and distance of that particular response from the actual force location. Again it is emphasised that the response locations should be concentrated within the vicinity of the force locations. The analysis was conducted on a finite element model of a plate and as a result did not include experimental verification or the effect of measurement noise.

Following the argument of Fabunmi, it is not possible to determine more than a single force for a lightly-damped structure in the vicinity of the resonant frequencies. This may prove to be highly undesirable, since the energy flows are usually a maximum in these regions. Lewit (1993) suggested the calculation of an equivalent force or forces, which will result in the same vibration output as the original force inputs. The total input power into the structure can then be calculated from the equivalent forces at the resonant frequencies.

Different matrix decomposition methods are used when dealing with ill-conditioned problems. Some of these include:

- The Moore-Penrose pseudo-inverse (Brandon, 1988; Hillary, 1983),
- QR decomposition (Fregolent and Sestieri, 1990),
- Singular Value Decomposition (Maia, 1991; Brandon, 1988),
- Second Order Epsilon Decomposition (Ojalvo and Zhang, 1993) and many more.

Singular Value Decomposition (SVD) of the frequency response function matrix can be used to improve the conditioning of the pseudo-inverse matrix. Powell and Seering (1984) calculated a threshold value from the coherence function corresponding to the measured frequency response functions. The singular values smaller than the threshold were truncated from the pseudo-inversion. Although the truncation reduced the resolution of the inputs, it prevented the prediction of large spurious forces.

Numerous regularisation methods are also available, which give a stable approximate solution to an ill-conditioned problem, e.g. Tikhonov regularisation (Sarkar *et al.*, 1981; Hashemi and Hammond, 1996).

Most of the successful applications that deal with the problem of multiple excitation forces have been for the least-squares method. These include work done by Flannely and Bartlett (1979), which produced results that can be compared to directly-measured harmonic forces acting on the hub of a laboratory model of a helicopter. The forces were accurately determined for combinations of two orthogonal forces from measurements of fourteen responses at three different frequencies.

In a similar case, Okubo *et al.* (1985) applied the least-squares technique to a number of applications. These include the identification of the cutting forces of a machine tool, the generated forces on mounts of an automobile engine and the transmitted forces to the piping system of an air conditioner. The frequency response functions were measured in advance at a stationary state, while the responses of the structure were measured under operating conditions. Although the frequency response functions often admittedly differ from those at operating conditions, this approach is more desirable since the frequency response function is usually very noisy under operating conditions.

When dealing with random forces, equation (1.3) can be defined in terms of the spectral density functions as

$$[G_{xx}(\omega)] = [H(\omega)][G_{ff}(\omega)][H(\omega)]^* \tag{1.6}$$

where

$[G_{xx}(\omega)]$ is the $(n \times n)$ response matrix,

$[G_{ff}(\omega)]$ is the $(m \times m)$ spectral matrix of the forces,

$[H(\omega)]$ is the $(n \times m)$ rectangular frequency response function matrix, and $[\cdot]^*$ denotes the complex conjugate transpose of $[H(\omega)]$.

The pseudo-inverse of equation (1.6) results in

$$[G_{ff}(\omega)] = [H(\omega)]^+ [G_{xx}(\omega)][H(\omega)]^{T+} \tag{1.7}$$

It is generally accepted that in the case of statistically uncorrelated forces, the cross-spectral density terms (off-diagonal terms) become equal to zero and the above equation reduces to:

$$\{G_{ff}(\omega)\} = \left[|H(\omega)|^2\right]^+ \{G_{xx}(\omega)\} \tag{1.8}$$

where

$\{G_{ff}(\omega)\}$ and $\{G_{xx}(\omega)\}$ are column vectors of the diagonal terms of the force and response spectral density matrices, respectively.

Conversely, it has been shown that this assumption is inadequate when solving the inverse problem for random forces. The cross-spectral densities of the response should be included with the real valued auto-spectral densities, since the former carries the phase information that in turn, establishes the correlation requirements among time variables (Varoto and McConnell, 1997).

Elliott *et al.* (1988) employed the SVD technique to predict acoustic forces on a thin panel. Force estimates were calculated from a strain frequency response function (SFRF) matrix and the corresponding strain response matrix. The measured strain response matrix was heavily influenced by noise. The measurement noise increased the rank of the strain responses, which in turn circumvented the force predictions. By applying singular value decomposition the noise contaminating the input measured strain can be reduced, but not completely rejected. It is shown that improvement in the force predictions was obtained by truncating singular values so that the rank of the measured strain response matrix resembles its true rank, without the effect of noise.

1.3.2 Modal Coordinate Transformation Method

The modal coordinate transformation method (also referred to as the modal model method) is based on the modal transformation theory. The system is expressed in terms of its modal parameters [i.e. the natural frequencies, modal damping factors and modal (eigen)vectors], which can be obtained from various experimental modal parameter estimation methods, widely used by the modal analysis community. The orthogonality criterion of the mass-normalised modal vectors is used to establish the transformation basis, and can be expressed as:

$$[\Phi]^T[M][\Phi]=[I] \quad \text{and} \quad [\Phi]^T[K][\Phi]=[\Lambda]$$
$$[\Phi]^T[C][\Phi]=[\beta] \tag{1.9}$$

where

$[M]$, $[K]$ and $[C]$ are the mass, stiffness and damping matrices, respectively;

$[\Phi]$ is the modal matrix;

$[I]$ is the identity matrix;

$[\Lambda]$ is the diagonal modal stiffness matrix with $\Lambda_r = \omega_r^2$, and ω_r the natural circular frequency of the r-th mode;

Assuming some type of proportional damping it follows that $[\beta]$ is the diagonal modal damping matrix, and $\beta_r = 2\zeta_r \omega_r$ with ζ_r the modal damping factor of the r-th mode.

Utilising the orthogonality criterion results in a set of uncoupled equations of motions and the response can be written in the frequency domain as follows:

$$\{X(\omega)\} = [\Phi]\left[-\omega^2[I] + i\omega[\beta] + [\Lambda]\right]^{-1}[\Phi]^T\{F(\omega)\} \tag{1.10}$$

The physical forces acting on the system are determined by an inverse coordinate transformation:

$$\{F(\omega)\} = \left[\Phi^T\right]^+\left[-\omega^2[I] + i\omega[\beta] + [\Lambda]\right][\Phi]^+\{X(\omega)\} \tag{1.11}$$

In the equation above, the forces are computed by transforming the operating response to the modal response. The modal forces are determined and then transformed back to the forces acting on physical coordinates of the system by an inverse coordinate transformation (Desanghere and Snoeys, 1985).

The modal coordinate transformation technique might just as well be implemented in the time domain (Genaro and Rade, 1998).

$$\{f(t)\} = \left[\Phi^T\right]^+\left([I]\{\ddot{p}(t)\} + [\beta]\{\dot{p}(t)\} + [\Lambda]\{p(t)\}\right) \tag{1.12a}$$

with

$$\{\ddot{p}(t)\} = [\Phi]^+\{\ddot{x}(t)\} \qquad \{\dot{p}(t)\} = [\Phi]^+\{\dot{x}(t)\}$$

$$\{p(t)\} = [\Phi]^+\{x(t)\} \tag{1.12b}$$

where

$\{\ddot{p}(t)\}$, $\{\dot{p}(t)\}$ and $\{p(t)\}$ are the modal (generalised) acceleration, velocity and displacement vectors.

The frequency response function method previously considered has two major drawbacks (Desanghere and Snoeys, 1985):

- The first is the ill-conditioned behaviour of the force estimates near and at the system's resonances.
- Secondly, the frequency response function matrix needs to be inverted at each frequency line and thus, increase the computational time required.

Both these limitations may be avoided by using the modal coordinate transformation method. The singularity problems are eliminated and the modal matrix needs to be inverted only twice.

Kim and Kim (1997) studied the effect of error propagation in the modal parameters on the force predictions. They concluded that, as was the case with the frequency response function technique, errors in the modal vectors are considered as the main source of error in the identified forces. A methodology is also proposed to recalculate the force estimates for inaccessible input locations.

Despite the advantages associated with the use of the modal coordinate transformation technique, Okubo *et al.* (1985) preferred to use the frequency response function technique, since the former requires the extraction of the modal parameters from the measured frequency response function. They argued that the modal parameters might be in error as a result of difficulties experienced by curve fitting algorithms, especially at resonances and anti-resonances. These modal parameters may in turn be detrimental to force identification. Recent advances in modal parameter extraction methods enables one to extract the modal parameters with greater accuracy, which makes the modal coordinate transformation technique more attractive.

Conversely, Desanghere and Snoeys (1985) found the method rather insensitive to measurement and curve-fitting perturbations. They successfully applied the modal coordinate transformation technique to identify the forces in a turbo compressor and a car-frame.

Hansen and Strakey (1990) extended the work of Starkey and Merrill (1989) by considering the condition number of this method. The findings revealed that the condition number, of the pseudo-inversion of the modal matrix can be ameliorated through proper selection of the sensor locations and the modes included in the analysis.

Most of the work done on modal coordinate transformation has been for the case where the locations of the input forces were known. The objective was then simply to resolve the amplitude and frequency content of these forces. Shih *et al.* (1989) proposed a method based on the modal coordinate transformation technique, where the number of forces, as well as the locations, is treated as unknowns. The modal response transformation (equation 1.10) is performed through a modal filter, calculated from frequency response function measurements and the modal parameters, rather than the pseudo-inverse of the modal matrix. The rank analysis of the modal force matrix (equation 1.11) can be evaluated to determine the number of incoherent force inputs to the structure. Once the number of excitation forces is known, their locations can be determined by various projection methods.

Genaro and Rade (1998) applied this technique on a simple numerically simulated structure and successfully identified harmonic and impact forces in the time domain. Another application consisted of a longitudinal beam of a car-frame where three random forces were accurately inferred (Desanghere and Snoeys, 1985). This method has also been demonstrated on a circular plate (Shih *et al.*, 1989; Zhang *et al.*, 1990).

Though the proposed method shows some success, the number of publications are limited. Accordingly it seems that further research is needed to clarify some of the difficulties to make the method more suitable for real-world applications.

1.3.3 Time Domain Methods

Since the focus of this work is primarily concerned with the assessment of force identification methods in the frequency domain, only some of the recent advances in the time domain methods will be summarised below. The time domain methods have the ability of exploring the transient behaviour of impulsive loads.

a) Sum of Weighted Accelerations Technique (SWAT)

This time domain method is the most widely known process in indirect force identification. As the name states, this method uses a sum of the weighted acceleration signals to experimentally predict the external forces, which excite the system.

$$f(t) = \sum_{i=1}^{n_a} \left(M_i \times A_i(t) \right) \tag{1.13}$$

where

$f(t)$ is the externally applied forces,

M_i is the i-th equivalent mass,

$A_i(t)$ is the i-th measured acceleration, and

n_a is the number of acceleration measurements.

The implementation of this method is confined to the computation of the sum of the external forces and moments about the center of mass of structures presenting free boundary conditions. The Rigid Body Modes (RBM) are explored in the preliminary tests to determine the optimal distribution of the weighting factors associated with an equivalent mass at each of the sensor locations. The weighting factors can be determined either from inverting the modal matrix or from the free-decay response of the structure (Carne *et al.*, 1992). Recently, the Max-Flat procedure was validated as an alternative for determining the weighting factors from frequency response functions and avoids possible errors resulting from mode shape estimation (Carne *et al.*, 1998). SWAT yielded excellent results in experiments conducted by Gregory *et al.* (1986) on a mass-loaded, free-free beam.

Kreitinger and Wang (1988) successfully applied this method to structures that exhibit non-linear behaviour. Other applications comprise of the impact force identification on nuclear shipping casks and energy absorbing noses (Bateman *et al*, 1991 and Bateman *et al.*, 1992).

b) Inverse William's Method

Ory *et al.* (1985 and 1986) analysed the reconstruction of transient loads from measured response-time histories on a beam. The use of an 'Inverse William's Method' improved the reconstructed force estimates. In the William's method, the response consists of a quasi-static component, which is superimposed on the dynamic component. The forcing functions were computed with a time-integration scheme. Providing that the stiffness matrix is known with sufficient accuracy, this matrix is combined with the measured displacements to produce the quasi-static forces. By extracting the quasi-static forces, the dynamic forces, which are the pure inertial forces pertaining to the significant modes, were reconstructed.

c) Central Difference Method

Among the applications is the work of Dubowski and Dobson (1985) where a central difference approach was applied to a cantilever structure suffering an impact load. The method yielded acceptable predictions of the excitation forces. However, in the post-shock period the method proved unstable as the force predictions continued to oscillate and diverged.

d) Time Domain Deconvolution Method

The convolution integral equation, which states the time domain relationship between the response of the structure and the applied forces, is given by Da Silva and Rade (1999) as:

$$\{x(t)\} = \int_0^t [h(t-\tau)]\{f(t)\}d\tau \qquad (1.14)$$

where

$\{x(t)\}$ is the $(n \times 1)$ time response vector,

$\{f(t)\}$ is the $(m \times 1)$ time force vector, and

$[h(t)]$ is the corresponding $(n \times m)$ Impulse Response Function (IRF) matrix.

Deconvolution of equation (1.14) produces an estimate of the force inputs from the vibration response. Unfortunately, this procedure is known to be ill-conditioned and requires the implementation of regularisation schemes to stabilise computations. The problem can be regularised by employing Tikhonov

regularisation (Fasana and Piombo, 1996), calculation of the inverse Markov parameters (Kammer, 1996) or application of the conjugate gradient method (Da Silva and Rade, 1999).

1.3.4 Continuous Systems

In the case of continuous systems one needs to solve partial differential equations from which solutions are available for every point on the structure. However, this limits the applications to relatively simple structures with well-defined boundary conditions. Some of the applications include a Timoshenko transformation technique, which was used to derive remote impact force-time histories from accelerations measured at remote locations (Whitson, 1984 and Jordan and Whitson, 1984). In another case, the impulse response functions for Euler-Bernouli and Timoshenko beams, subjected to transverse impact forces were also investigated (Park and Park, 1994). The impulse response functions, which state the relationship between the force and strain, were obtained by using the wave propagation approach in the time domain.

1.4 OUTLINE AND SCOPE OF THIS WORK

The force identification in this work will be performed in the frequency domain. The advantages of using the frequency domain and the theory relating to the frequency response function's formulation, measurement and modal parameter extraction are presented in Chapter 2.

The work presented in this dissertation can be roughly divided into three sections:

- Formulation of the frequency response function method as applied to the force identification process,
- Formulation of the modal coordinate transformation method, and
- An experimental study performed on a beam with different boundary conditions to assess the performance of the above mentioned methods.

Each section is dealt with in a separate chapter.

Chapter 3 presents the derivation of the frequency response function method. The limitations regarding the use of this method is highlighted as well as presenting some of the regularisation methods in dealing with the inverse problem. The results of a numerical study of a two degree-of-freedom system and Finite Element Analysis (FEA) of a beam are presented. The significance of the condition number on the force estimates is discussed.

Chapter 4 is entirely devoted to the modal coordinate transformation method. The numerical studies investigate the application of the method on a two degree-of-freedom system and the factors influencing the condition number of the modal matrix. This chapter also describes applying the modal filter to force reconstruction, which is validated by a numerical simulation.

The ultimate objective of this research is to implement these methods in an experimental investigation on a simple well-behaved structure, given the lack of experimental work pertaining to especially the modal coordinate transformation method. The aim is to determine a single harmonic force on an aluminium beam subjected to different boundary conditions. The work is then extended to predict two point sinusoidal forces from measured acceleration signals. Strain measurements have also been employed and the results noted.

In the work presented we will only focus on harmonic force inputs applied at discrete locations while reference is made to random forces, distributed loading and unknown forcing locations.

Assumptions:

- The frequency response functions measured at stationary state are the same as those at operating conditions.
- Discrete force inputs at known locations.
- An existing structure or representative scale model is already available for the acquisition of the frequency response functions and response measurement.

CHAPTER 2

Frequency Domain Analysis

2. FREQUENCY DOMAIN ANALYSIS

The force identification techniques will be performed in the frequency domain. This section motivates the use of the frequency domain and highlights the related theory used in Fourier Transforms, as well the frequency response function's formulation, measurement and modal parameter extraction.

2.1 ADVANTAGE OF USING FREQUENCY DOMAIN

The frequency response function is one of the functions used to describe the input-output relation in a linear system, in the frequency domain. Equation (1.3) is repeated as an example:

$$\{X(\omega)\}=[H(\omega)]\{F(\omega)\} \tag{2.1}$$

where

$\{X(\omega)\}$ is the $(n\times 1)$ response vector,

$[H(\omega)]$ is the $(n\times n)$ frequency response function matrix,

$\{F(\omega)\}$ is the $(n\times 1)$ force vector.

One important benefit, which is evident from the equation above, is that the Fourier Transform, transforms a convolution in the time domain, into a multiplication in the frequency domain (Randall, 1977). The equivalent convolution in the time domain is evidently a much more complicated procedure. This is one of the reasons for the great success of the Fourier Transform technique in signal processing.

Dealing with stationary random excitations also benign the use of the frequency domain. As examples we can mention flow-induced vibration in a piping system and the fluctuating pressure gusts on the wing of an airplane in flight. These systems can only be formulated in terms of their statistical properties and can be completely defined by the spectral density functions.

It may also be justifiable to mention some of the disadvantages associated with the frequency domain. Windowing functions need to be enforced on the time signals to suppress the affect of 'leakage'. Furthermore, the Auto Spectral Density (ASD) functions contain no phase information and are unable to capture transient phenomena of systems.

2.2 DISCRETE FOURIER TRANSFORM

The Discrete Fourier Transform (DFT) technique will be employed to transform any time function, $x(t)$ into the frequency domain by use of the following equation (Broch, 1990):

$$X(n) = \frac{1}{N}\sum_{k=0}^{N-1} x(k)\, e^{-i2\pi\frac{jk}{N}} \tag{2.2}$$

where

$x(k)$ is a discrete series of a sampled time function $x(t)$,

N is the number of sampled points,

$X(n)$ is the Fourier series coefficients,

for $j = 0, 1, 2, \ldots, N-1$; $k = 0, 1, 2, \ldots, N-1$.

Conversely, a discrete time series may be calculated from knowledge of the Fourier series coefficients:

$$x(k) = \sum_{j=0}^{N-1} X(n)\, e^{i2\pi\frac{jk}{N}} \tag{2.3}$$

which is the Inverse of the Discrete Fourier Transform (IDFT). The DFT and IDFT equations are implemented in *Matlab*®, which uses efficient Fast Fourier Transform (FFT) algorithms.

Thus, the use of DFT permits any time response to be transformed into the frequency domain. The force identification technique will yield the estimated forces. These forces may be transformed back into discrete time series, using the IDFT. The flowchart for this procedure is as follows:

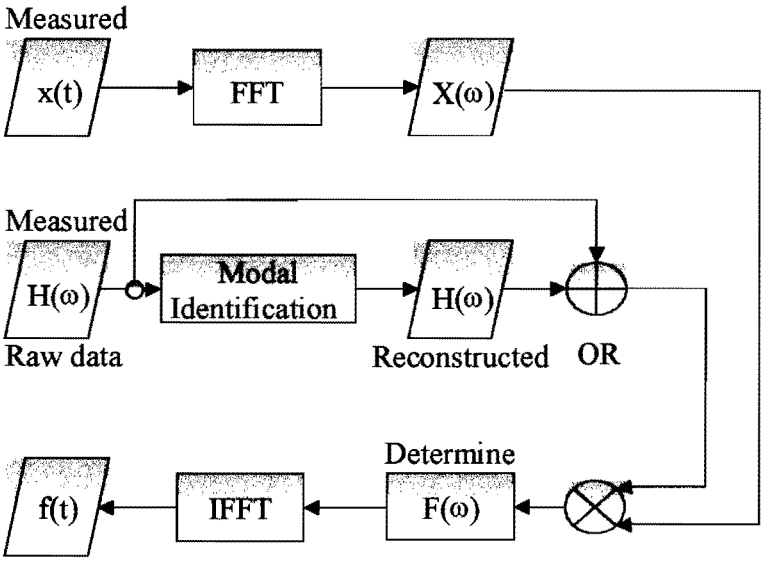

Figure 2.1 - Flowchart of a typical force identification procedure

For more detailed information on the discrete Fourier transform, the FFT algorithms or implementation of Fourier analysis in the *Matlab*® environment the interested reader is referred to the original references (Randall, 1977; Broch, 1990; McConnell, 1992 and *Matlab*®, *Version 5.3*).

2.3 FREQUENCY RESPONSE FUNCTION MODELLING

The *Structural Dynamics Toolbox*® (Balmès, 1997) provides a framework for the modelling of the input/output response of a linear system. Many engineering structures may be considered as lightly-damped structures. That is structures for which the damping is small so that the low frequency response is characterised mostly by the mass and stiffness contributions. Consequently, a normal mode model is used.

The eigenvalue problem of the normal modes may be defined as follows:

$$-[M]\{\phi\}_r \omega_r^2 + [K]\{\phi\}_r = \{0\} \tag{2.4}$$

where

$[M]$ and $[K]$ are the $(N \times N)$ mass and stiffness matrices, respectively.

$\{\phi\}_r$ denotes $(N \times 1)$ independent eigenvectors (normal modes),

ω_r^2 is N independent eigenvalues (eigenfrequencies squared), and $r = 1, \ldots, N$ where N is the number of degrees-of-freedom in the system.

The solutions of the eigenvalue problem of equation (2.4) yield the following mass-normalised modal matrix orthogonality properties:

$$[\Phi]^T[M][\Phi] = [I] \quad \text{and} \quad [\Phi]^T[K][\Phi] = [\Lambda] \tag{2.5}$$

The state space formulation of the normal mode model for the *damped system*, as expressed in terms of the principal coordinates, is as follows:

$$[[I]s^2 + [\beta]s + [\Lambda]]\{p\} = [[\Phi]^T[b]]\{u\} \tag{2.6a}$$

$$\{y\} = [[c][\Phi]]\{p\} \tag{2.6b}$$

where

$s = i\omega$ is the Laplace variable,

$[\Lambda]$ is the diagonal modal stiffness matrix (eigenfrequency squared),

$[\beta]$ is the modal damping matrix, and $[\beta] = [\Phi]^T[C][\Phi]$,

$[[\Phi]^T[b]]$ is the modal input matrix,

$[b]$ is the input shape matrix, which is time invariant and characterises the spatial properties of the applied forces,

$[[c][\Phi]]$ is the modal output matrix,

$[c]$ is the output shape matrix, which is time invariant and characterises the spatial properties of the sensors,

$\{u\}$ is the input vector to the system,

$\{y\}$ is the output vector of the system,

$\{p\}$ is the principal/modal coordinates.

Assuming a unity modal mass matrix, the first-order state space model takes the form

$$\begin{Bmatrix}\{\dot{p}\}\\ \{\ddot{p}\}\end{Bmatrix}=\begin{bmatrix}[0] & [I]\\ -[\Lambda] & -[\beta]\end{bmatrix}\begin{Bmatrix}\{p\}\\ \{\dot{p}\}\end{Bmatrix}+\begin{bmatrix}[0]\\ [\Phi]^T[b]\end{bmatrix}\{u\} \tag{2.7a}$$

$$\{y\}=[[c][\Phi]\ [0]]\begin{Bmatrix}\{p\}\\ \{\dot{p}\}\end{Bmatrix} \tag{2.7b}$$

In the case of proportional damping, the diagonal modal damping matrix, $[\beta]$, may be expressed in terms of the damping ratios $\beta_r = 2\zeta_r\omega_r$.

The frequency response function is, by definition, the Fourier Transform of the system's response divided by the Fourier Transform of the applied force. The frequency response function for the linear system, which corresponds to the partial fraction expansion, can be written as:

$$[\alpha(s)]=\sum_{r=1}^{N}\frac{\{[c]\{\phi\}_r\}\{[b]^T\{\phi\}_r\}^T}{s^2+2\zeta_r\omega_r s+\omega_r^2}=\sum_{r=1}^{N}\frac{[T]_r}{s^2+2\zeta_r\omega_r s+\omega_r^2} \tag{2.8}$$

where

ω_r is the natural circular/normal mode frequencies for each mode,

ζ_r is the modal damping factor for each mode, and

$[T]_r$ is the residue matrix, which is equal to the product of the normal mode $[[c]\{\phi\}_r]$ and $[\{\phi\}_r^T[b]]$.

Equation (2.8) is generally referred to as the *receptance*, since it gives the relation between the displacement and force. Usually, an alternative formulation known as *inertance* is used, which is the ratio of the acceleration to the force. This formulation is desired, since piezoelectric accelerometers are used for the measurement of the frequency response functions and responses. The inertance can be obtained simply by multiplying the receptance by $-\omega^2$, as follows:

$$[A(s)]=-\omega^2[\alpha(s)] \tag{2.9}$$

In practice, one can measure only a limited number of modes, N, within the frequency range of interest. However, the contribution of the modes outside this frequency range is evident in the measured frequency response function, and needs to be accounted for when one desires to reconstruct measured frequency response functions. Equation (2.8) is rewritten to include the high- and low-frequency corrections or generally referred to as residuals.

$$[\alpha(s)] = \sum_{j=1}^{N} \left(\frac{[T]_j}{s^2 + 2\zeta_j \omega_j s + \omega_j^2} \right) + [E] + \frac{[F]}{s^2} \tag{2.10}$$

where

$[E]$ denotes the high-frequency residual, and

$[F]$ is the low-frequency residual.

Figure 2.2 shows a typical reconstructed frequency response function with and without the residual terms included.

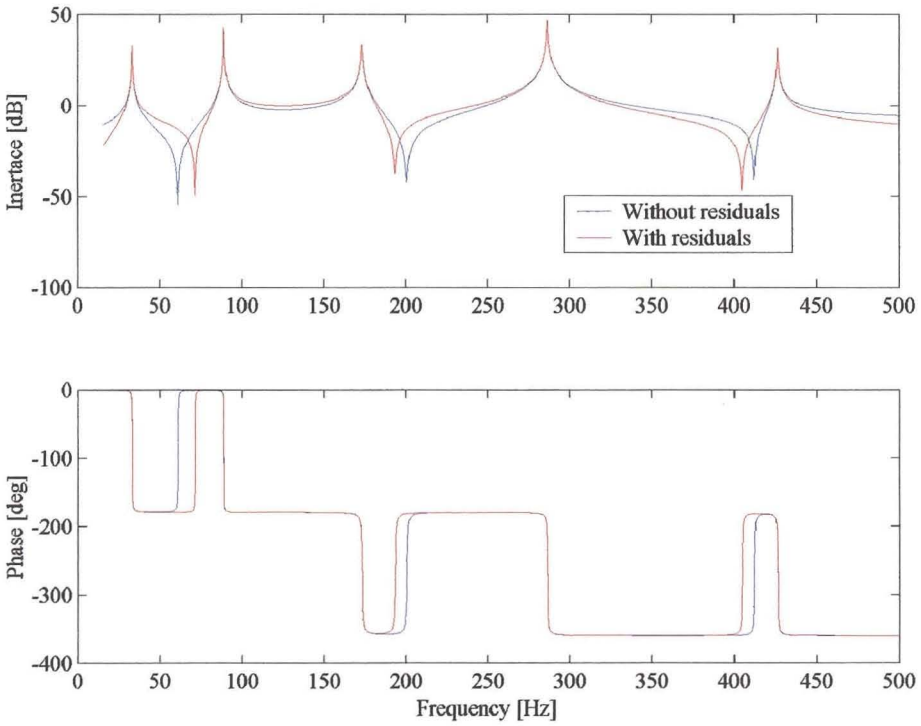

Figure 2.2 – Contribution of the residual terms for a typical system

2.4 MULTIPLE INPUT MULTIPLE OUTPUT EXCITATION

In the case of a single input excitation, the structure is excited sequentially at each of the desired locations, while measuring the responses, from which columns of the frequency response function are obtained successively.

Alternatively, Multiple Input Multiple Output (MIMO) excitation is used in an attempt to obtain the information from several rows or columns of the frequency response function matrix simultaneously during a single excitation run. This does not only reduce the test time required, but also contributes to better estimates of the natural frequencies, modal damping factors and modal vectors in the case of closely spaced modes. A more detailed mathematical treatment of the MIMO excitation can be found in Maia and Silva (1997) and Zaveri (1984).

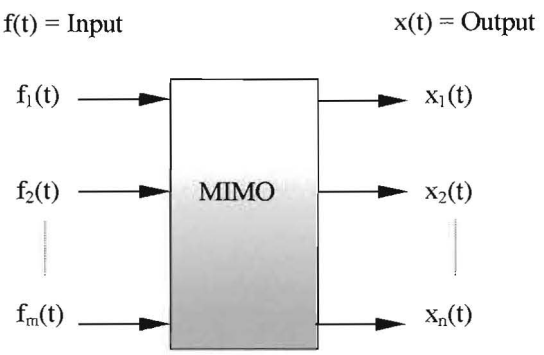

Figure 2.3 – Multiple-input multiple-output model

Consider the above MIMO system, which is excited at m input locations and whose response is measured at n points. The frequency response function matrix for this system can be written as:

$$[H(\omega)]=\begin{bmatrix} H_{11}(\omega) & H_{12}(\omega) & \cdots & H_{1m}(\omega) \\ H_{21}(\omega) & H_{22}(\omega) & \cdots & H_{2m}(\omega) \\ \vdots & \vdots & & \vdots \\ H_{n1}(\omega) & H_{n2}(\omega) & \cdots & H_{nm}(\omega) \end{bmatrix} \tag{2.11}$$

where $H_{ij}(\omega)$ is the frequency response function for excitation at point j and the response measured at point i.

The structure may be excited with two or more exciters simultaneously. For the sake of simplicity we will consider a dual-input, single-output system as shown in Figure 2.4.

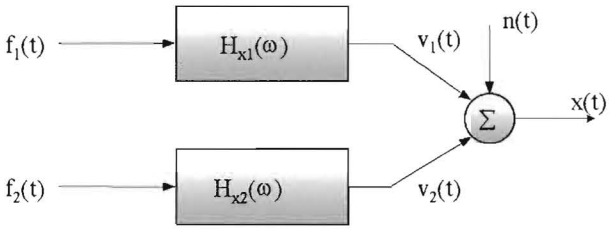

Figure 2.4 – Dual-input, single-output system

The Fourier Transform of the response $X(\omega)$ is given by

$$X(\omega) = H_{x1}(\omega)F_1(\omega) + H_{x2}(\omega)F_2(\omega) + N(\omega) \tag{2.12}$$

where

$F_1(\omega)$ and $F_2(\omega)$ are the Fourier Transform of the inputs at points 1 and 2, respectively,

$N(\omega)$ is the noise contaminating the response.

Assuming that averaging is employed it can be shown that

$$XF_1^* = H_{x1}F_1F_1^* + H_{x2}F_2F_1^* \tag{2.13a}$$

$$XF_2^* = H_{x1}F_1F_2^* + H_{x2}F_2F_2^* \tag{2.13b}$$

where

$*$ denotes the complex conjugate.

These equations can be expressed in terms of the auto- and cross-spectrums as:

$$G_{1x} = H_{x1}G_{11} + H_{x2}G_{12} \tag{2.14a}$$

$$G_{2x} = H_{x1}G_{21} + H_{x2}G_{22} \tag{2.14b}$$

Equation (2.14) can be solved for H_{x1} and H_{x2}, i.e.

$$H_{x1} = \frac{G_{1x}G_{22} - G_{2x}G_{12}}{G_{11}G_{22} - |G_{12}|^2} = \left(\frac{G_{1x}}{G_{11}}\right)\left\{\frac{1 - \dfrac{G_{2x}G_{12}}{G_{1x}G_{22}}}{1 - \gamma_{12}^2}\right\} \tag{2.15a}$$

$$H_{x2} = \frac{G_{11}G_{2x} - G_{21}G_{1x}}{G_{11}G_{22} - |G_{12}|^2} = \left(\frac{G_{2x}}{G_{22}}\right)\left\{\frac{1 - \frac{G_{2x}G_{12}}{G_{2x}G_{22}}}{1 - \gamma_{12}^2}\right\} \qquad (2.15b)$$

providing that the coherence function, γ_{12}^2 between the inputs $F_1(\omega)$ and $F_2(\omega)$ is not equal to unity, i.e.

$$\gamma_{12}^2 = \frac{|G_{12}|^2}{G_{11}G_{22}} \neq 1$$

When $G_{12} = G_{21}^* = 0$, $\gamma_{12}^2 = 0$, equation (2.15) reduces to the single-input expressions

$$H_{x1} = \frac{G_{1x}}{G_{11}} \qquad (2.16a)$$

$$H_{x2} = \frac{G_{2x}}{G_{22}} \qquad (2.16b)$$

As long as the inputs are uncorrelated, equation (2.15) can be used to obtain the frequency response functions when two inputs are acting simultaneously. The above analysis can be extended to apply to any arbitrary number of inputs and outputs.

MIMO Applied To Experimental Setup:

Despite the advantages referred to earlier, associated with the MIMO excitation the use of this type of excitation was motivated by the exciter-structure interaction. The exciter-structure interaction inherently creates difficulties, since the dynamic characteristics of the exciter becomes combined with those of the structure (the exciter adds some of its own mass, stiffness and damping to that of the structure). From experiments conducted on a beam-like structure Han (1998) confirmed that the exciter-structure interaction distorted the natural frequencies and damping values of the structure. In the experimental studies that follow in Chapter 5 two exciters were attached to the beam, in some instances. The distortion of the natural frequencies of the beam due to the two exciters were so severe that the frequency response functions obtained from single-input excitation could not be reconciled with the frequency response functions measured with both exciters attached.

2.5 EXPERIMENTAL MODAL ANALYSIS

The aim of Experimental Modal Analysis is to construct a mathematical model of the structure, which will resemble the characteristics of the experimentally measured data. In the case of measured frequency response functions, one needs to curve-fit an expression to the measured data and thereby finding the appropriate modal parameters (i.e. natural frequencies, damping ratios and mode shapes).

Reducing the frequency response function to terms involving only the modal parameters as in equation (2.10) leads to considerable reduction in the amount of data to be handled. The frequency response function may now be reconstructed for any frequency, simply from use of the modal parameters. Another advantage is that the regenerated frequency response curve is smoother than the experimentally measured data, which always contains noise.

The author made extensive use of the *Structural Dynamic Toolbox*® (Balmès, 1997 (1)) to identify the modal parameters and reconstruct the frequency response functions.

It is not the intention of this work to include a detailed discussion regarding the experimental modal analysis technique. However, the author has spent a considerable amount of time and effort mastering this Toolbox and gaining insight into the technique proposed by Balmès. Only the methodology that has been followed in the analysis will be discussed briefly.

Experimental Modal Analysis Methodology:

Step 1: The measured frequency response function data is imported into the Toolbox, in the desired format.

Step 2: At this stage, the user needs to specify the appropriate type of model that will be used in the identification. The type of model may be either a complex mode model or a normal mode model. An experimentally identified model will have complex eigenvectors. The normal mode model can then be obtained through the use of a transformation procedure, which allows the identification of the normal mode model (i.e. real modes) from the complex mode identification result (Balmès, 1997 (2)).

Step 3: Next, one iteratively computes an approximation of the measured response. This is done in three separate procedures:

a) First, finding initial complex pole estimates. The Toolbox obtains estimates of the poles by searching for the minima of the Multivariable Mode Indicator Function (MMIF) within a frequency region specified by the user. Additional poles may be added or removed to obtain the best fit to the data.

b) Once the user is satisfied with the set of complex poles, the Toolbox continues to estimate the residues and residual terms for the given set of poles.

c) These complex poles and residues are then optimised using a broad or narrow band update algorithm.

Step 4: The poles, damping ratios and complex mode shapes at the sensor locations are extracted from the mathematical model. If the user requires the normal mode model the above-mentioned transformation will be performed and will produce the modal parameters corresponding to the normal mode model.

Step 5: Lastly the frequency response functions may be reconstructed from use of the modal parameters.

The above procedure is depicted in Figure 2.5.

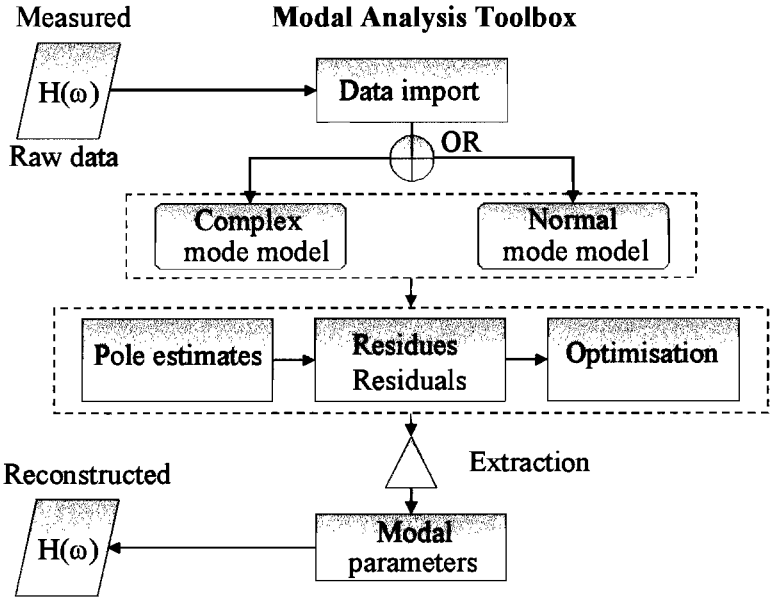

Figure 2.5 - Flowchart of a typical modal analysis and frequency response function reconstruction procedure

CHAPTER 3

The Frequency Response Function Method

3.1 THEORY

Preamble

The intent of this section is twofold: Firstly, we will formulate the relevant theory relating to the frequency response function method as applied to the force identification process. We will start with the more familiar inverse of a square matrix and progress to the pseudo-inverse of a rectangular matrix. The second objective is concerned with the calculation of the pseudo-inverse itself. There are currently a number of different matrix decomposition methods that are used in the calculation of the pseudo-inverse. It is not the intention to present a detailed mathematical explanation of the derivation of the pseudo-inverse, but rather to highlight some of the important issues. This is explained on the basis of the frequency response function method, but is also relevant to other force identification procedures, among others the modal coordinate transformation method which also features in this work.

3.1.1 Direct Inverse

By assuming that the number of forces to be identified and the number of responses are equal $(m = n)$, the frequency response matrix becomes a square matrix and thus an ordinary inversion routine can be applied, as follows:

$$\{F(\omega)\} = [H(\omega)]^{-1}\{X(\omega)\} \tag{3.1}$$

The above equation suppresses many of the responses for computational purposes, since the number of forces is usually only a few even if the structure is very complex or many responses are available.

3.1.2 Moore-Penrose Pseudo-Inverse

Accordingly, it is proposed to use a method of least-squares regression analysis, which allows the use of more equations than unknowns, whence the name over-determined. The advantage of being able to use redundant information minimises the consequence of errors in measured signals due to noise, which are always present. Adopting the least-squares method the following set of inconsistent linear equations are formulated:

$$\{X(\omega)\} = [H(\omega)]\{F(\omega)\} \tag{3.2}$$

where

$\{X(\omega)\}$ is the $(n \times 1)$ response vector,

$[H(\omega)]$ is the $(n \times m)$ frequency response function matrix,

$\{F(\omega)\}$ is the $(m \times 1)$ force vector.

The difference between the above equation and equation (3.1) is that here m unknowns (forces) are to be estimated from n equations (responses), with $n \geq m$. The least-squares solution of equation (3.2) is given by:

$$\{\hat{F}(\omega)\} = [H(\omega)]^{+} \{X(\omega)\} \tag{3.3.a}$$

where

$$[H(\omega)]^{+} = \left([H(\omega)]^{*}[H(\omega)]\right)^{-1}[H(\omega)]^{*} \tag{3.3.b}$$

which is known as the Moore-Penrose pseudo-inverse of the rectangular matrix $[H(\omega)]$. Since the force and response vectors are always functions of the frequency, the functional notation (ω) will be dropped in further equations.

The least-squares solution $\{\hat{F}\}$ is thus given by:

$$\{\hat{F}\} = \left([H]^{*}[H]\right)^{-1}[H]^{*}\{X\} \tag{3.4}$$

where

$[\cdot]^{*}$ is the complex conjugate transpose of the indicated matrix and $(\cdot)^{-1}$ is the inverse of a square matrix.

Now, we would like to investigate the conditions under which the pseudo-inverse, as stated in equation (3.4), are valid. For this reason, we first need to consider what is meant by the rank of a matrix.

a) *The Rank of a Matrix*

The rank of a matrix can be defined as the number of linearly independent rows or columns of the matrix. A square matrix is of full rank if all the rows are linearly independent and rank deficient if one or more rows of the matrix are a linear combination of the other rows. Rank deficiency implies that the matrix is singular, i.e. its determinant equals zero and its inverse cannot be calculated. An $n \times m$ rectangular matrix with $n \geq m$ is said to be 'full rank' if its rank equals m, but rank deficient if its rank is less than m. (Maia, 1991)

b) *Limitation Regarding the Moore-Penrose Pseudo-Inverse*

It should be noted that equation (3.4) is only unique when $[H]$ *is of full column rank* ($rank([H]) = m$; m = number of forces), i.e. the equations in (3.2) are linearly independent. Or in other words, the inverse of $\left([H(\omega)]^{*}[H(\omega)]\right)^{-1}$ in equation (3.4) is

only feasible if all the columns and at least m rows of the $(n \times m)$ rectangular matrix $[H]$ are linearly independent.

If $[H]$ is rank deficient ($rank([H]) < m$), the matrix to be inverted will be singular and the pseudo-inverse cannot be computed. This, however, does not mean that the pseudo-inverse does not exist, but merely that another method needs to be employed for its determination.

Based on the above-mentioned requirement Brandon (1988) refers to the Moore-Penrose pseudo-inverse as the 'restricted' pseudo-inverse. He investigated the use of the restricted pseudo-inverse method in modal analysis and only his conclusions will be represented here.

- "The most common representation of pseudo-inverse, in modal analysis is the full rank restricted form. This will fail if the data is rank deficient, due to the singularity of the product matrices. In cases where the data is full rank, but is poorly conditioned (common in identification problems), the common formulation of the restricted pseudo-inverse will worsen the condition *unnecessarily*.

- In applications where the rank of the data matrix is uncertain, the singular value decomposition gives a reliable numerical procedure, which includes an explicit measure of the rank."

It is to be hoped that the reader will be convinced in view of the above that certain restrictions exist regarding the use of the Moore-Penrose pseudo-inverse. The Singular Value Decomposition will prove to be an alternative for calculating the pseudo-inverse of a matrix.

c) *Further Limitations Regarding the Least-Square Solution*

Up to now, it may seem possible to apply the least-squares solution to the force identification problem, simply by ensuring that the columns of $[H]$ are all linearly independent. But this in itself introduces further complications. The number of significantly participating modes, as introduced by Fabunmi (1986), plays an important role in the linear dependency of the columns of the frequency response function matrix.

The components of the forces acting on a structure are usually independent. Conversely, the different responses caused by each one of the forces may have quite similar spatial distributions. As a result, the columns of the frequency

response function matrix are "almost" linearly dependent, resulting in a rank deficient matrix. This can be circumvented by taking more measurements, or by moving the measurement positions along the structure. However, situations exist where the above action will have little effect.

As is generally known, the response at a particular frequency will be dominated only by a number of significantly participating modes, p. This is particularly true at or near resonance. In such a situation only a limited number of columns of the frequency response function matrix are linearly independent, while some can be written as linear combinations of the dominated modes. The linear dependency may be disguised by measurement errors. This leads to ill-conditioning of the matrix, which can be prone to significant errors when inverted.

In order to successfully implement the least-squares technique, Fabunmi (1986) suggests that the number of forces one attempts to predict should be less or equal to the significantly participating modes at some frequency ($m \leq p$). This will ensure that all the columns and at least m rows will be linearly independent.

To conclude:

- The number of response coordinates must be at least as many as the number of forces. In the least-squares estimation, the response coordinates should considerably outnumber the estimated forces ($n \geq m$).

- Furthermore, the selection of the response coordinates must be such as to ensure that at least m rows of the frequency response function matrix are linearly independent. If there are fewer than m independent rows, the estimated forces will be in error, irrespective of how many rows there are altogether ($p \geq m$).

3.1.3 Singular Value Decomposition (SVD)

In the force identification the number of modes that contribute to the data is not always precisely known. As a result the order of the data matrix may not match the number of modes represented in the data. Another method must then be employed to calculate the pseudo-inverse, for instance Singular Value Decomposition (SVD).

It is not the intent to present a detailed mathematical explanation of the derivation of the SVD technique, but rather to highlight some of the important issues. The reader is referred to the original references for specific details (Menke, 1984; Maia, 1991; Brandon, 1988).

The SVD of an $n \times m$ matrix $[H]$ is defined by:

$$[H]=[U][\Sigma][V]^T \tag{3.5}$$

where

$[U]$ is the $(n \times n)$ matrix, the columns comprise the normalised eigenvectors of $[H][H]^T$,

$[V]$ is the $(m \times m)$ matrix and the columns are composed of the eigenvectors of $[H]^T[H]$, and

$[\Sigma]$ is the $(n \times m)$ matrix with the singular values of $[H]$ on its leading diagonal (off-diagonal elements are all zero).

The following mathematical properties follow from the SVD:

a) The Rank of a Matrix

The singular values in the matrix $[\Sigma]$ are arranged in decreasing order $(\sigma_1 > \sigma_2 > ... > \sigma_m)$. Thus,

$$[\Sigma]=\underbrace{\left.\begin{bmatrix} \sigma_1 & & 0 \\ & \sigma_2 & \\ & & \ddots \\ 0 & & \sigma_m \\ \hline & 0 & \end{bmatrix}\right\}m}_{m}\Bigg\}n \tag{3.6}$$

Some of these singular values may be zero. The number of non-zero singular values defines the rank of a matrix $[\Sigma]$. However, some singular values may not be zero because of experimental measurements, but instead are very small compared to the other singular values. The significance of a particular singular value can be determined by expressing it as the ratio of the largest singular value to that particular singular value. This gives rise to the condition number.

b) Condition Number of Matrix

After decomposition, the condition number, $\kappa_2([H])$, of a matrix can be expressed as the ratio of the largest to the smallest singular value.

$$\kappa_2([H])=\|[H]\|_2\left\|[H]^+\right\|_2=\sigma_{max}/\sigma_{min} \tag{3.7}$$

If this ratio is so large that the smaller one might as well be considered zero, the matrix $[H]$ is 'almost singular' and has a large condition number. This reflects an ill-conditioned matrix. We can establish a criterion whereby any singular value smaller than a tolerance value will be set to zero. This will avoid numerical problems, as the inverse of a small number is very large and would, falsely, dominate the pseudo-inverse if not excluded. By setting the singular value equal to zero, the rank of the matrix $[H]$ will in turn be reduced, and in effect the number of force predictions allowed, as referred to in Section 3.1.2.c.

c) *Pseudo-Inverse*

Since the matrices $[U]$ and $[V]$ are orthogonal matrices, i.e.,

$$[U][U]^T = [U]^T[U] = [V][V]^T = [V]^T[V] = [I] \tag{3.8a}$$

and

$$[U]^T = [U]^{-1} \quad \text{and} \quad [V]^T = [V]^{-1} \tag{3.8b}$$

the pseudo-inverse is related to the least-squares problem, as the value of $\{\hat{F}\}$ that minimises $\left\|[H]\{\hat{F}\} - \{X\}\right\|_2$ and can be expressed as:

$$[H]^+ = ([V]^T)^+[\Sigma]^+[U]^+ \tag{3.9}$$

Therefore,

$$[H]^+ = [V][\Sigma]^+[U]^T \tag{3.10}$$

where

$[H]^+$ is an $(m \times n)$ pseudo-inverse of the frequency response matrix,

$[V]$ is an $(m \times m)$ matrix containing the eigenvectors of $[H][H]^T$,

$[U]^T$ is an $(n \times n)$ unitary matrix comprising the eigenvectors of $[H]^T[H]$,

$[\Sigma]^+$ is an $(m \times n)$ real diagonal matrix, constituted by the inverse values of the non-zero singular values.

The force estimates can then be obtained as follows:

$$\{\hat{F}\} = [V][\Sigma]^+[U]^T\{X\} \tag{3.11}$$

3.1.4 QR Decomposition

The QR Decomposition (Dongarra *et al.*, 1979) provides another means of determining the pseudo-inverse of a matrix. This method is used when the matrix is ill-conditioned, but not singular.

The QR Decomposition of the $(n \times m)$ matrix $[H]$ is given as:

$$[H]=[Q][R] \tag{3.12}$$

where

$[Q]$ is the $(n \times m)$ orthogonal matrix, and

$[R]$ is the $(m \times m)$ upper triangular matrix with the diagonal elements in descending order.

The least-squares solution follows from the fact that

$$[H]^T[H]=[R]^T[Q]^T[Q][R] \tag{3.13}$$

and taking the inverse of the triangular and well-conditioned matrix $[R]$ it follows that

$$\{\hat{F}\}=[R]^{-1}[Q]^T\{X\} \tag{3.14}$$

3.1.5 Tikhonov Regularisation

As described earlier, the SVD deals with the inversion of an ill-conditioned matrix by setting the very small singular values to zero and thus, averting their contribution to the pseudo-inverse. In some instances the removal of the small singular values will still result in undesirable solutions. The Tikhonov Regularisation (Sarkar *et al.*, 1981; Hashemi and Hammond, 1996) differs from the previously mentioned procedures in the sense that it is not a matrix decomposition method, but rather a stable approximate solution to an ill-conditioned problem, and whence the name regularisation methods. The basic idea behind regularisation methods is to replace the unconstrained least-squares solution by a constrained optimisation problem which would force the inversion problem to have a unique solution.

The optimisation problem can be stated as the minimising of $\left\|[H]\{\hat{F}\}-\{X\}\right\|^2$ subjected to the constraint $\left\|[\hat{L}]\{\hat{F}\}\right\|^2$, where $[\hat{L}]$ is a suitably chosen linear operator.

It has been shown that this problem is equivalent to the following one

$$\min_{\hat{F}} \left\{ \left\| [H]\{\hat{F}\} - \{X\} \right\|^2 + \mu^2 \left\| [\hat{L}]\{\hat{F}\} \right\|^2 \right\} \tag{3.15}$$

where

μ plays the role of the Lagrange multiplier.

The following matrix equation is equivalent to equation (3.14):

$$\left([H]^*[H] + \mu^2 [\hat{L}]^*[\hat{L}] \right) \{\hat{F}\} = [H]^*\{X\} \tag{3.16}$$

leading to

$$\{\hat{F}\} = \left([H]^*[H] + \mu^2 [\hat{L}]^*[\hat{L}] \right)^{-1} [H]^*\{X\} \tag{3.17}$$

3.2 TWO DEGREE-OF-FREEDOM SYSTEM

Noise, as encountered in experimental measurements, consists of correlated and uncorrelated noise. The former includes errors due to signal conditioning, transduction, signal processing and the interaction of the measurement system with the structure. The latter comprises errors arising from thermal noise in electronic circuits, as well as external disturbances. (Ziaei-Rad and Imregun, 1995)

The added effect of noise, as encountered in experimental measurements, may further degrade the inversion process. This is especially true for a system with a high condition number, indicating an ill-conditioned matrix. As was stated previously, the inverse of a small number is very large and would, falsely, dominate the pseudo-inverse.

There are primarily two sources of error in the force identification process. The first is the noise encountered in the structure's response measurements. Another source of errors arises from the measured frequency response functions and the modal parameter extraction. Bartlett and Flannelly (1979) indicated that noise contaminating the frequency response measurements could create instabilities in the inversion process. Hillary (1983) concluded that noise in both the structure's response measurement and the frequency response function can affect the force estimates. Elliott *et al.* (1988) showed that the measurement noise increased the rank of the strain response matrix, which circumvented the force predictions.

The measured frequency response functions can be applied directly to the force identification process. As an alternative, the frequency response functions can also be reconstructed from the modal parameters, but this approach requires that an

experimental modal analysis be done in advance. The latter has the advantage that it leads to a considerable reduction in the amount of data to be stored. The curve-fitted frequency response functions can be seen as a way of filtering some of the unwanted noise from the frequency response functions. However, the reconstruction of the frequency response functions from the identified eigensolutions might give rise to difficulties in taking into account the effect of out-of-band modes in the reconstruction.

To illustrate the ill-conditioning of a system near and at the resonant frequencies, consider the following lumped-mass system:

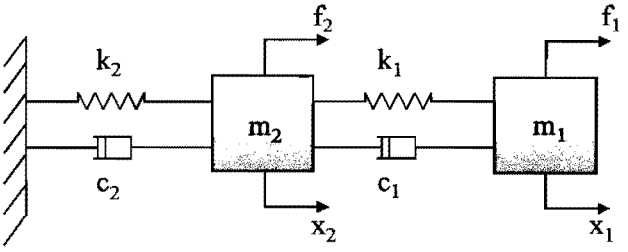

$m_1 = 0.5$ kg	$k_1 = 1.4212 \times 10^5$ N/m	$\zeta_1 = 0.001$
$m_2 = 1.0$ kg	$k_2 = 2k_1$ N/m	$\zeta_2 = 0.001$

Figure 3.1 – 2 DOF lumped mass system

A harmonic forcing function is used to excite each of the masses.

$$f_1(t) = 150\cos(60\pi t) \qquad f_2(t) = 100\cos(60\pi t) \tag{3.18}$$

It can be shown that the natural frequencies and mass-normalised mode-shapes for the undamped system are:

$$\begin{aligned} \omega_1 &= 60\ Hz \\ \omega_2 &= 120\ Hz \end{aligned} \qquad [\Phi] = \begin{bmatrix} 1.1547 & 0.8165 \\ 0.5773 & -0.8165 \end{bmatrix} \tag{3.19}$$

The forward problem was solved to obtain the response for each degree-of-freedom from

$$\{\ddot{X}(\omega)\}_{EXACT} = [A(\omega)]_{EXACT}\{F(\omega)\}_{APPLIED} \tag{3.20}$$

where

$\{\ddot{X}(\omega)\}$ is the (2×1) acceleration vector,

$[A(\omega)]$ is the (2×2) inertance matrix,

$\{F(\omega)\}$ is the (2×1) force vector.

The frequency response function was recalculated for the perturbated modal parameters. The inverse problem was solved subsequently to obtain the force estimates

$$\{\hat{F}(\omega)\} = [\tilde{A}(\omega)]^{+} \{\tilde{\tilde{X}}(\omega)\} \tag{3.25}$$

where

$(\tilde{\ })$ denotes the contaminated values.

The relative error is given by the Force Error Norm (FEN), $\varepsilon_f(\omega)$, of the forces, evaluated at each frequency line, and is defined as

$$\varepsilon_f(\omega) = \frac{\| \{F(\omega)\} - \{\hat{F}(\omega)\} \|_2}{\| \{F(\omega)\} \|_2} \times 100\,\% \tag{3.26}$$

where

$\{F(\omega)\}$ is the actual/applied force vector,

$\{\hat{F}(\omega)\}$ is the estimated force vector,

$\| \cdot \|_2$ is the vector 2-norm.

Results and Discussion

Figures 3.2 and 3.3 show the ill-conditioning of equation (3.25) in the vicinity of the modes, where the force estimates are in error. The FEN at the first mode (Figure 3.4) is considerably higher than at the second mode. Since the applied forces are not in the vicinity of the system's resonances, they are not affected by this ill-conditioned behaviour and are correctly determined.

The modes of this system are well-separated, and near and at the resonant frequencies the response of the system is dominated by a single mode. As Fabunmi (1986) concluded, the response of which content is primarily that of one mode only cannot be used to determine more than one force.

In another numerical simulation of the same system, the influence of the perturbation of the different modal parameter on the force identification was considered. The force estimates were calculated for the case where a single modal parameter was polluted to the prescribed error level. It was concluded that the perturbation of the mode-shapes had the most significant effect in producing large errors in the force estimates. This result confirmed findings of Hillary (1983) and Okubo *et al.* (1985).

Although the frequency response function matrix is a square matrix, it is still singular at the resonant frequencies. This implies that the pseudo-inverse of the frequency response function can only be obtained by the SVD.

Since two forces were determined from two response measurements the least-square solution is of no use. In practice one would include as many response measurements as possible to utilise the least-squares solution for the over-determined case.

The maximum error levels were considered as realistic of what one could expect during vibration testing. These values were gathered from similar perturbation analyses performed by Hillary (1983), Genaro and Rade (1998), and Han and Wicks (1990). No explanations or references were provided for the error levels adopted. A literature survey conducted by the author concerning this issue also failed to produce satisfactory information. These error values proved to produce very large errors in the identified forces, beyond the point where the estimated forces could be meaningful.

To conclude, the aim of this section was to prove that small errors can have adverse effects on the force identification at the resonant frequencies of a system.

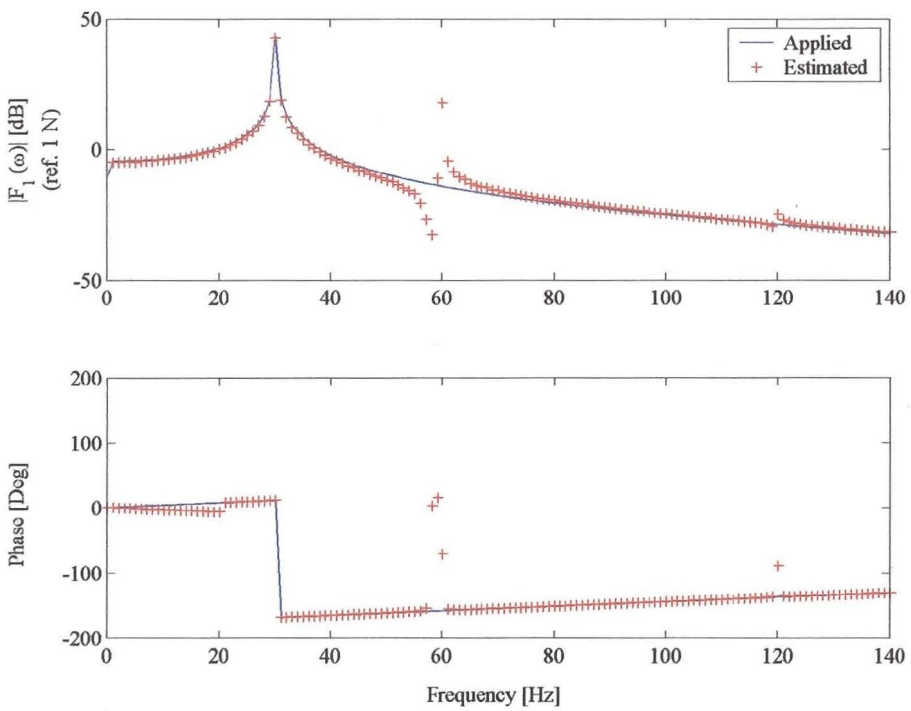

Figure 3.2 – Applied and estimated force no.1 for the 2 DOF lumped-mass system in the frequency domain

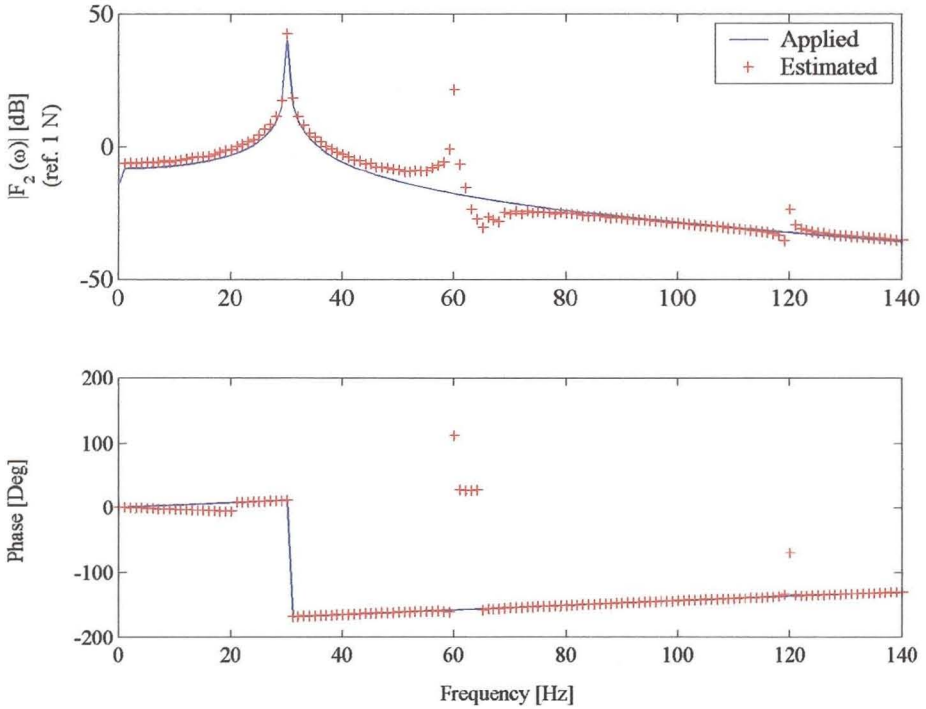

Figure 3.3 – Applied and estimated force no.2 for the 2 DOF lumped-mass system in the frequency domain

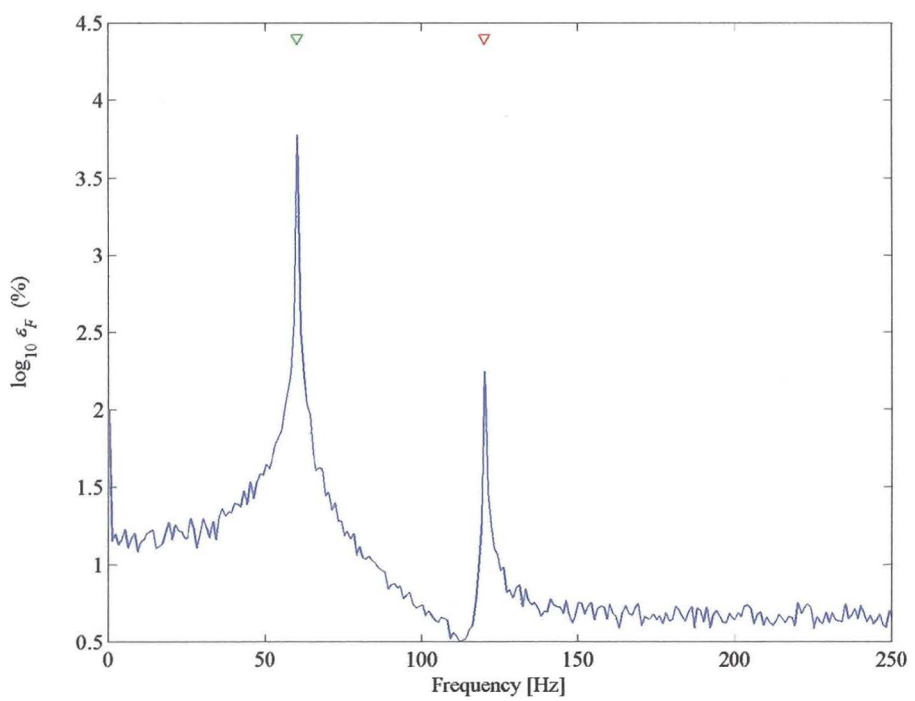

Figure 3.4 – Force Error Norm (FEN) of the estimated forces, ∇ indicates the 2 DOF systems' resonant frequencies

3.3 SIGNIFICANCE OF THE CONDITION NUMBER

In the previous section the effect of noise in the force identification was introduced. Consequently, errors will always be present in the measurements. In this section it is suggested that the condition number of the frequency response function matrix serves as a measure of the sensitivity of the pseudo-inverse.

Again consider the 2 DOF lumped-mass system. This time the system was subjected to randomly generated forces with uniform distribution on the interval $[-1, 1]$. The responses were obtained utilising the forward problem. The contaminated frequency response function matrix was generated through the perturbation of the modal parameters, as previously described. Finally, the inverse problem was solved to obtain the force estimates. The above procedure was repeated 100 times. In each run new random variables were generated. Figure 3.5 represents the average FEN, $\varepsilon_f(\omega)$ for these 100 runs.

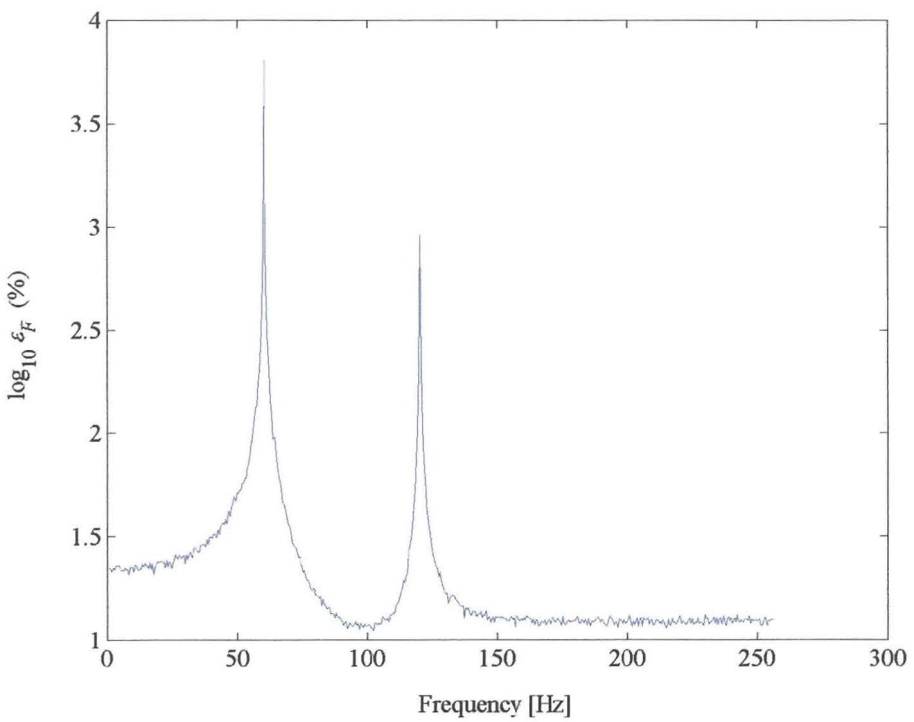

Figure 3.5 – Average Force Error Norm of estimated forces for the 2 DOF lumped-mass system

Golub and Van Loan (1989) describe the error propagation using the condition number, of the matrix to be inverted, as an error boundary for perturbation of linear systems of equations. Referring to the above case where only the frequency response function matrix was perturbated, errors in the calculation of $\{F(\omega)\}$ will be restricted by

$$\frac{\left\| \{F(\omega)\} - \{\hat{F}(\omega)\} \right\|_2}{\left\| \{F(\omega)\} \right\|_2} \leq \kappa_2([H])^2 \frac{\left\| [\delta H(\omega)] \right\|_2}{\left\| [H(\omega)] \right\|_2} \tag{3.27}$$

where

$\{F(\omega)\}$ is the actual force vector,

$\{\hat{F}(\omega)\}$ is the estimated force vector,

$\kappa_2([H])$ is the condition number of $[H]$,

$[\delta H(\omega)]$ is the difference between the actual and perturbated $[H]$,

$\|\cdot\|_2$ is the vector 2-norm.

Similar expressions could be obtained for perturbation of the response, $\{X(\omega)\}$. Unfortunately, these expressions are of little practical use, since the actual force and response are unknown.

It was suggested that the condition number of the matrix to be inverted, should be used as a measure of the sensitivity of the pseudo-inverse (Starkey and Merrill, 1989). Although the exact magnitude of the error bound of the system at a particular frequency remains unknown, the condition number enables one to comment on the reliability of the force estimates within a given frequency range. A high condition number indicates that the columns of the frequency response function are linearly or "almost" linearly dependent, i.e. rank deficient. This can result in large errors in the identified forces. Conversely, a condition number close to unity indicates that the columns of the frequency response function are almost mutually perpendicular. One should not expect any large amplification of the measurement noise when inverting the frequency response function matrix. Figure 3.6 shows the condition number of the frequency response function matrix for the 2 DOF lumped-mass system. From this it is evident that the condition number follows the same trend as the relative error in the force estimates given in Figure 3.5.

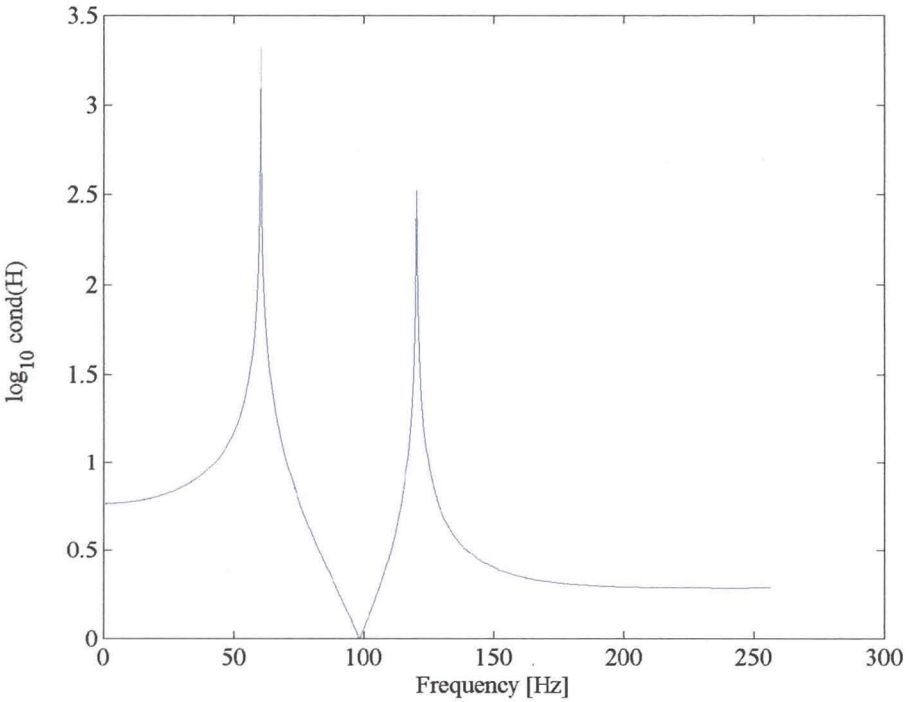

Figure 3.6 – Condition number of frequency response function matrix

In the next half of this section we would like to investigate the factors that have an influence on the value of the condition number. A more complex structure will be considered for this purpose.

A Finite Element Model (FEM) of a freely supported beam was constructed. Ten equally spaced beam elements were used to simulate the 2 metres long beam. The model was restricted to two dimensions, since only the transverse bending modes were of interest, for which the natural frequencies and normal modes were obtained solving the eigenvalue problem. The first eight bending modes were used in the reconstruction of the frequency response function matrix of which, the first three modes were the rigid body modes of the beam. A uniform damping factor of 0.001 was chosen. Each node point was considered as a possible sensor location.

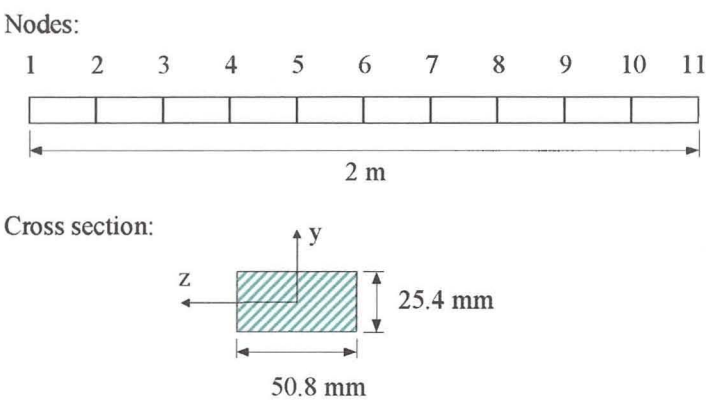

Figure 3.7 – FEM of free-free beam and response locations

3.3.1 Effect of the Number of Forces

Eleven response 'measurements' were taken and four sets of excitation forces were applied to the beam. These sets consisted of 1, 2, 3 and 4 forces, respectively and are shown in Figure 3.8.

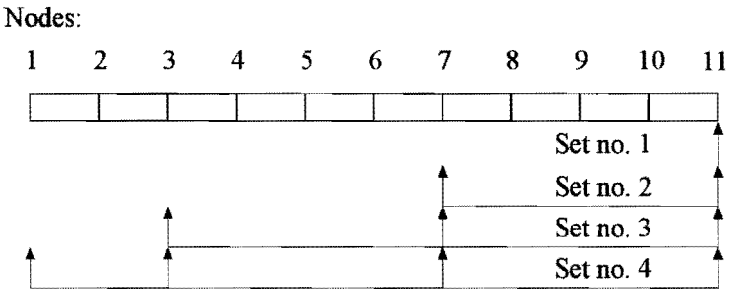

Figure 3.8 - FEM of free-free beam and force locations

Figure 3.9 shows the condition number of the frequency response function matrix for each of these sets. It is evident from the results that the condition number increases drastically as the number of force predictions increase. The condition number for a single force prediction is equal to unity over the entire frequency range. If an additional force is added, it implies that the column corresponding the force location be included in the frequency response function matrix, which in turn increases the condition number of the matrix. The number of force predictions is, however, limited by the number of modes included in the analysis (Fabunmi, 1986).

3.3.2 Effect of the Damping

The effect of the damping on the condition number was evaluated next. Only three forces were applied, while still measuring eleven responses. From Figure 3.10 one notices that the condition number varies for different modal damping factors. In fact, as the damping factors increase, the condition number decreases, especially at the beam's resonances. This can be attributed to higher modal overlap due to the higher damping. It was mentioned earlier that at a resonant frequency the system's response is dominated by that particular mode. In a system with higher damping the neighbouring modes have a larger contribution to the response of the system at that frequency.

3.3.3 Effect of the Number of Response Measurements

Figure 3.11 shows the condition number as a function of the number of response measurements across the frequency range of interest. The beam is once again subjected to three forces while considering 3 (locations 3, 7 and 11), 6 (locations 2, 3,

5, 7, 9 and 11) and 9 (locations 2, 3, 4, 5, 7, 8, 9, 10 and 11) response measurements, respectively.

The results show that there is a significant improvement in the condition number by increasing the number of response measurements. Since there is a direct relation between the condition number and force error, over-determination will improve the force estimates as well. Adding a response measurement implies that an additional row, and thus a new equation, is added to the frequency response function matrix. Mas *et al.* (1994) showed that the ratio of the number of response measurements to the number of force predictions should preferably be greater than or equal to 3 (i.e. $n/m \geq 3$).

3.3.4 Effect of the Response Type

Both accelerometers and strain gauges have been employed by Hillary and Ewins (1984) to determine sinusoidal forces on a uniform cantilever beam. The strain responses gave more accurate force estimates, since the strain responses are more influenced by the higher modes at low frequencies. Han and Wicks (1990) also studied the application of displacement, slope and strain measurements. From both these studies it is evident that proper selection of the measurement type can improve the condition of the frequency response function matrix and hence obtain better force predictions.

3.3.5 Conclusion

It is suggested that the condition number of the frequency response function matrix serves as a measure of the sensitivity of the pseudo-inverse. The frequency response function matrix needs to be inverted at each discrete frequency, and as a result the condition number varies with frequency. Large condition numbers exist near and at the system's resonances.

The condition number of the pseudo-inverse is a function of the number of response points included. The number of force predictions, system's damping, as well as the selection of the response type also influence the condition number.

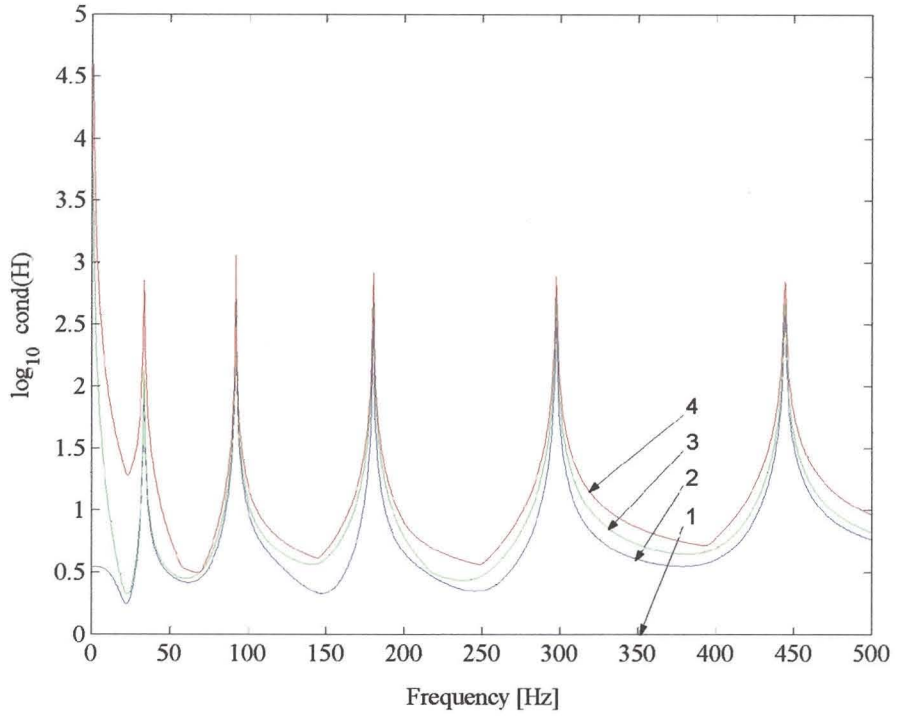

Figure 3.9 – Effect of the number of forces on the condition number

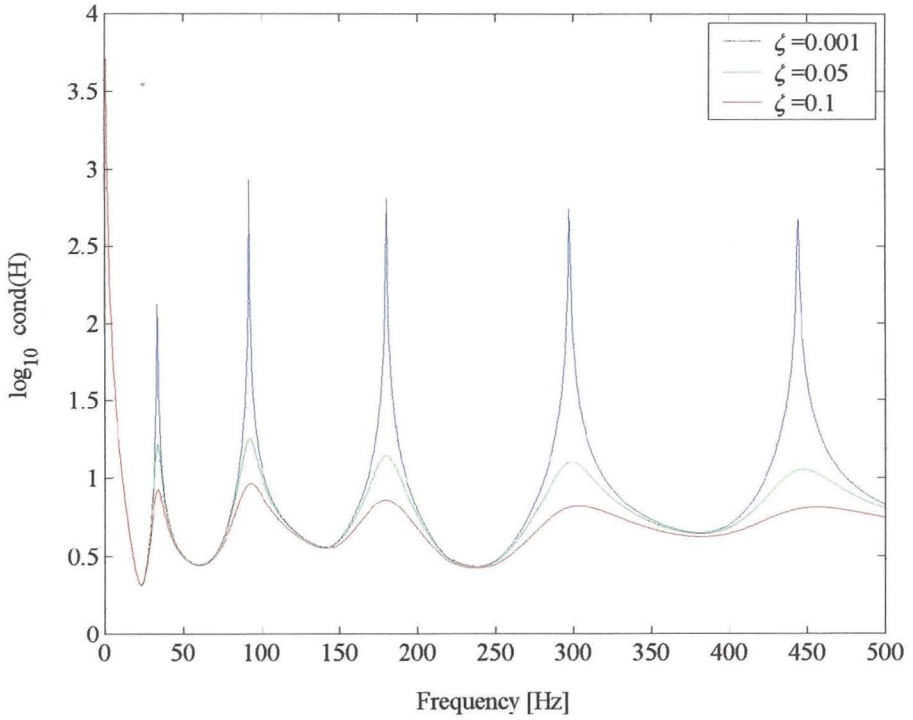

Figure 3.10 – Effect of the damping on the condition number

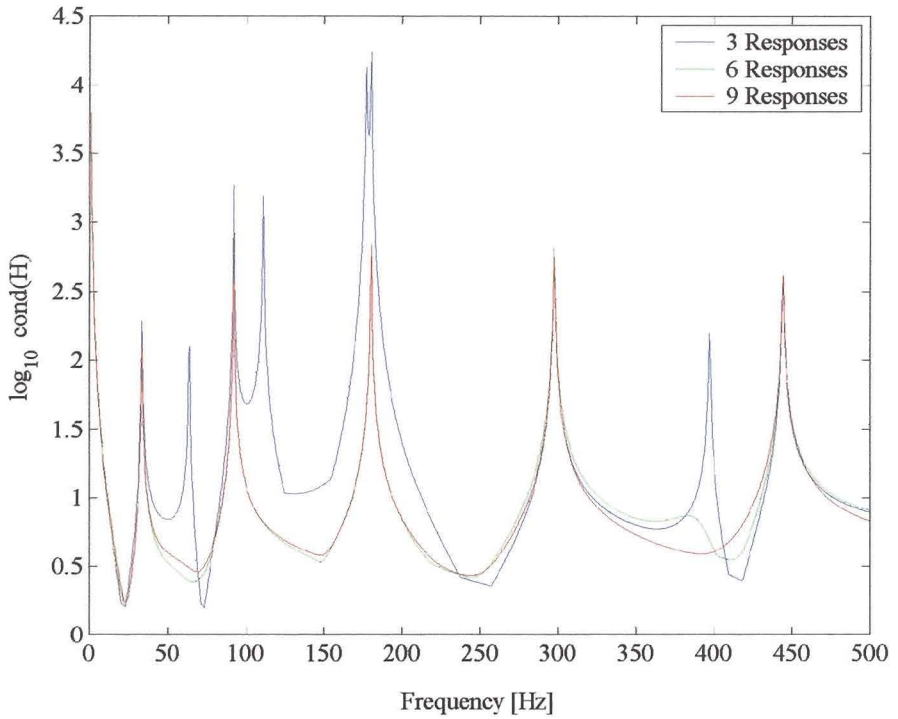

Figure 3.11 – Effect of the number of response measurements on the condition number

3.4 NUMERICAL STUDY OF A FREE-FREE BEAM

This section examines the different matrix decomposition and regularisation methods employed for the calculation of the pseudo-inverse. For this purpose it was decided to continue using the FEM of the freely supported aluminium beam, as introduced in Section 3.3.

The eigenvalue problem was solved to obtain the natural frequencies and mode shapes. In addition to the RBM, five bending modes were in the chosen frequency range of 0 to 500 Hz. The natural frequencies and mode shapes were taken as the 'exact' values. A proportional damping model was assumed with values obtained from the experimental modal analysis performed on a similar beam.

The beam was then subjected to two simultaneous harmonic forces applied at positions 5 and 11 with forcing frequencies of 220 Hz and 140 Hz, respectively. The frequency content of the force signals was not determined with an FFT algorithm, thus presenting zero amplitude values in the frequency range except at the discrete forcing frequencies.

The 'exact' response at each of the eleven sensor locations was calculated from:

$$\{\ddot{X}(\omega)\}_{EXACT} = [A(\omega)]_{EXACT}\{F(\omega)\}_{APPLIED} \tag{3.28}$$

where

$\{\ddot{X}(\omega)\}$ is the (11×1) acceleration vector,

$[A(\omega)]$ is the (11×2) inertance matrix,

$\{F(\omega)\}$ is the (2×1) force vector.

The $[A(\omega)]$ matrix was constructed from the RBM and five bending modes, while omitting the residual terms. The response and modal parameters were perturbated, as described in Section 3.2, to resemble experimental data. Successively, the force identification problem was solved while including only six response locations (positions 1, 3, 5, 6, 9 and 11) in the analysis.

$$\{\hat{F}(\omega)\} = [\tilde{A}(\omega)]^{+}\{\tilde{\ddot{X}}(\omega)\} \tag{3.29}$$

where

$(\tilde{\ })$ denotes the contaminated values.

Figure 3.12 shows the effect of the perturbation analysis on the reconstructed inertance matrix $[\tilde{A}(\omega)]$.

Each of the previously explained pseudo-inverse methods was employed to evaluate their ability to correctly determine the two harmonic forces.

A major difficulty associated with the Tikhonov regularisation is the choice of the regularisation parameter μ (Da Silva and Rade, 1999). The value of this parameter was obtained from using the L-curve (Hansen and O'Leary, 1991). The L-curve is a plot of the semi-norm $\left\|[\hat{L}]\{\hat{F}\}\right\|$, as a function of the residual norm $\left\|[H]\{\hat{F}\}-\{X\}\right\|$ for various values of μ. The corner of the L-curve is identified and the corresponding regularisation parameter μ is returned. This procedure has to be performed at each discrete frequency line and a result is computationally very expensive.

The results of the analysis are presented in Table 3.2. Only, the Tikhonov regularisation failed to predict the two forces correctly. This constraint optimisation algorithm identified the force applied at position 11 correctly, but calculated a significant force amplitude with the same frequency content as the force applied at node 11 at the other force location, position 5. Furthermore, it also under-estimated the force at node 5. Increasing the number of response locations had no improvement on the result.

Table 3.2 - Force results of the different matrix decomposition and regularisation methods

	$\lvert F_1 \rvert$ [N]	$\lvert F_2 \rvert$ [N]
Applied Force amplitudes	10.000 0	0 23.000
Singular Value Decomposition	9.338	21.432
QR Decomposition	9.338	21.432
Moore-Penrose	9.338	21.432
Tikhonov Regularisation	5.2139	19.512

Next, the author evaluated the force identification process for the entire frequency range. In this case, the frequency content of the harmonic force time signals was determined with an FFT-algorithm, thus presenting non-zero values in the frequency range considered. Figure 3.13 illustrates the ill-conditioning of the force estimates at the resonant frequencies of the beam. The ill-conditioning in this particular case is a result of the perturbation analysis, the FEM approximations and the FFT-algorithms. Changing the excitation points on the beam produced the same trends. Once again the Tikhonov regularisation produced poorer results than the other methods. The Singular Value Decomposition, QR Decomposition and Moore-Penrose pseudo-inverse produced exactly the same results.

In view of the above-mentioned the author decided to use the SVD from here onwards for the calculation of the pseudo-inverse matrix. The motivation being the ease of the implementation of this algorithm in the *Matlab®* environment. Another advantage of the SVD is the ability to ascertain the rank of a matrix and to truncate the singular values accordingly.

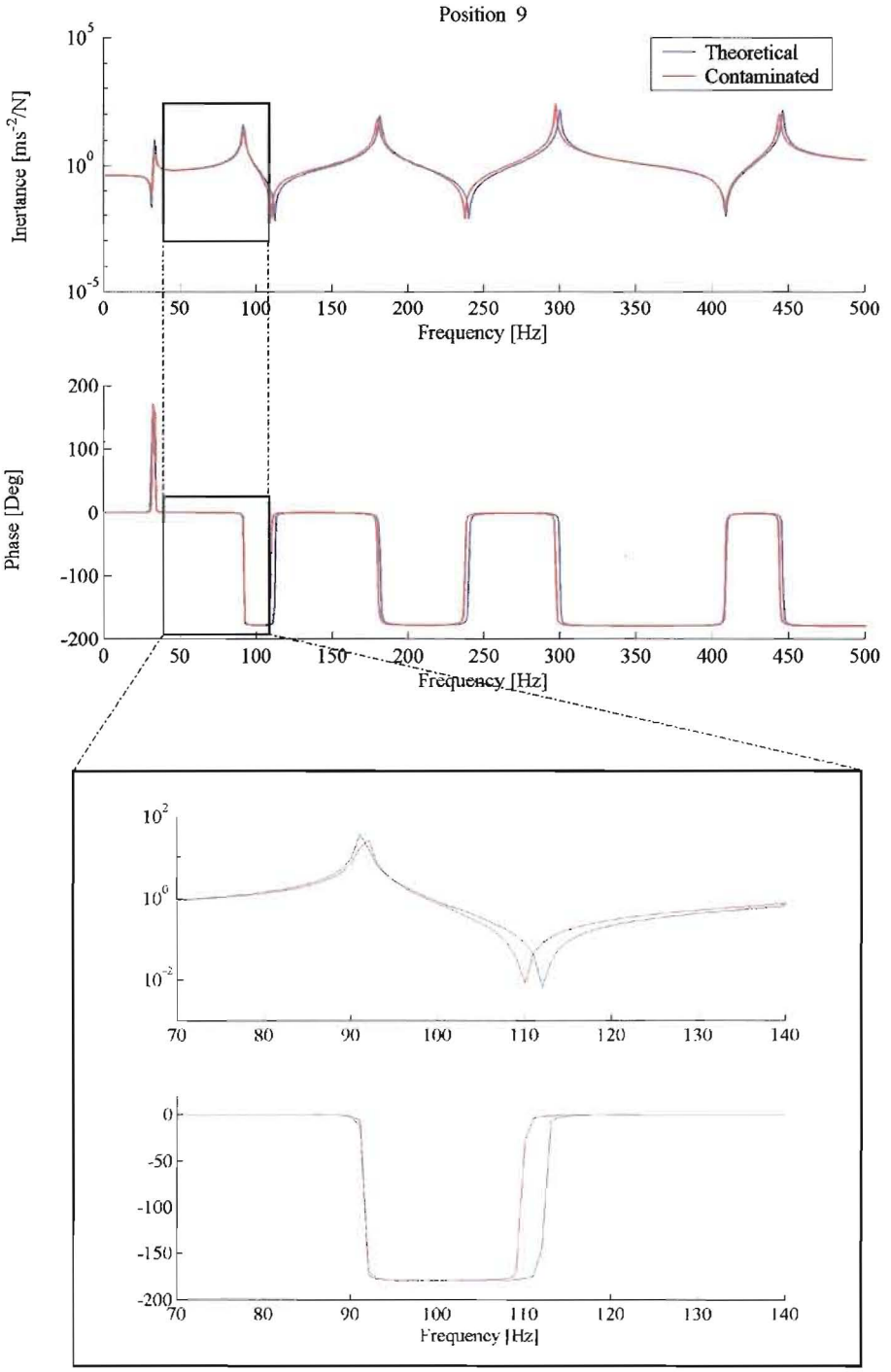

Figure 3.12 - Comparison of the 'exact' and perturbated inertance frequency response function

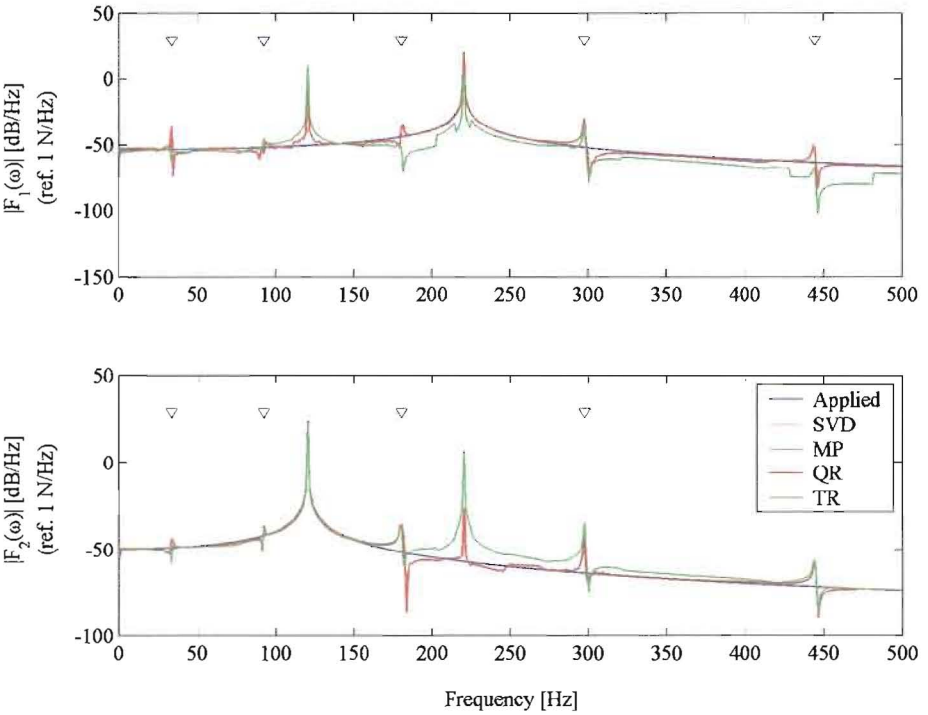

Figure 3.13 – Comparison of the different decomposition and regularisation methods. ∇ indicates the resonant frequencies

CHAPTER 4

The Modal Coordinate Transformation Method

4.1 THEORY

Preamble

This chapter is devoted entirely to the modal coordinate transformation method (Kim and Kim, 1997; Desangehere and Snoeys, 1985). A detailed derivation of the modal coordinate transformation method is presented. The numerical studies investigate the application of the method on a two degree-of-freedom system and the factors influencing the condition number of the modal matrix. This chapter also describes applying the modal filter to force reconstruction, which is validated by a numerical simulation.

For a proportionally damped multi-degree-of-freedom system, with N degrees of freedom, the governing equations of motion can be written in matrix form as:

$$[M]\{\ddot{x}(t)\}+[C]\{\dot{x}(t)\}+[K]\{x(t)\}=\{f(t)\} \tag{4.1}$$

where

$[M]$, $[K]$ and $[C]$ are the $(N\times N)$ mass, stiffness and damping matrices, respectively,

$\{\ddot{x}(t)\}$, $\{\dot{x}(t)\}$ and $\{x(t)\}$ are the $(N\times 1)$ acceleration, velocity and displacement vectors, respectively, and

$\{f(t)\}$ is the $(N\times 1)$ applied force vector.

The eigenvalue problem for the conservative (undamped) structure is written as:

$$[K][\Phi]=[M][\Phi][\Lambda] \tag{4.2}$$

where

$[\Phi]=[\{\phi\}_1,\{\phi\}_2,\ldots,\{\phi\}_N]^T$ is the modal matrix, consisting of N modal vectors,

$[\Lambda]=diag\{\lambda_1,\lambda_2,\ldots,\lambda_N\}$ is the modal stiffness matrix and $\lambda_r=\omega_r^2$ for $r=1,N$

Substitute the following coordinate transformation into equation (4.1)

$$\{x(t)\}=[\Phi]\{p(t)\} \tag{4.3}$$

and pre-multiplying the resulting equation by $[\Phi]^T$ yields

$$[\overline{M}]\{\ddot{p}(t)\}+[\overline{C}]\{\dot{p}(t)\}+[\overline{K}]\{p(t)\}=[\Phi]^T\{f(t)\} \tag{4.4}$$

where

$[\overline{M}]$, $[\overline{K}]$ and $[\overline{C}]$ are the modal mass, stiffness and damping matrices, respectively.

For a mass-normalised modal matrix it follows that

$$[\Phi]^T[M][\Phi]=[I] \quad \text{and} \quad [\Phi]^T[K][\Phi]=[\Lambda]$$
$$[\Phi]^T[C][\Phi]=[\beta] \tag{4.5}$$

where

$[\beta]=diag\{\beta_1,\beta_2,...,\beta_N\}$ is the modal damping matrix and $\beta_r=2\zeta_r\omega_r$,

ζ_r is the modal damping factor for the r-th mode.

It will be assumed that the following relation holds:

$$[C][M]^{-1}[K]=[K][M]^{-1}[C] \tag{4.6}$$

Satisfying this condition, the damped system will possess the same mode shapes as its undamped counterpart. Thus, the eigenvectors will be real and equation (4.4) will contain N uncoupled system equations.

Transforming equation (4.4) to the frequency domain and using equation (4.5), it follows for steady state conditions that

$$\left[-\omega^2[I]+i\omega[\beta]+[\Lambda]\right]\{P(\omega)\}=[\Phi]^T\{F(\omega)\} \tag{4.7}$$

where

$\{P(\omega)\}$ denotes the Fourier Transform of the modal coordinates ($\{p\}$ refers to the modal coordinates as a function of time),

Rearranging equation (4.7) it follows

$$\{P(\omega)\}=\left[-\omega^2[I]+i\omega[\beta]+[\Lambda]\right]^{-1}[\Phi]^T\{F(\omega)\} \tag{4.8}$$

Introducing equation (4.8) back into equation (4.3) in the frequency domain results in:

$$\{X(\omega)\}=[\Phi]\left[-\omega^2[I]+i\omega[\beta]+[\Lambda]\right]^{-1}[\Phi]^T\{F(\omega)\} \tag{4.9}$$

Equation (4.9) can be represented in a more familiar form, as the frequency response function

$$\{X(\omega)\}=\sum_{r=1}^{N}\frac{\{\phi\}_r\{\hat{\phi}\}_r^T}{\omega_r^2-\omega^2+i2\zeta_r\omega_r\omega}\{F(\omega)\} \tag{4.10}$$

where

$\{\phi\}_r$ is the $(N\times 1)$ modal vector corresponding to the measurement points,

$\{\hat{\phi}\}_r$ is the $(N \times 1)$ modal vector corresponding to the excitation points.

In real-world applications the mode shapes are usually identified at n $(n < N)$ sensor locations while only p $(p < N)$ of all possible modes are included. If the number of forces, m and positions are known *a priori*, equation (4.10) reduces to

$$\{X(\omega)\} = \sum_{r=1}^{p} \frac{\{\phi\}_r \{\hat{\phi}\}_r^T}{\omega_r^2 - \omega^2 + i2\zeta_r\omega_r\omega} \{F(\omega)\} \qquad (4.11)$$

where

$\{\phi\}_r$ is the $(n \times 1)$ modal vector corresponding to the measurement points,

$\{\hat{\phi}\}_r$ is the $(m \times 1)$ modal vector corresponding to the excitation points.

Employing matrix notation, equation (4.11) can be rewritten as

$$\{X(\omega)\} = [\Phi][S(\omega)]\left[\hat{\Phi}\right]^T \{F(\omega)\} \qquad (4.12)$$

where

$[S(\omega)]$ is an $(p \times p)$ diagonal matrix having the following terms on the diagonal:

$$s_r = \frac{1}{\omega_r^2 - \omega^2 + i2\zeta_r\omega_r\omega}$$

4.1.1 The Modal Coordinate Transformation Methodology:

The modal coordinate transformation method uses equation (4.12) to identify the input forces. This method comprises the following steps (Desanghere and Snoeys, 1985):

Step 1: Computation of the modal responses.

Successive integration of the measured acceleration signals to obtain the displacements. The displacements at the physical coordinates are transformed to the modal coordinates by multiplying the displacements with the pseudo-inverse of the modal matrix.

$$\{P(\omega)\} = [\Phi]^+ \{X(\omega)\} \qquad (4.13)$$

where

$\{P(\omega)\}$ is a $(p \times 1)$ vector and denotes the Fourier Transform of the modal coordinates ($\{p\}$ refers to the modal coordinates as a function of time),

$[\Phi]^+$ denotes the pseudo-inverse of the $(n \times p)$ modal matrix, and
$\{X(\omega)\}$ is the $(n \times 1)$ physical response vector at the sensor locations.

Step 2: Computation of the modal forces.

$$\{F_m(\omega)\} = [S(\omega)]^{-1}\{P(\omega)\} \tag{4.14}$$

where
$\{F_m(\omega)\}$ is the $(p \times 1)$ modal force vector.

Step 3: Computation of the physical forces

$$\{\hat{F}(\omega)\} = [\Phi^T]^+\{F_m(\omega)\} \tag{4.15}$$

where
$\{F(\omega)\}$ is the $(m \times 1)$ input force vector, and
$[\Phi^T]^+$ indicates the pseudo-inverse of $[\Phi]^T$.

The least-squares estimation of the pseudo-inverse is used twice in the modal force identification. These pseudo-inverse matrices can be calculated using any of the methods previously described in Section 3.1.

The above procedure can be summarised in a single equation as:

$$\{\hat{F}(\omega)\} = [\Phi^T]^+[S(\omega)]^{-1}[\Phi]^+\{X(\omega)\} \tag{4.16}$$

4.1.2 Limitations Regarding the Modal Coordinate Transformation

Since the over-determined case is the most common in engineering problems, the same approach will be followed in force identification. This means that the pseudo-inverse is obtained by normal least-squares solutions while avoiding minimum norm solutions associated with the under-determined case. Consider the direct problem of equation (4.15) as

$$\{F_m(\omega)\} = [\Phi]^T\{F(\omega)\}$$

The number of responses, n, generally exceeds the number of modes, p, resulting in a rectangular modal matrix. Thus, solving the forces at the physical coordinates from knowledge of the modal forces, equation (4.16) is under-determined (i.e. more unknowns than data). If the number and positions of the forces are known *a priori*, the

rows of $[\Phi]$ which correspond to these forces are grouped into the $(m \times p)$ matrix $[\Theta]$, while eliminating the positions from the force vector, $\{F(\omega)\}$, at which forces will be constrained to act, making it an $(m \times 1)$ vector. In this case, the solution for $\{F(\omega)\}$ becomes over-determined (i.e. more data than unknowns).

Thus, to obtain a least-squares solution, it is required that $n \geq p \geq m$ be satisfied, i.e. the number of response measurements should exceed or be equal to the number of modes, which in turn should be greater than or equal to the number of forces estimated.

4.2 TWO DEGREE-OF-FREEDOM SYSTEM

In this section the modal coordinate transformation technique is implemented on a simple 2 DOF lumped-mass system. Once again the system's response and modal parameters will be subjected to perturbation in order to simulate experimental measurements. It will be shown that the modal coordinate transformation technique does not suffer from the ill-conditioning of the force estimates at the system's resonance due to the matrix inversion, as was encountered for the frequency response function technique.

There are primarily two sources of error present in the modal coordinate transformation technique. These are the noise encountered in the structure's response measurements and the modal parameter extraction. Errors in the modal parameters will propagate to the identified forces through the double pseudo-inverse of the modal matrix. Kim and Kim (1997) studied the error propagation and found that for a lightly damped structure, errors in the damping values induce fewer error in the force identification than errors in the natural frequencies. Errors in the modal vectors were considered to have the most adverse effect on force predictions. Desanghere and Snoeys (1985) considered the modal coordinate transformation technique rather insensitive to measurement and curve-fitting perturbations. They claim that the precision of the identified forces were almost constant over the frequency range covered by the modes included in the analysis, regardless of the system's resonances.

Consider the following lumped-mass system.

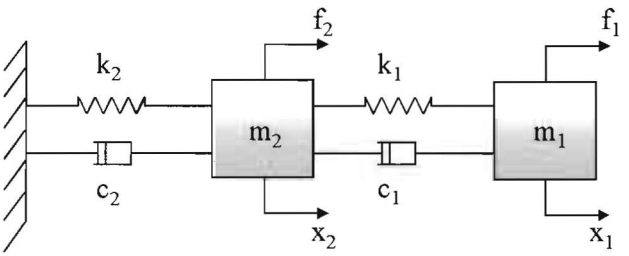

$m_1 = 0.5$ kg	$k_1 = 1.4212 \times 10^5$ N/m	$\zeta_1 = 0.001$
$m_2 = 1.0$ kg	$k_2 = 2k_1$ N/m	$\zeta_2 = 0.001$

Figure 4.1 - 2 DOF lumped-mass system

Once again, a harmonic forcing function is used to excite each of the masses.

$$f_1(t) = 150\cos(60\pi t) \qquad f_2(t) = 100\cos(60\pi t) \tag{4.17}$$

The response for each degree-of-freedom was solved analytically.
Perturbation of the natural frequencies, modal damping factors, mode-shapes and accelerations was conducted similar to that described in Section 3.2, for the frequency response function method. The same maximum error levels were used as before.

The contaminated modal parameters and responses were used to solve the forces.

Results and Discussion

This technique was successfully implemented to identify the two harmonic forces applied to the 2 DOF lumped-mass system.

It is evident from Figures 4.2, 4.3 and 4.4 that the modal coordinate transformation technique does not suffer from the ill-conditioning of the force estimates at the system's resonance due to the inversion of the modal matrix. Figure 4.2 shows the force magnitudes as a function of the frequency.

Although it is general practice to take acceleration measurements, the formulation of the modal coordinate transformation method, as expressed by equation (4.16), uses displacements. The successive integration of the accelerations to displacements will amplify the errors in the low frequency range. This type of behaviour is evident in Figures 4.3 and 4.4 where the small numerical errors from the perturbation and the DFT are amplified prior to the excitation frequency.

The Moore-Penrose pseudo-inverse method was used to determine the pseudo-inverse of the modal matrix, since the columns of the modal matrix represent the individual mode-shapes and are orthogonal with respect to each other.

The FEN is depicted in Figure 4.5. The FEN is initially high in the low-frequency range, for the above-mentioned explanation, but decreases rapidly as it approaches the excitation frequency. At the excitation frequency the force estimates are in good agreement with the applied forces and the FEN reaches a minimum value. From here onward the FEN increases steadily, as the force estimates deviate from the applied forces.

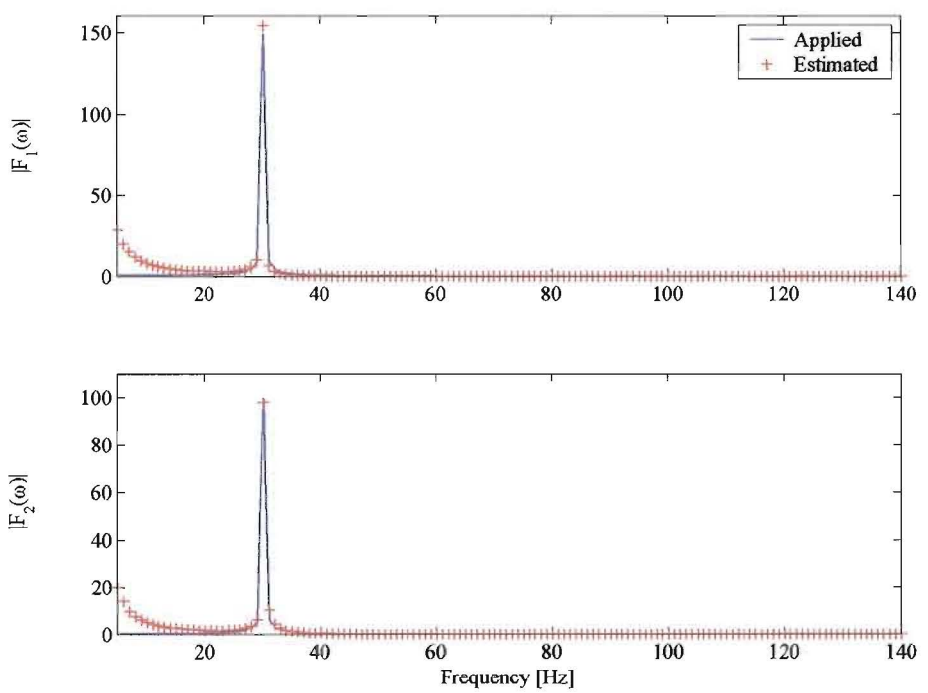

Figure 4.2 – Applied and estimated force magnitudes for the 2 DOF lumped-mass system in the frequency domain

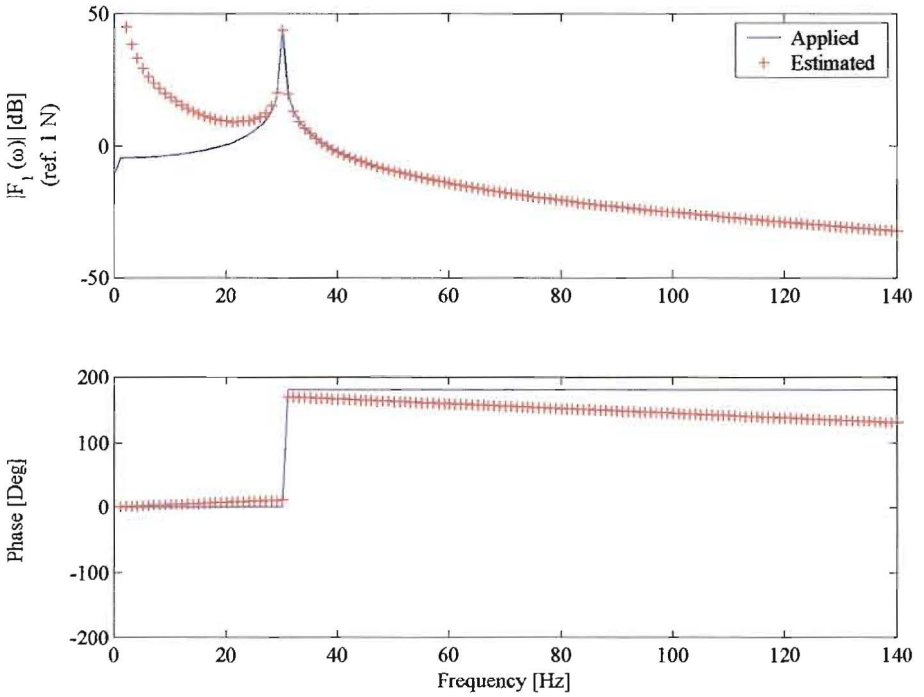

Figure 4.3 – Applied and estimated force no.1 for the 2 DOF lumped-mass system in the frequency domain

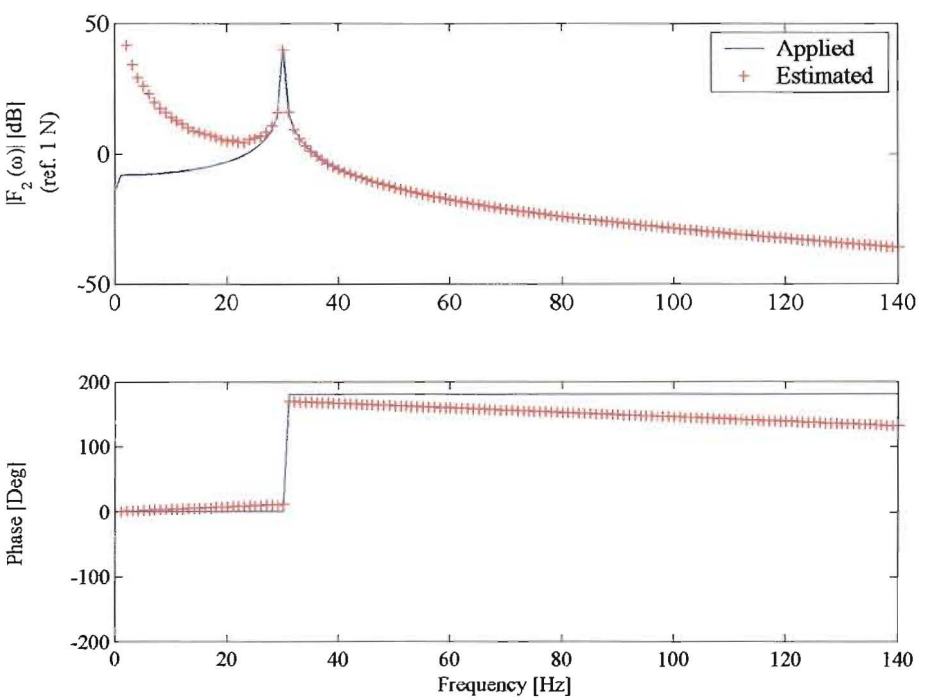

Figure 4.4 – Applied and estimated force no.2 for the 2 DOF lumped-mass system in the frequency domain

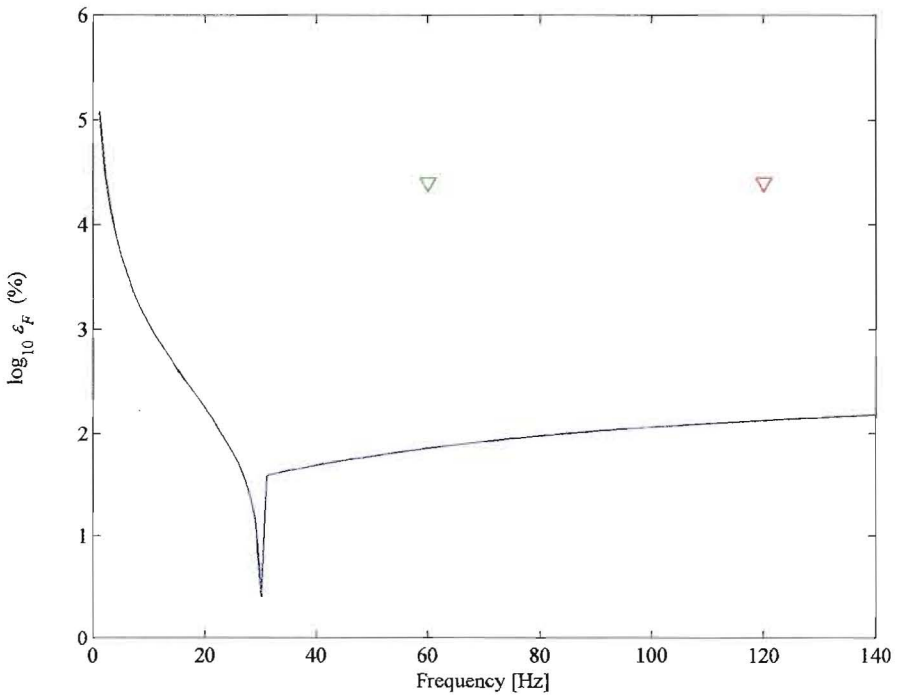

Figure 4.5 – Force Error Norm (FEN) of the estimated forces,
∇ indicates the 2 DOF systems' resonant frequencies

In view of the above numerical simulation we would like to comment on some of the advantages and disadvantages regarding the use of the modal coordinate transformation technique in general.

Advantages of Modal Coordinate Transformation

This technique requires that the pseudo-inverse be calculated only twice, regardless of the number of discrete frequencies included in the analysis. This reduces the computational time required to analyse large systems (Kim and Kim, 1997).

The points on a structure where the actual forces are applied may be inaccessible. Another point can then be artificially excited to extract the modal parameters while measuring the responses at the actual input locations. The force estimates at the inaccessible points can then be determined based on the reciprocity theorem (Kim and Kim, 1997).

Disadvantages of Modal Coordinate Transformation

The modal coordinate transformation technique requires a good set of modal parameters. This may prove hard to obtain for a complex structure.

Another disadvantage is that the estimated forces are limited to the frequency range based on the modes selected for the modal transformation (Shih *et al.*, 1989).

4.3 SIGNIFICANCE OF THE CONDITION NUMBER

As mentioned earlier, the definition of the condition number for a rectangular matrix can be stated as:

$$\kappa_2 = \frac{\sigma_{\max}([A])}{\sigma_{\min}([A])} \tag{4.18}$$

where

$\sigma([A])$ is the singular value of the matrix $[A]$.

From equations (4.13) and (4.15) it is apparent that the modal coordinate transformation method only requires the pseudo-inverse of the modal matrix, $[\Phi]$ and $[\Phi]^T$. The condition number of this technique will, thus be bounded by the product of the condition number of the individual pseudo-inverses.

$$\kappa_{modal} = \kappa_2([\Phi^T]) \cdot \kappa_2([\Phi]) \tag{4.19}$$

A large condition number will indicate an ill-conditioned system, i.e. a system that is prone to significant errors in the force estimates when inverted. The source of this ill-conditioning lies in the pseudo-inverse of $[\Phi]$ and $[\Phi]^T$. It is also important to note from equation (4.19), that the condition number remains constant for the entire frequency range of interest.

Hansen and Starkey (1990) extended the work of Starkey and Merrill (1989) by considering the condition of the modal coordinate transformation technique. They established a criterion for which some types of systems are ill-conditioned while others are not. Based on the fact that there is a close relationship between the singular values of a matrix $[A]$ and the eigenvalues of $([A]^T[A])$, they concluded that the condition number of the pseudo-inverse will be a function of the set of sensor locations, as well as of which modes are included.

The same FEM, as described in detail in Section 3.3, was used to investigate the factors that contribute to the condition number of the modal coordinate transformation technique.

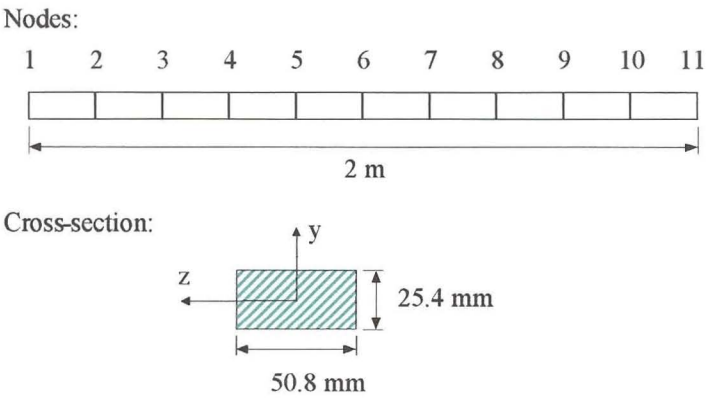

Figure 4.6 - FEM of free-free beam and response locations

4.3.1 Effect of the Response Selection

Firstly, we investigated how the different combinations of response locations influenced the condition number of the modal matrix. Three sets of response measurements were chosen, each consisting of four response locations. The first five bending modes were included in the analysis, while disregarding the rigid body modes. From the results in Table 4.1 we can conclude that the choice of response locations included in the modal matrix, can greatly affect the condition of the pseudo-inverse and subsequently influence the force predictions.

Table 4.1 – Effect of different response sets on the condition number

Sets of response points	Condition Number
(8, 5, 6, 11)	3.05
(1, 7, 4, 10)	18.88
(1, 2, 3, 4)	23.00

For a real-world structure involving a large number of sensors, selecting the appropriate response set that corresponds to the lowest condition number, from all possible sensor locations may prove to be a formidable task. In order to choose r sensor locations out of a possible n, we would need to evaluate

$$\frac{n!}{r!(n-r)!} \tag{4.20}$$

combinations in search for the optimal modal matrix. Therefore, to choose 4 sensor locations out of a possible 11 for the above FEM example, 330 combinations must be evaluated, which is not practical.

Kammer (1990) introduced the effective independent algorithm that measures how each sensor location contributes to the rank of the modal matrix. Shelley *et al.* (1991) found this algorithm to be both effective and computationally efficient in selecting sensor locations in the application of modal filters.

Kammer's algorithm is supported in the *Structural Dynamics Toolbox*®(Balmès, 1997) and is accessed using the `fe_sens` function. This function sorts the selected sensor locations contained in the vector `sdof`, from most too least important. Applying this function to the FEM the following result was obtained:

```
sdof=[8; 5; 6; 11; 1; 7; 4; 10; 2; 3; 9]
```

The first four digits in `sdof` correspond to the first response set in Table 4.1. It can be seen that this response set produced the lowest condition for the particular choice of modes. Important to note is that Krammer's algorithm is dependent on the modes included in the analysis. Reducing the number of modes to include only the first four bending modes will result in a different set of sensor locations, as shown below:

```
sdof=[11; 7; 5; 1; 6; 4; 9; 3; 8; 2; 10]
```

Similar to the frequency response function technique, the inclusion of more response measurements will reduce the condition number of the modal matrix.

4.3.2 The Effect of the Number of Modes

The effect of the number of modes included in the modal matrix was considered next. The same combinations of response measurements were considered as before, but with different ranges of modes included. Table 4.2 shows the condition number for each of these cases.

Table 4.2 – Effect of different modes on the condition number

Response points	Modes 1-5	Modes 2-5	Modes 1-4	Modes 2-4
(8, 5, 6, 11)	3.05	4.85	22.37	3.49
(1, 7, 4, 10)	18.88	20.37	20.09	17.12
(1, 2, 3, 4)	23.00	46.79	98.12	14.49

The result shows that the modes included or excluded from the modal matrix can influence the condition number significantly. In general the condition number is smaller when more modes are included, than when fewer modes are used.

These results confirm Hansen's findings.

4.3.3 Conclusion

The modal coordinate transformation technique is generally well-conditioned, as long as a convenient set of sensor locations is chosen. Care should be taken during the selection of the response measurements and number of modes included to ensure the lowest possible condition number for the calculation of the pseudo-inverse.

4.4 MODAL FILTERS

4.4.1 Preamble

This section describes applying modal filters to the force identification process. First, modal filters are described and discussed. The modal filter is then applied to the modal coordinate transformation technique, which is validated by a numerical simulation.

The modal filter was originally introduced to deal with the spillover problem in the control of distributed-parameter systems (Meirovitch and Baruh., 1983), but has recently been extended to include other applications in vibration analysis. These include active vibration control (Meirovitch and Baruh, 1985), correlation between analytical and experimental models, vibration force identification (Zhang *et al.*, 1990) and on-line parameter estimation (Shelley *et al.*, 1992).

A modal filter works on the basis that it transforms the physical response coordinates to the modal coordinates and may be performed in either the time or frequency domain. For instance, by multiplying the measured response vector, $\{x\}$, by the modal filter matrix, $[\psi]^T$, the physical response vector is uncoupled into a vector of the single-degree-of-freedom modal coordinates responses, $\{p\}$.

$$\{p\}=[\psi]^T\{x\} \tag{4.21}$$

The first step in the force identification by means of the modal coordinate transformation method requires the computation of the modal responses. This is done by multiplying the measured displacement vector with the pseudo-inverse of the modal matrix.

$$\{P(\omega)\} = [\Phi]^{+} \{X(\omega)\} \tag{4.22}$$

In equation (4.22) the pseudo-inverse of the modal matrix performs in essence the role of the modal filter as described in equation (4.21). A problem with this approach is that complete and accurate estimations of all the modal vectors in the frequency range of interest are required. Furthermore, it is assumed that for an undamped or proportionally damped system the modal vectors are orthogonal with respect to the physical mass matrix, which is analytically imposed but may be violated during the parameter extraction process. If a particular modal vector contains errors this will propagate to all of the modal vectors through calculation of the pseudo-inverse.

The Reciprocal Modal Vector (RMV) can be employed as an alternative method for calculating the modal filter of a system. The reciprocal modal vectors are defined to be orthogonal to the modal vectors and are calculated from measured frequency response functions and modal parameters. The modal filter estimate for a given mode is not affected by errors associated with other modes.

4.4.2 Formulation

A brief description of the formulation of the reciprocal modal vector method follow (Zhang *et al.*, 1990). Specific details regarding the derivation of RMV and other modal filters can be found in Zhang *et al.* (1989); Shelley and Allemang (1992) and He and Imregun (1995).

The frequency response function was previously derived in terms of modal parameters as

$$\{X(\omega)\} = \sum_{r=1}^{N} \frac{\{\phi\}_r \{\hat{\phi}\}_r^T}{\omega_r^2 - \omega^2 + i2\zeta_r \omega_r \omega} \{F(\omega)\} \tag{4.23}$$

In the above equation the orthogonality criterion of the modal vectors is used to perform the transformation from the physical to the modal coordinates. Thus, for mass-normalised modal vectors it follows that

$$\{\phi\}_i^T [M] \{\phi\}_j = \delta_{ij} \tag{4.24}$$

where

δ_{ij} is the Kronecker delta function, and δ_{ij} is equal to zero for $i \neq j$ and is equal to 1 for $i = j$.

Since the physical mass matrix is usually not available in practice, this orthogonality criterion can be restated as:

$$\{\psi\}_i^T \{\phi\}_j = \delta_{ij} \tag{4.25}$$

where

$\{\psi\}_i^T$ is the reciprocal modal vector, corresponding to mode i.

The reciprocal modal vector is defined as the product of the transposed modal vector and the mass matrix:

$$\{\psi\}_i^T \equiv \{\phi\}_i^T [M] \tag{4.26}$$

Zhang *et al.* (1990) constructed the reciprocal modal vector of a particular mode, using mode vectors, eigenvalues and frequency response functions. If the p-th column of the frequency response function matrix may be expressed as

$$\{H_p(\omega)\} = \sum_{r=1}^{N} \left[\frac{\{\phi\}_r \phi_{pr} Q_r}{(i\omega - \lambda_r)} + \frac{\{\phi\}_r^* \phi_{pr}^* Q_r^*}{(i\omega - \lambda_r^*)} \right] \tag{4.27}$$

where

λ_r and $\{\phi\}_r$ are the r-th complex eigenvalue and the associated modal vector,

Q_r is the modal scaling factor, and

$*$ denotes the complex conjugate.

Premultiplying the reciprocal modal vector and rearranging the expression Zhang produced the following results:

$$\left\{ \{H_p(\omega)\} - \frac{\{\phi\}_r^* \phi_{pr}^* Q_r^*}{(i\omega - \lambda_r^*)} \right\}^T \{\psi\}_r = \frac{\phi_{pr} Q_r}{(i\omega - \lambda_r)} \tag{4.28}$$

Equation (4.28) may be evaluated at a sufficient number of discrete frequencies to form an over-determined problem, which may be solved for $\{\psi\}_r$ in a least-squares manner. The resulting reciprocal modal vector will be orthogonal to the modal vectors within this frequency range.

The minimum number of sensors required to calculate the modal filter should be equal to or greater than the number of modes in the frequency range of interest.

The modal filter calculated from use of the reciprocal modal vector will replace the pseudo-inverse of the modal vector in the first step of the force identification process.

4.4.3 Seven Degree-of-Freedom System

A numerical simulation involving a seven DOF system, with non-proportional damping, is employed to illustrate the effectiveness of the proposed method. Although the formulation of the modal coordinate transformation method was developed based on the hypothesis of proportional damping, this simulation shows that for lightly damped structures the non-proportional damping model does not lead to significant errors in the force estimates.

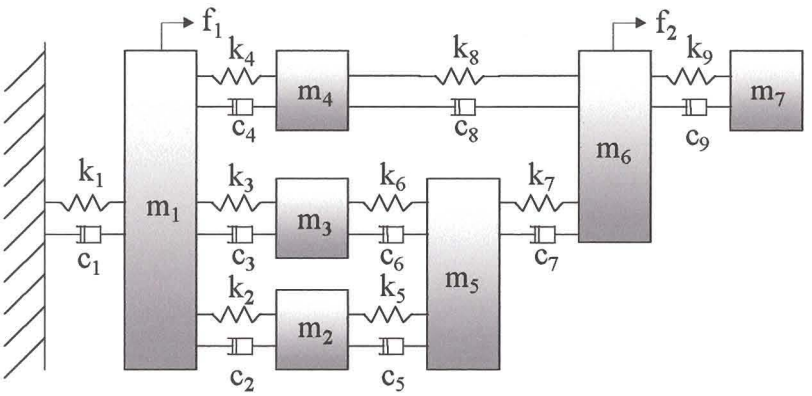

Figure 4.7 - 7 DOF lumped-mass system

Table 4.3 Properties of the 7 DOF lumped-mass system

Mass [kg]	Stiffness [N/m]	Modal damping factors	Natural frequencies [Hz]
m_1=3.0	k_1=5.0 x 10^6	2.5 x 10^{-3}	68.02
m_2=2.0	k_2=2.0 x 10^6	1.0 x 10^{-3}	135.56
m_3=1.0	k_3=1.0 x 10^6	3.0 x 10^{-3}	173.55
m_4=2.0	k_4=2.0 x 10^6	2.0 x 10^{-3}	212.86
m_5=1.5	k_5=1.0 x 10^6	0.0 x 10^{-3}	250.10
m_6=2.0	k_6=1.5 x 10^6	5.0 x 10^{-3}	316.76
m_7=1.0	k_7=2.0 x 10^6	1.0 x 10^{-3}	335.16
-	k_8=2.0 x 10^6	-	-

The system's natural frequencies and corresponding modal vectors were determined. The modal vectors were contaminated with uniformly distributed random errors with a maximum error level of 10 %, to simulate experimentally obtained data. This was done in accordance with the error model described in Section 3.2. These contaminated modal vectors will then be used to calculate the modal filter and the force estimates by means of the modal coordinate transformation method.

The modal filter was calculated as follows:

Columns 2 and 6 of the frequency response function matrix were constructed at 15 discrete frequencies, distributed equally throughout the frequency range and depicted as circles in Figure 4.8. These values, as well as the modal parameters of the mode of interest, were substituted into equation (4.28), from which the reciprocal modal vector was solved. This procedure was repeated for all seven modes. Each reciprocal modal vector represented a column of the modal filter matrix.

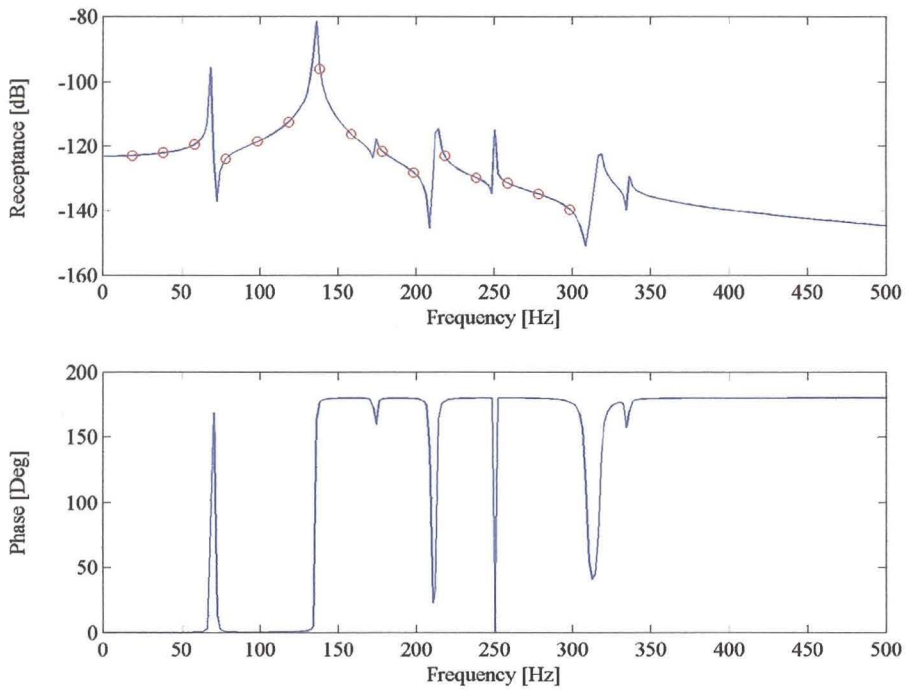

Figure 4.8– Receptance, $\alpha_{12}(\omega)$ and discrete frequency points used in modal filter construction

The validity of the modal filter can be checked based on the orthogonality criterion stated in equation (4.25). This equation can be rewritten in matrix notation as:

$$[\Phi]^T[\psi]=[I] \tag{4.29}$$

Substituting the previously obtained modal filter and modal matrix into the above equation, the following matrix was obtained:

$$[\Phi]^T[\psi] = \begin{bmatrix} 0.999 & 0.0 & 0.0 & 0.0 & 0.0 & 0.0 & 0.0 \\ 0.0 & 0.994 & 0.0 & 0.0 & 0.0 & 0.0 & 0.0 \\ 0.0 & 0.0 & 0.977 & 0.001 & 0.0 & 0.0 & 0.0 \\ 0.0 & 0.003 & -0.004 & 0.989 & 0.0 & 0.0 & 0.0 \\ 0.0 & 0.001 & -0.002 & 0.003 & 1.0 & 0.0 & 0.0 \\ -0.003 & 0.0 & 0.004 & -0.002 & 0.0 & 0.988 & 0.0 \\ 0.005 & 0.003 & 0.0 & 0.003 & 0.0 & 0.004 & 1.0 \end{bmatrix}$$

This matrix differs from the expected identity matrix due to the contaminated modal vectors included in the calculation of the reciprocal modal vectors and the modal truncation errors caused by the limited frequency range. However, it can be seen that the dominant values are still situated on the diagonal and are very close to unity.

The seven DOF-system was subjected to two harmonic forces with the same excitation frequency, acting on masses 1 and 6, respectively. The modal coordinate transformation method was used to calculate the force estimates, with the exception that the reciprocal modal vector was used for the modal coordinate transformation, rather than the pseudo-inverse of the modal matrix.

As can be seen from Figures 4.9 and 4.10, the estimated forces correspond well with the actual forces.

To conclude:

The modal filter, calculated from use of the reciprocal modal vector, might replace the pseudo-inverse of the modal vector in the first step of the force identification process.

Since the reciprocal modal vector method only requires the frequency response function matrix and modal parameters for only the mode of interest, the modal filter estimate for a given mode is not affected by errors associated with other modes.

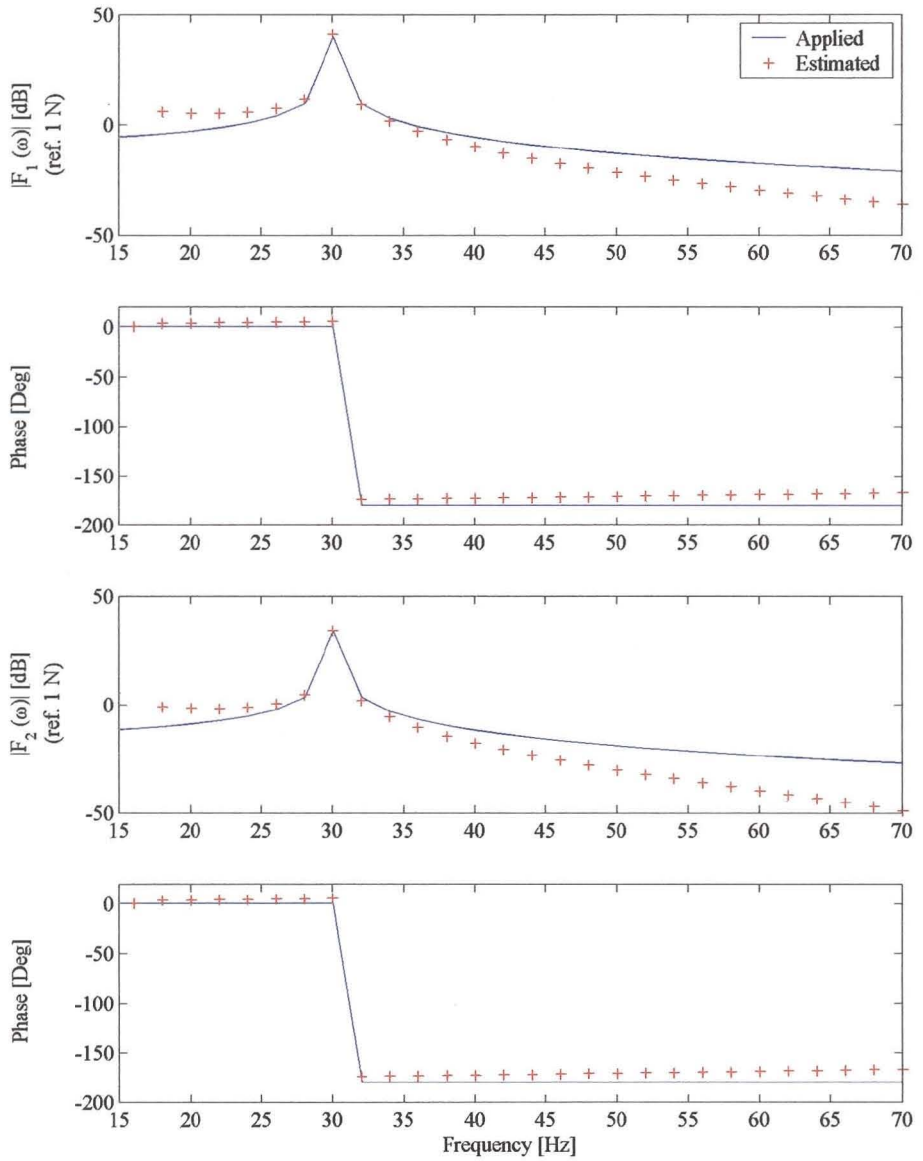

Figure 4.9 – Applied and estimated forces in the frequency domain

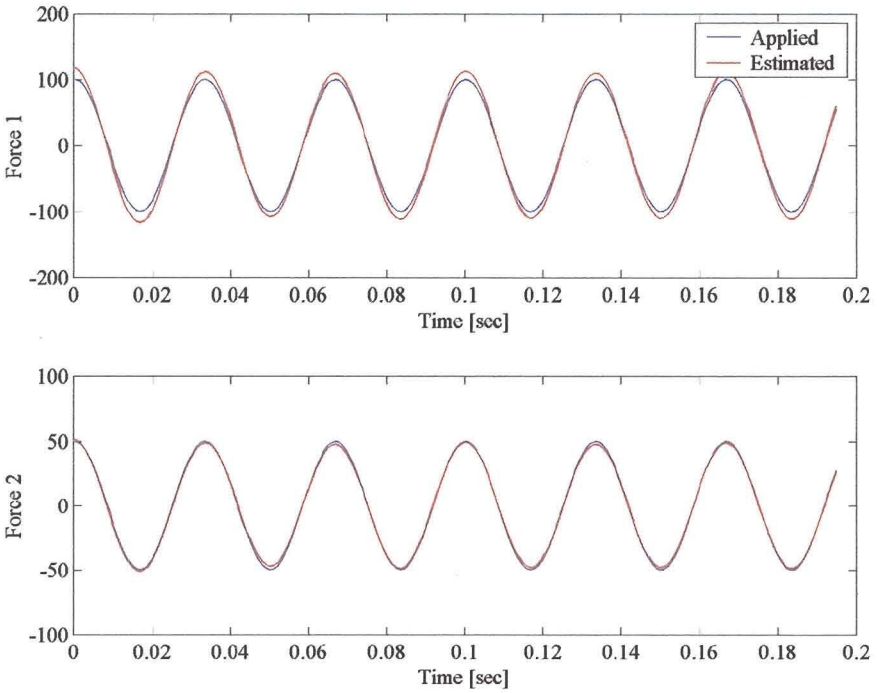

Figure 4.10 – Applied and estimated forces in the time domain

CHAPTER 5

Experimental Studies

"In many respects the practice of vibration testing is more of an art than a science."
Maia *et al.* (1997)

5. EXPERIMENTAL STUDIES

The majority of the effort will be devoted to the determination of harmonic forces, since all other forms of excitation, be they transient, periodic or random, may be represented as a Fourier series. The likelihood of being able to determine these forces will depend on the success obtained for the harmonic case. The first part of each section describes the experimental setup, which is followed by the issues relating to the measurement process and finally concludes with the results and conclusions drawn from the study.

5.1 SINGLE HARMONIC FORCE: FREE-FREE BEAM

This section presents the first attempt to apply the previously derived theory to determine a single harmonic force on a free-free beam.

5.1.1 Details of the Experimental Set-up

The test piece consisted of an aluminium beam with the same geometrical dimensions as the beam considered in the FEA. The beam was discretised with eleven equally spaced node points, each constituted a potential sensor location, as depicted in Figure 5.1.

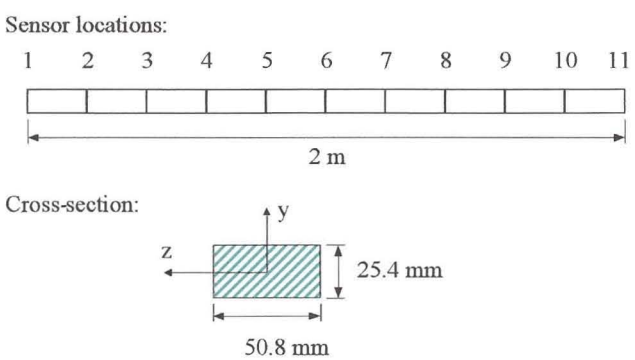

Figure 5.1 – Free-free aluminum beam and response locations

The beam was suspended on very soft elastic bands to approximate free-free boundary conditions. This type of suspension causes the theoretical 0 Hz Rigid Body Modes (RBM) to shift to slightly higher frequencies. Different lengths of elastic band and different points of attachment to the structure were considered to ensure that the suspension did not influence the beam's dynamic characteristics. The beam was excited in the y-direction through the use of an electromagnetic exciter/shaker. A stinger was used to connect the shaker to the force transducer that was mounted on the

beam. Piezoelectric accelerometers were attached at the sensor locations with beeswax.

The layout of the measurement system is shown in Figure 5.2, the core of which is the *DSPT ™ Siglab 24-40*. This piece of equipment performs the role of a signal generator, as well as a data acquisition and processing mechanism and can easily be controlled with a mini-computer. Details of the other components of the measurement system and their calibration can be found in Appendix A.

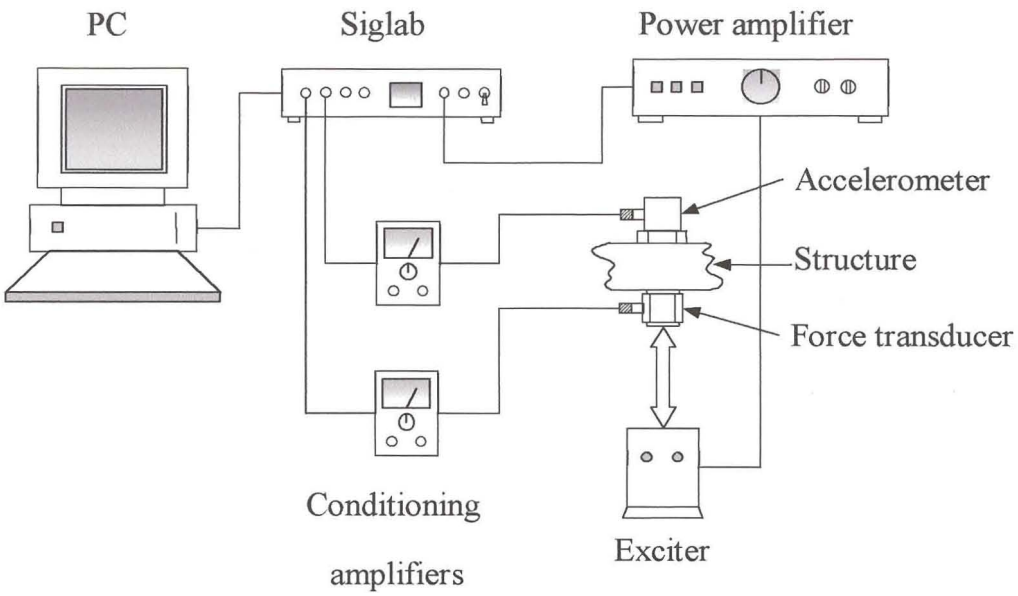

Figure 5.2 – Measurement system used for the identification of a single harmonic force

5.1.2 The Measurements

The test was conducted to cover the chosen range of frequencies from 0 Hz to 500 Hz, which included the first five bending modes. The excitation was applied at position 11, while measuring at 11 response locations with a single roving accelerometer. The excitation point was chosen since it is the only point that properly excites all the modes in the direction of excitation. The accelerometer was small enough so that its inertia loading on the beam was considered negligible.

Inertance frequency response functions were measured for each of the response locations. A lot of time was spent to ensure proper definition of the resonance peaks and anti-resonances. This resulted in changing the excitation point and considering different stinger configurations.

Another factor that influenced the quality of the resonance peaks was the excitation function used in determining the frequency response functions. At first a true random signal was used to excite the structure. The true random excitation violates the periodicity requirement of the FFT process, since neither the force nor the response is periodic within the measurement time. This results in an error known as 'leakage'. The effect of leakage can be reduced by applying a 'window' (typically a Hanning window), but not completely eliminated. The frequency response function is computed by dividing the output spectrum by the input spectrum, and since each spectrum is different, the effect of the convolution (see Section 2.1) does not divide or ratio out. Especially, the peak values in the frequency response function measurements will be influenced by leakage most heavily, and may appear blunt and poorly defined. Furthermore, the coherence function is not unity at the resonances and anti-resonances. Hence, the structure will appear to be more damped than what is actually the case. This is particularly true for lightly damped structures. (Olsen, 1984 and Avitabile, 1999)

In view of the above-mentioned difficulties associated with the true random signal, the chirp-sine function, or swept sine burst, was used instead. This signal satisfies the periodicity requirement and will not experience the 'leakage' phenomenon. The peaks on the frequency response function were much sharper and better defined. There was also an improvement in the coherence function.

The frequency response function is, by definition, the Fourier transform of the system's response divided by the Fourier Transform of the applied force. This relation is only valid if the system is assumed to behave linearly. A linear system will also obey Maxwell's reciprocity theorem, which will yield symmetric mass, stiffness, damping and frequency response function matrices. Since the frequency response function matrix is symmetric, it is theoretically at least possible to determine the entire matrix by simply considering one column (or row) of the frequency response function. To check the reliability of the frequency response function measurements, a second column of the inertance matrix was measured by exciting position seven. Figure 5.3 illustrates the reciprocity check for the beam structure and confirms that the beam behaves linearly.

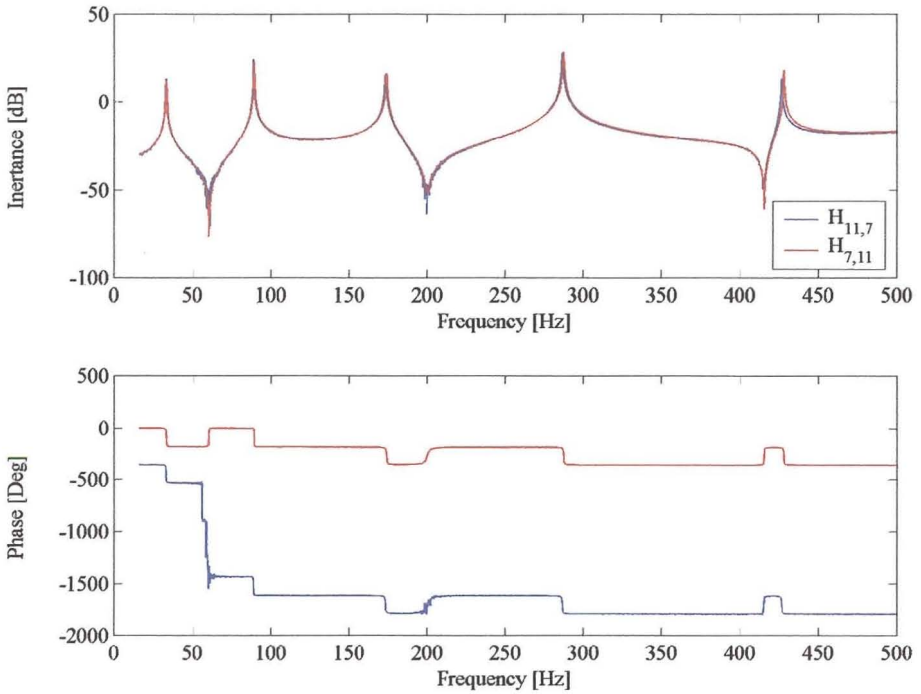

Figure 5.3 – Reciprocity check of frequency response functions for the aluminium beam

The point inertance of the measured frequency response function is presented in Figure 5.4 (the entire set being represented in Appendix B) and exhibits the expected anti-resonance after each resonance.

The beam was then excited with a harmonic forcing function of a 100 Hz. The applied force was measured directly with the force transducer for comparison with the force predictions. The Auto Spectral Densities (ASD) of the acceleration signals corresponding to each sensor location were also measured taking 30 frequency domain averages.

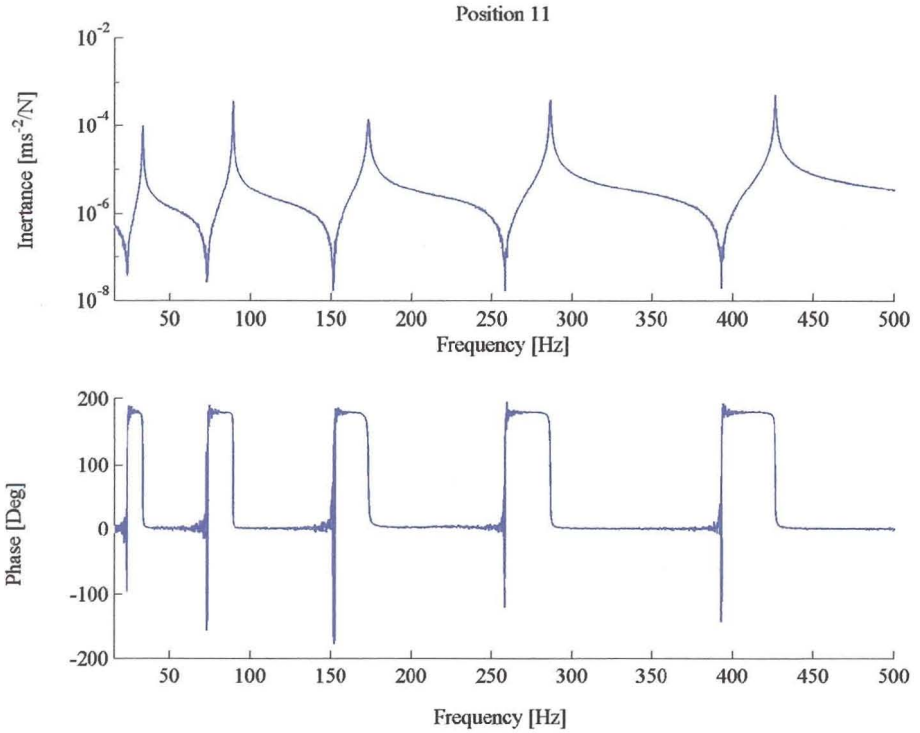

Figure 5.4 – Measured point inertance (position 11) for the free-free beam.

5.1.3 Force Determination Results

a) Frequency Response Function Method

From the measured frequency response functions it is evident that the noise is particularly acute at the anti-resonances. In these regions the response signal tends to become very small and is susceptible to pollution and noise. It was decided to 'smooth' the frequency response functions by performing the experimental modal analysis given in Section 2.3. The RBM were excluded from the analysis, since they were not properly excited and were below the frequency range of the accelerometer and exciter used in the analysis. The point inertance of the measured frequency response function data and the reconstructed normal mode model (residual terms included) are presented in Figure 5.5 (the entire set and modal parameters being represented in Appendix B).

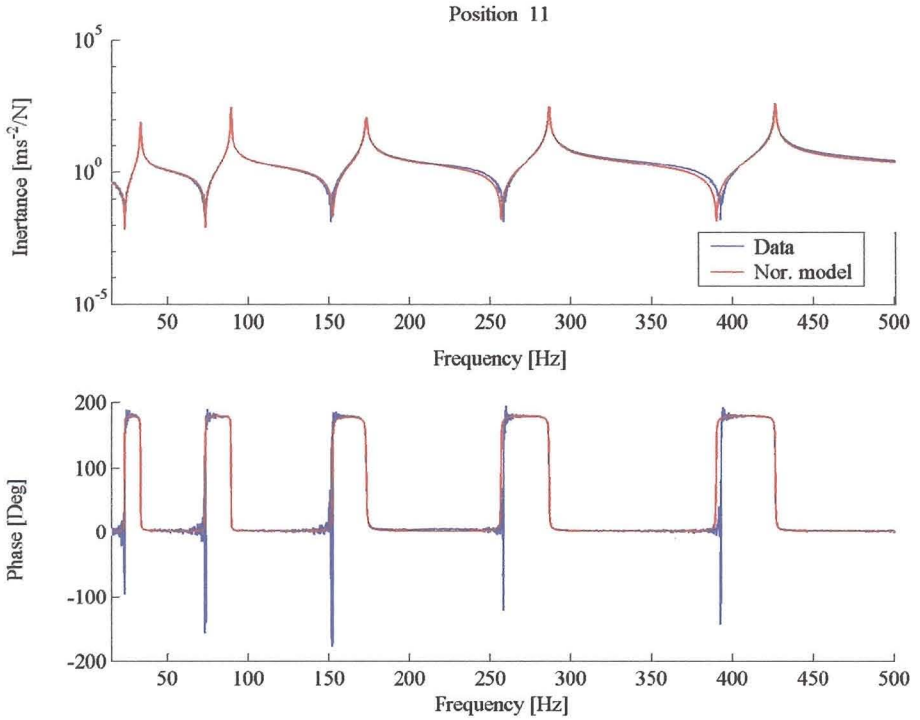

Figure 5.5 – Measured and reconstructed point inertance (position 11) for the free-free beam.

Having measured the frequency response function matrix and the accelerations due to the applied force, the force could be determined from

$$\{\hat{F}(\omega)\} = [A(\omega)]^{+}\{\ddot{X}(\omega)\} \tag{5.1}$$

Only four sensor locations were included in the calculations, these being positions 6, 8, 9 and 11. SVD was used to calculate the pseudo-inverse of the reconstructed frequency response function matrix. The force estimates are shown in Figure 5.6 where they may be compared with the directly measured force. Since we only measured the ASD of the force and responses the terms in equation 5.1 are real, and as a result there is no phase information available.

It is obvious from the results (Figure 5.6) that the frequency response function method accurately identified the single harmonic force acting on the free-free beam, with a FEN of only 0.141 per cent at the excitation frequency.

Increasing the number of response measurements is likely to improve the quality of the force estimate by averaging the errors.

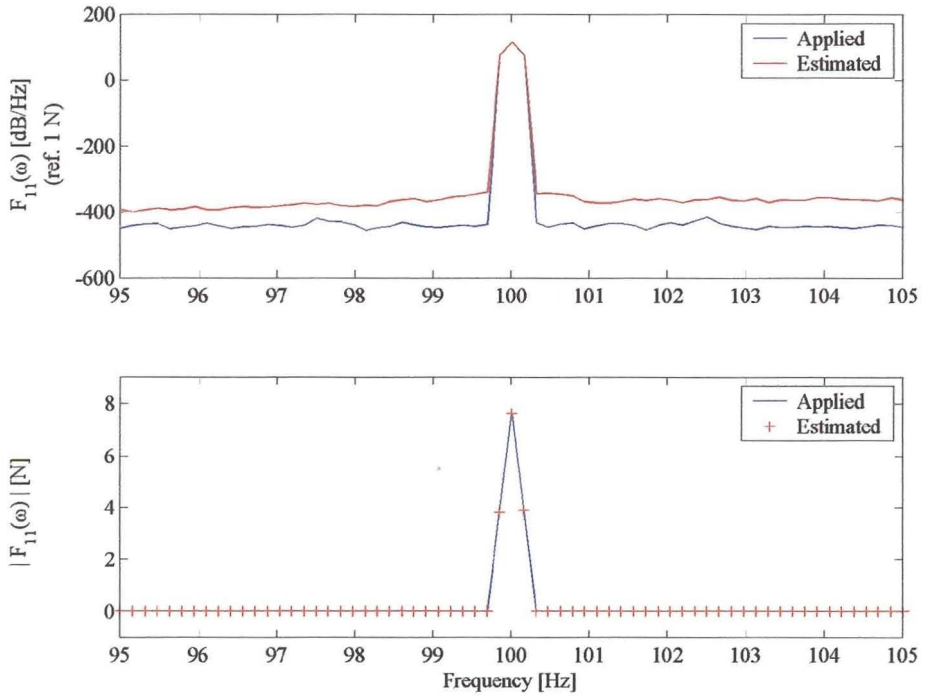

Figure 5.6 – Comparison of the measured and estimated force for free-free beam corresponding to position 11

b) Modal Coordinate Transformation Method

The single harmonic force was calculated from equation (4.16), i.e.

$$\{\hat{F}(\omega)\} = [\Phi^T]^+ [S(\omega)]^{-1} [\Phi]^+ \{X(\omega)\} \tag{5.2}$$

All five modes in the range of frequencies were included in the analysis. This method failed to predict the correct force amplitudes. The source of error may be attributed to poor modal identification, which can be explained as follows:

The formulation of the two frequency domain methods, considered in this work, is essentially the same. Both use the frequency response function to express the relation between the applied force(s) and the associated response. The only difference being the calculation of the pseudo-inverse. In the case of the frequency response function method the pseudo-inverse of the whole frequency response matrix is calculated, while the modal coordinate transformation method considers only the pseudo-inverse of the modal matrix. Thus, while the former allows the incorporation of the residual terms corresponding to the truncated modes, there is no manner in which one can account for these terms in the latter. Figure 5.7 illustrates this point. Here the normal mode model for the free-free beam, with and without the residual

terms, is compared to the originally measured frequency response function. It can be seen that the exclusion of the residual terms has a significant effect on the accuracy of the frequency response function, and subsequently on the success of the modal coordinate transformation method.

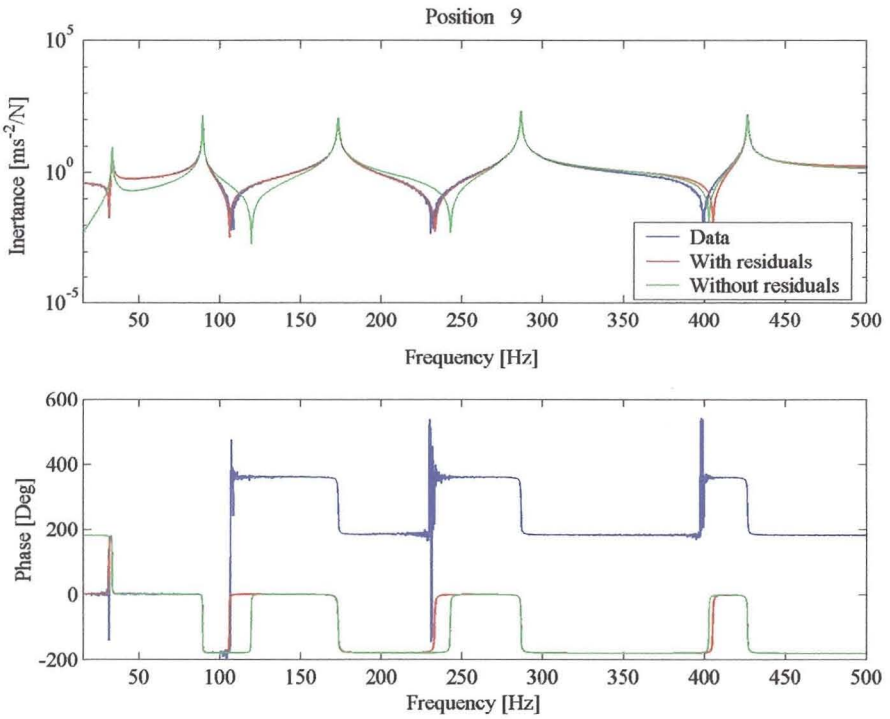

Figure 5.7 – Measured and reconstructed normal mode model of the frequency response function, $A_{9\ 11}(\omega)$ for free-free beam.

A numerical simulation of the free-free beam revealed that the low frequency contribution, i.e. the RBM, had the most adverse affect on the accuracy of the frequency response functions at the excitation frequency (100 Hz).

The implication this has is that the frequency range should consist of the entire modal space of the model. This means that the residual contributions from modes outside the analysis frequency range, which are not represented in the modal matrix, must be small. (Warwick and Gilheany, 1993). As a result one would need to include a larger frequency range in the experimental modal analysis, than the frequency range for which one would like to estimate the forces (Clark *et al.*, 1998).

It is important to note that the frequency response function matrix may either be reconstructed with the residual terms included, as was the situation in the former subsection, or without the residual terms. From here onwards the term -

reconstructed frequency response function - will refer to the case where residual terms are omitted.

5.2 SINGLE HARMONIC FORCE: HINGED-HINGED BEAM

The aim of this section is to ascertain a single harmonic force on a hinged-hinged beam.

5.2.1 Details of the Experimental Set-up

The aluminium beam was fixed at the ends to approximate a hinged-hinged beam (also referred to as a simply supported beam). In theory, at least, this type of constraint will only allow rotations at the supports, while restraining the beam from any translations. However, in practice, this constraint is much more difficult to implement, since the construction of the clamping often causes significant resonance frequency and mode shape differences. Figure 5.8 shows the construction of the supports.

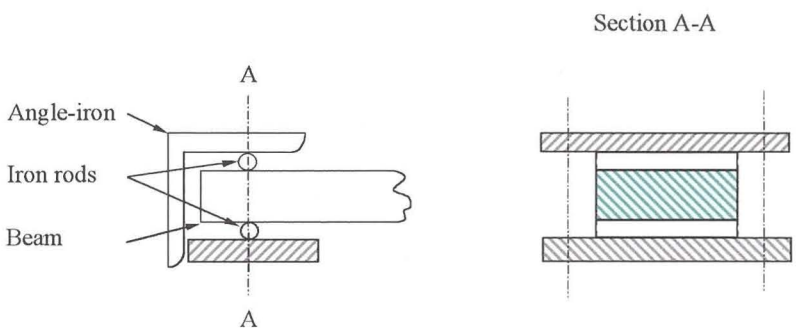

Figure 5.8 – Construction of the support for the hinged-hinged beam

The basic idea was to keep the contact area between the beam and the support as small as possible to allow the beam to rotate about a single point. In order to accomplish this the beam was fastened between two iron rods with a diameter of approximately 5 millimetres. An angle-iron section was placed on top and bolted to concrete-filled blocks.

Although it was the initial intention to approximate a hinged-hinged beam, the dynamic characteristics of the beam may be quite different from those of the theoretical boundary condition. However, no attempt was made to confirm that the imposed boundary conditions satisfied the requirements of that of a hinged-hinged beam. It was assumed that the test boundary conditions matched that of the operating boundary conditions of a specific beam in practice. Having said this, the boundary conditions will still be referred to as hinged-hinged.

The same sensor locations were retained as before, the only difference being the exclusion of positions 1 and 11 from the measurements, since the response of these points were considered to be zero. The sensor locations are depicted in Figure 5.9.

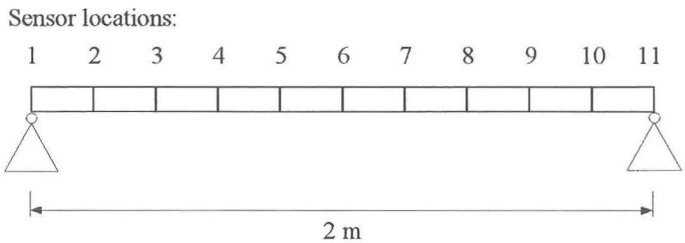

Figure 5.9 – Hinged-hinged aluminium beam and response locations

Since the beam was 'grounded' there are no RBMs contributing to the response of the beam.

The measurement system remained unchanged and was used for measuring frequency response functions, accelerations and force levels.

5.2.2 The Measurements

The test was conducted to cover the chosen range of frequencies from 0 Hz to 500 Hz, which included the first six bending modes. The excitation was applied at position 8, while measuring at nine response locations (sensor location 2 to 10) with two roving accelerometers. The accelerometers were small enough so that their inertia loading on the beam were considered as negligible.

Despite attempts to improve the quality of the frequency response functions through the use of a chirp-sine excitation, the author still experienced difficulties associated with the measured frequency response functions. Especially, when an experimental modal analysis had to be performed on the data to extract the necessary modal parameters the curve-fitting algorithm failed to produce satisfactory results. One of the likely reasons may be attributed to the fact that the beam can be considered as a lightly damped structure, which requires a very small frequency resolution to ensure proper definition of the resonance peaks. The *Structural Dynamics Toolbox*® (Balmès, 1997) identifies the maximum value of the frequency response function plot within a specified frequency band as the natural frequency of that particular mode. Once the natural frequency has been obtained a curve is fitted to the frequency response function plot, originating from the maximum value, to estimate the damping of the mode in question. Failing to properly excite or measure the resonance will result not only in the wrong natural frequency, but also over-estimate the damping values. This is especially acute where the boundary conditions interfere with the resonances. A

thin rubber strip was glued to the one side of the aluminium beam to increase the damping values. This modification definitely improved the definition of the resonance peaks – nicely curved and not spiky (Figure 5.10). Another advantage of the increased damping is the decrease in the condition number due to higher modal overlap, which may prove to be beneficial to the force identification process.

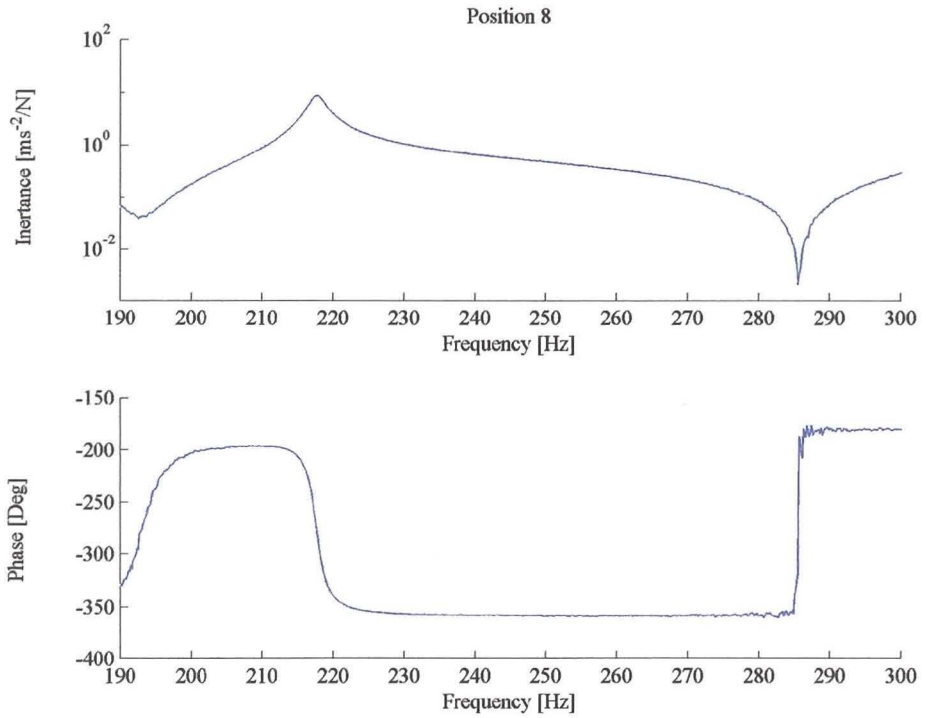

Figure 5.10 – Improvement in the resonance peaks of the point inertance (position 8) due to the attachment of a thin rubber strip.

Inertance frequency response functions were measured for each of the nine sensor locations. Figure 5.11 shows the measured point inertance for the hinged-hinged beam (the entire set being represented in Appendix C).

Successively, the beam was excited with a harmonic forcing function of a 250 Hz, while measuring 30 frequency domain averages of the applied force and acceleration signals.

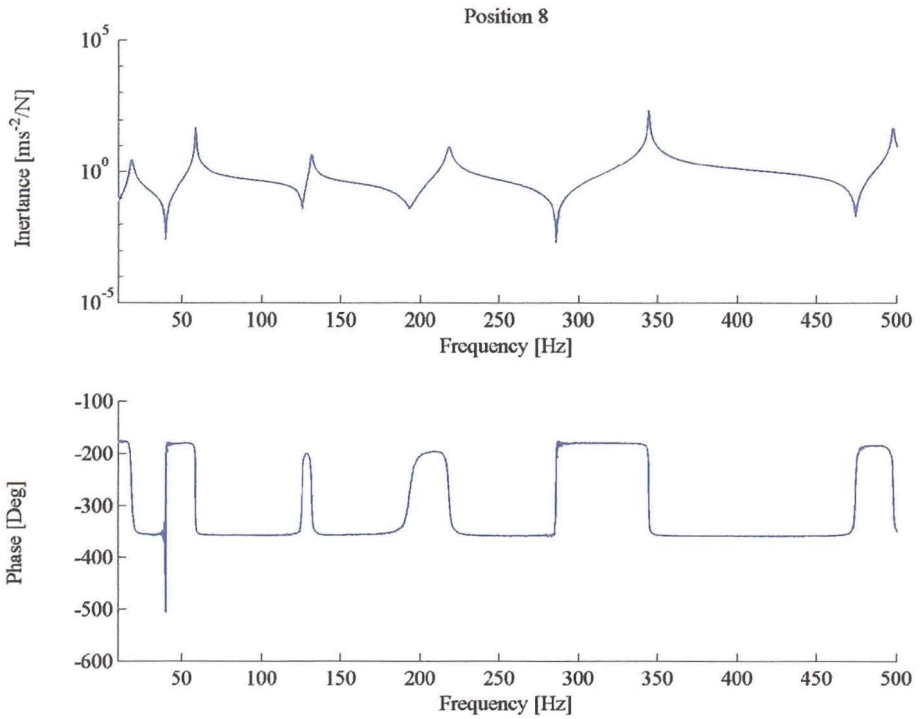

Figure 5.11 – Measured point inertance (position 8) for the hinged-hinged beam.

5.2.3 Force Determination Results

a) Frequency Response Function Method

The actual force may be reconstituted from

$$\{\hat{F}(\omega)\} = [A(\omega)]^{+}\{\ddot{X}(\omega)\} \tag{5.3}$$

by considering only four sensor locations (positions 7, 8, 9 and 10). Unlike the case for the free-free beam the 'raw' frequency response function measurements were used in the force identification process. This resulted in a FEN of 4.202 per cent at 250 Hz and the forces are compared in Figure 5.12.

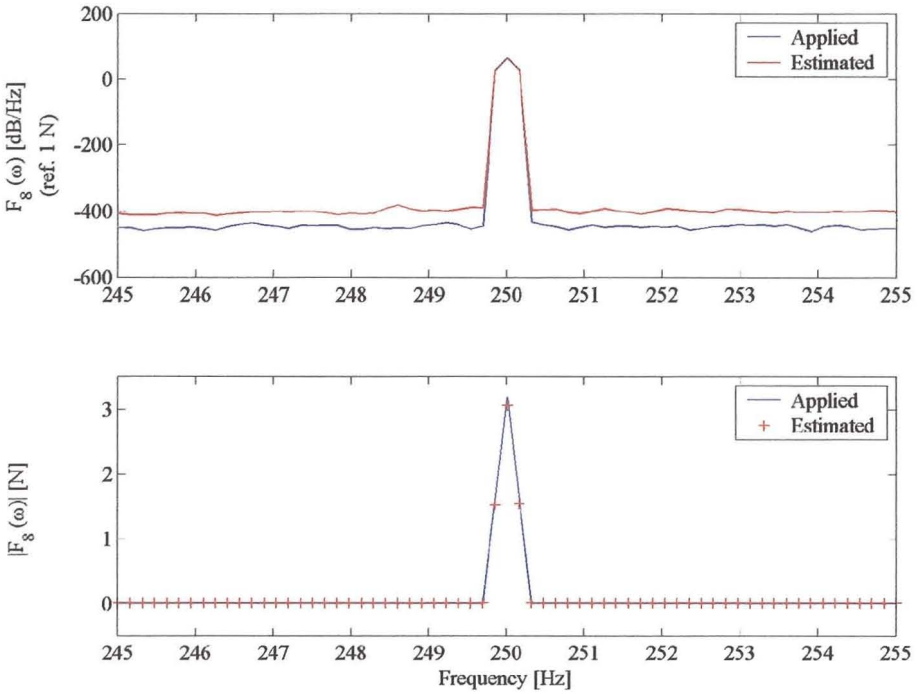

Figure 5.12 – Comparison of the measured and estimated forces for hinged-hinged beam

b) Modal Coordinate Transformation Method

The force estimates were obtained from using equation (5.2). Five modes were included in the analysis. Once again the reconstructed frequency response functions deviated noticeably from the measured values at the excitation frequency. Based on the explanation given in the previous section, in practice one would have no other choice than to increase the frequency range to include more modes, thereby ensuring that the residual contributions from the modes outside the frequency range are small enough. Instead, it was decided to alter the forcing frequency and only repeat the force and response measurements, rather than the laborious frequency response function matrix. The excitation frequency was reduced to a 100 Hz. Six sensor locations (positions 6, 10, 4, 2, 8 and 3) were necessary to obtain acceptable force estimates. These sensor locations were selected from all possible sensor locations with Krammer's effective independent algorithm (refer to Section 4.3.1) and are sorted from most to least important. The force results were presented in Figure 5.13. Interesting to note is that the actual and predicted forces have a much higher noise floor, as a result of a larger frequency resolution applied during the measurements.

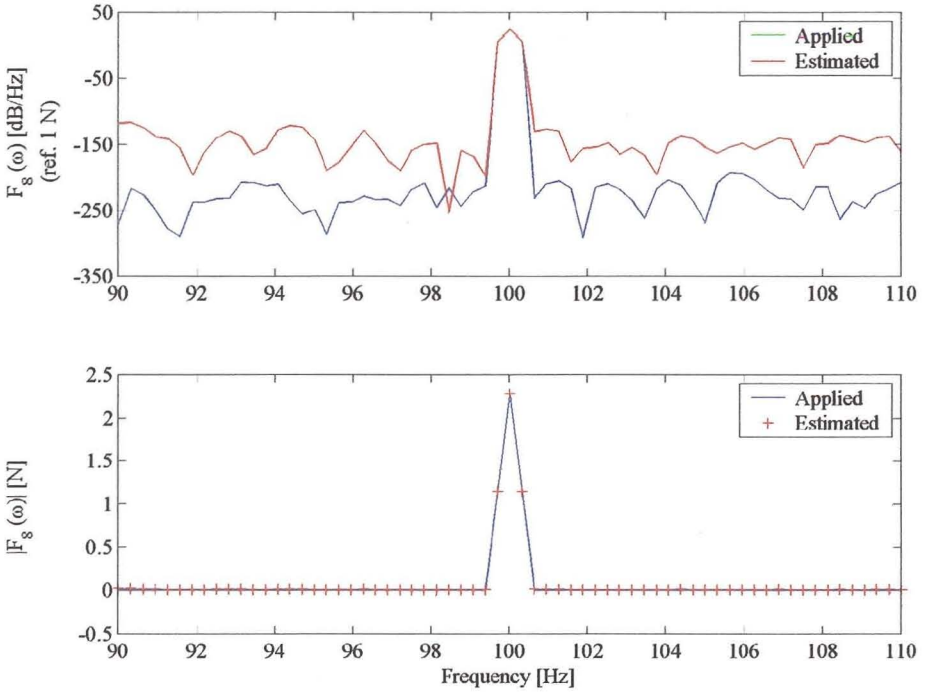

Figure 5.13 - Comparison of the measured and estimated forces for the hinged-hinged beam.

Application of the RMV, outlined in Section 4.4, produced similar results to the pseudo-inverse of the modal matrix, although the former required a lot more computational effort.

The FEN for each case is listed in Table 5.1.

Table 5.1 Force Error Norm of the estimated force

Modal matrix [%]	RMV [%]
5.014	5.048

5.3 TWO HARMONIC FORCES: FREE-FREE BEAM

The previous applications were limited to the estimation of a single harmonic force. In this section the free-free beam was invoked once again to investigate the extension of the force identification methods in the frequency domain to determine two harmonic forces acting on the beam.

5.3.1 Details of the Experimental Set-up

The components of the measurement system are essentially the same as before, but have been extended to cater for two exciters and are shown in Figure 5.14.

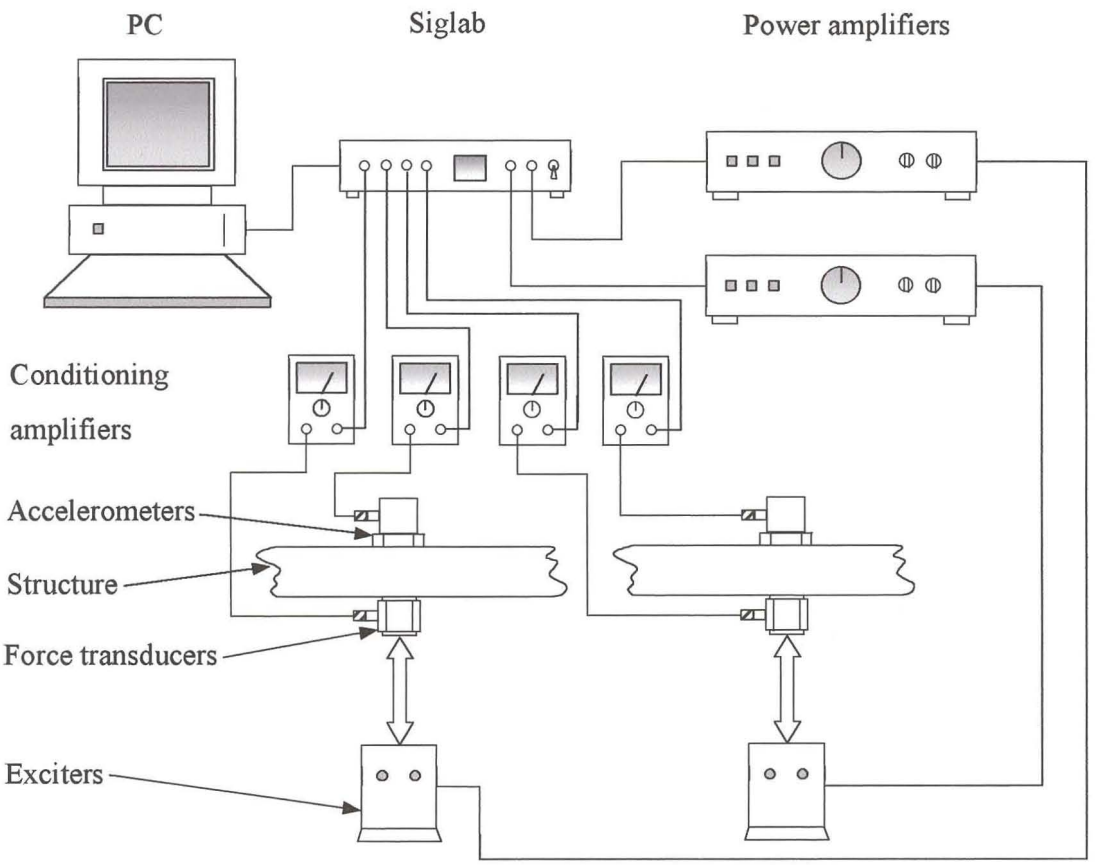

Figure 5.14 – Measurement system used for the identification of two harmonic forces

5.3.2 The Measurements

Eleven acceleration signals were recorded with two roving accelerometers. The two harmonic forces, with frequency content 380 Hz and 250 Hz, were applied to the free-free aluminium beam at two different positions (position 5 and 8 respectively), the inertance frequency response functions having already been determined with the MIMO excitation (refer to Section 2.4). As mentioned before, this was done to

account for the distortion of the natural frequencies of the beam due to the attachment of the two exciters. It can be seen from Figures 5.15 and 5.16 that the first five bending modes spanned the chosen frequency range from 0 Hz to 500 Hz.

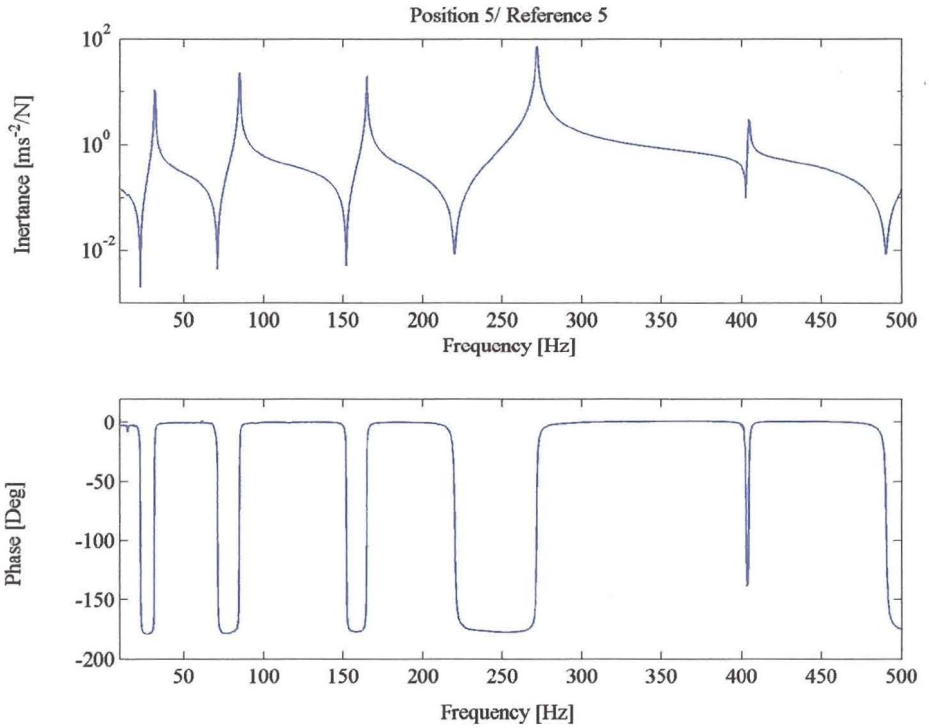

Figure 5.15 – Measured point inertance for the free-free beam corresponding to reference position 5

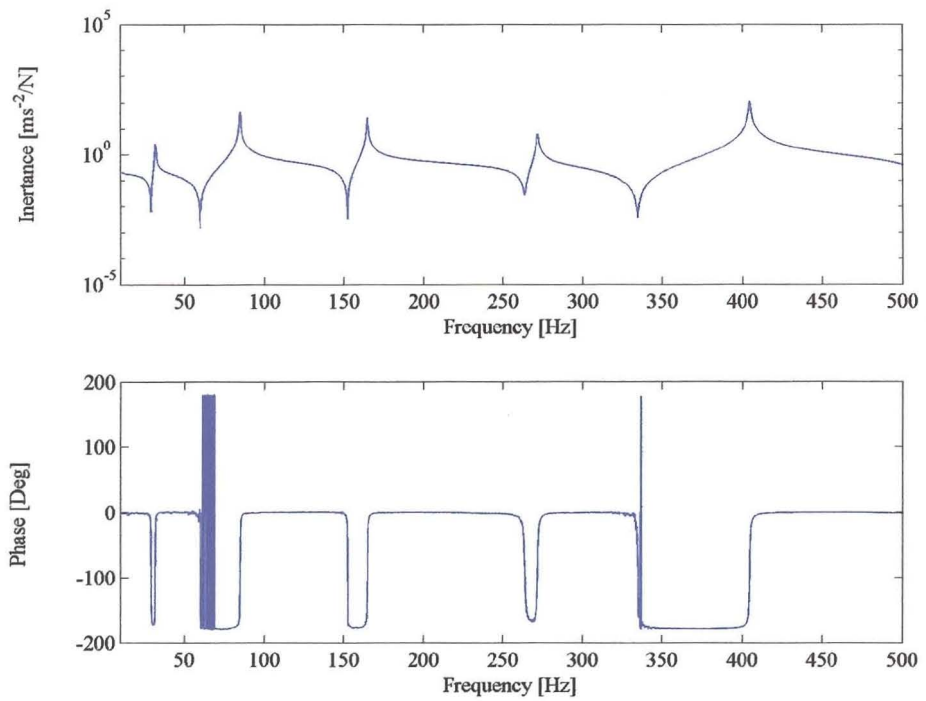

Figure 5.16 – Measured point inertance for the free-free beam corresponding to reference position 8

Figure 5.17 shows the ASD of the actual input forces as measured directly with the force transducers. In the figure, F_a denotes the force measured at position 8, while F_b is the force measured at position 5. Even though the drive signals to the shakers were completely uncorrelated, the measured force signals exhibited some correlation due to the interaction of the excitation system with the structure (Maia *et al.*, 1997). The correlation between the input forces was also evident in the Cross Spectral Densities (CSD) of the input forces, F_{ab}. The correlation components were significant in magnitude so that it was deemed advisable to include their contribution in the force identification process.

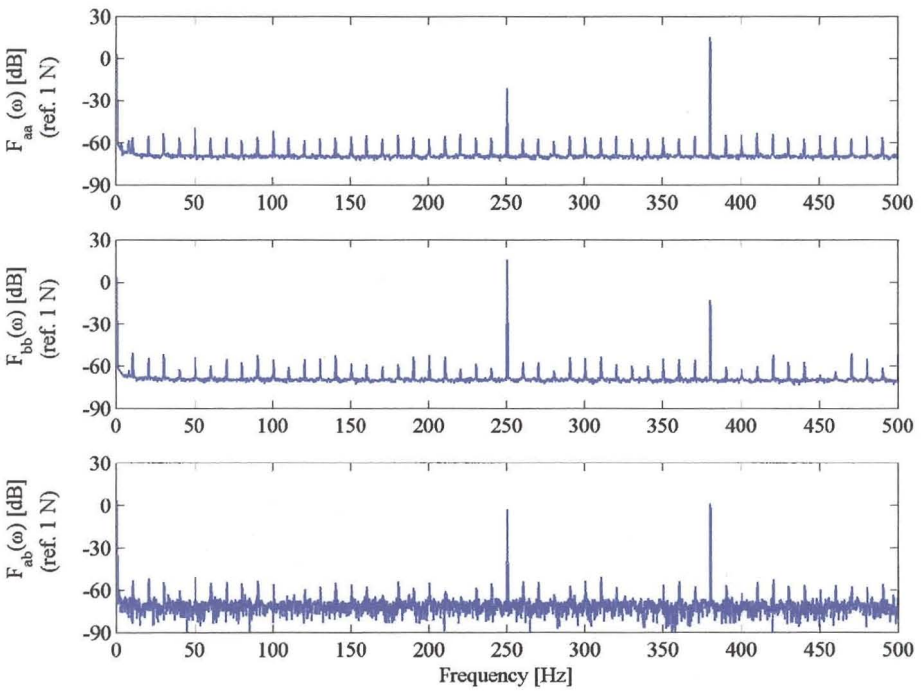

Figure 5.17 – ASD (F_a and F_b) and CSD (F_{ab}) of the two harmonic forces applied to the free-free beam

5.3.3 Force Determination Results

Equation (5.1) can be defined in terms of the spectral density function as:

$$[G_{ff}(\omega)] = [H(\omega)]^{+}[G_{xx}(\omega)][H(\omega)]^{T+} \tag{5.4}$$

For the noise-free case, the rank of the measured acceleration matrix, $[G_{xx}]$, should be equal to the number of linearly independent forces exciting the beam. The rank of the response matrix can be evaluated by applying SVD to the matrix. However, if the forces are not independent, the rank will be less than the number of forces (Elliott *et al.*, 1988).

The measured acceleration matrix was of full rank. This can be attributed to the presence of the measurement noise that spuriously increased the rank of the response matrix. Figure 5.18 shows the singular values of $[G_{xx}]$ and gives no clear indication of the 'true' rank because of the noise contaminating the response.

The full rank matrix $[G_{xx}]$ cannot be substituted into equation (5.4) since the small singular values can falsely dominate the pseudo-inversion and render inaccurate force estimates. Truncating the singular values to reflect the number of independent forces can ameliorate the force estimates. In practice the truncation point of the number of singular values is not always clear, especially when considerable measurement noise is present in the data (Elliott *et al.*, 1988).

The forward problem was solved with the directly measured forces.

$$[G_{xx}(\omega)] = [H(\omega)][G_{ff}(\omega)][H(\omega)]^T \tag{5.5}$$

and the SVD of $[G_{xx}]$ revealed that the rank of the acceleration matrix is indeed one, as depicted in Figure 5.19. The absolute values of the higher-order singular values were of the order 10^{-4} and below and can for all practical purposes be considered as negligible.

Unfortunately, in a real-world application the direct forces will not be available and it may be difficult to determine the 'true' rank of the noise contaminated response matrix.

The $[G_{xx}]$ matrix was recalculated for the truncated singular values and the discrete forces were estimated from equation (5.4). It is apparent from the results in Figure 5.20 that there is some difficulty in predicting the accurate forces at the forcing frequencies. This resulted in an elaborated investigation to find probable causes and explanations for the behaviour noted. The response matrix, as calculated from the forward problem, was substituted into the force identification algorithm and produced excellent force predictions. Next, the accuracy of the inertance matrix and measured accelerations were considered. The individual frequency response functions from the MIMO excitations were compared with previous frequency response functions obtained from single input excitations and found to be satisfactory.

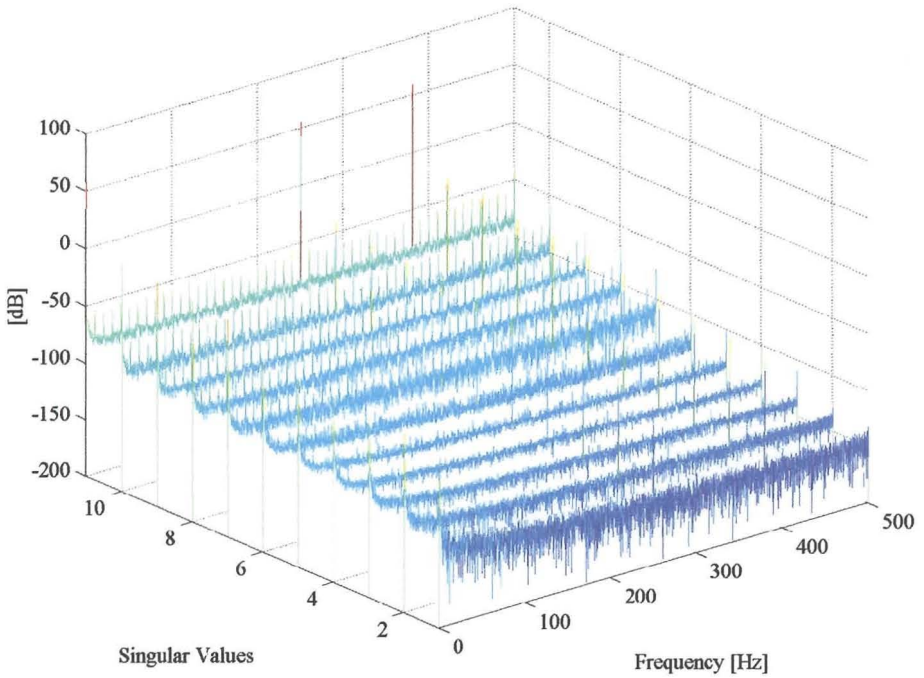

Figure 5.18 - Singular values of the measured response matrix, $[G_{xx}]$

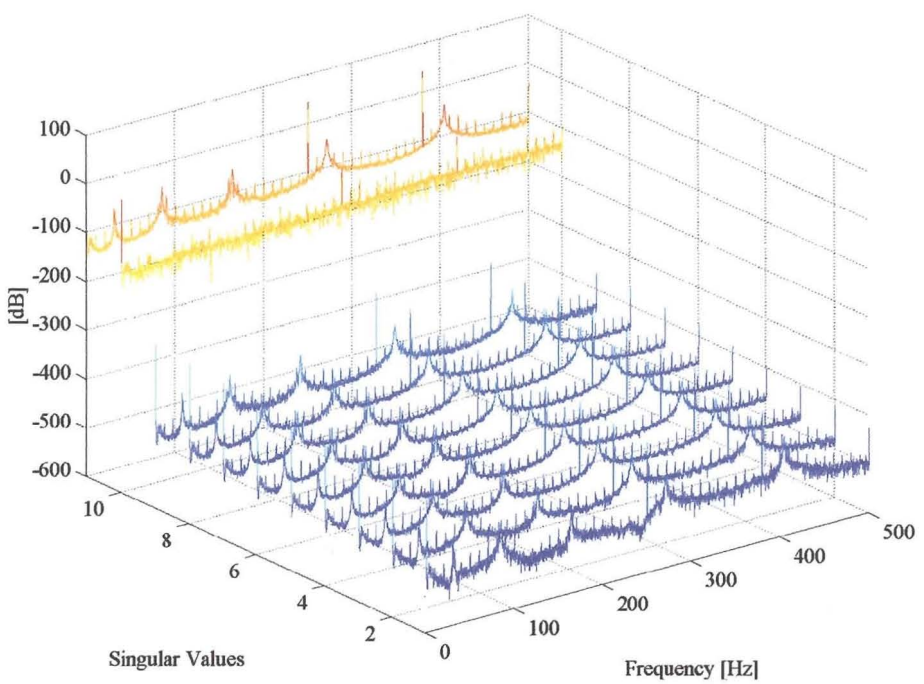

Figure 5.19 - Singular values of the response matrix, $[G_{xx}]$, determined from the forward problem

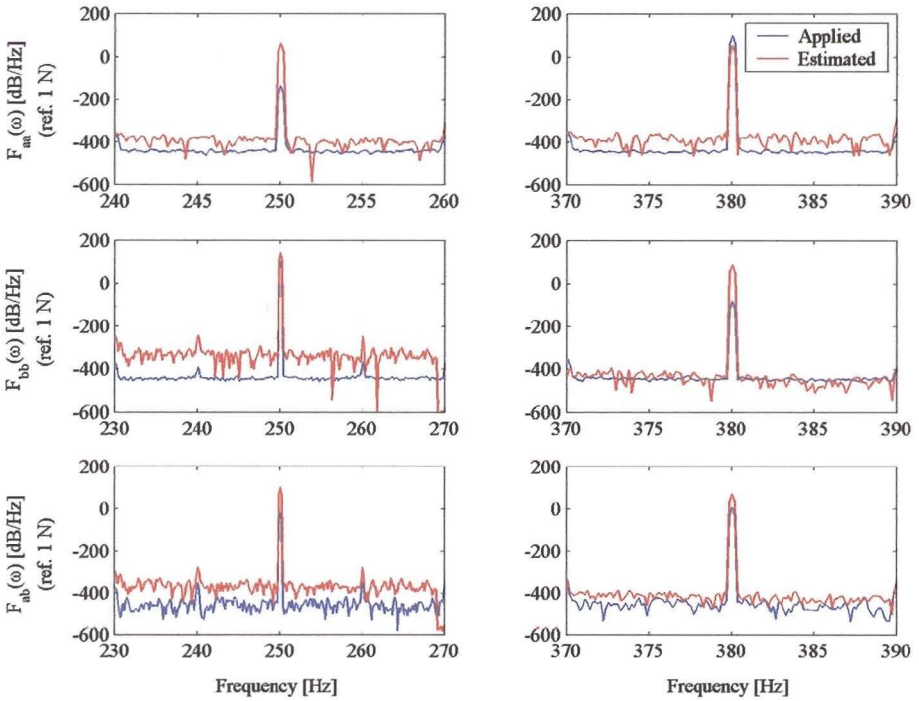

Figure 5.20 – Comparison of measured and estimated forces for the free-free beam

Comparison between the measured accelerations and accelerations computed from equation (5.5) differed significantly (Figure 5.21). Although the presence of considerable noise may contaminate the measured accelerations, the deviation might not be attributed solely to the influence of measurement noise. At first the measured accelerations were thought to consist of the acceleration of the center of mass superimposed on the beam's response subjected to the force inputs. Further investigation revealed this to be an unlikely cause, since the strain measurements strange enough exhibited the same type of behaviour. The only probable explanation was found in a work published by Ojalvo and Zhang (1993: pp. 171):

"Since the ill-conditioning of algebraic equations is dependent upon the zero and near-zero eigenvalues of the coefficient matrix, it is possible to interpret the original equations as those associated with the forced response of a free-free system, or one for which an otherwise structurally stiff system is suspended by very soft springs. In such cases, the zero (or near-zero) eigenvalues represent rigid (or near-rigid) body modes ... small errors in the right hand side may be viewed as static imbalance terms. These would have little effect if the system were restrained (i.e. no zero frequency) but are disastrous for unrestrained systems, and over time can produce large drifts in the system."

The above explanation was taken as the probable cause for the observed behaviour. In addition it was decided to refrain from continuing the force identification on this experimental setup and to progress to the assessment of a restrained system.

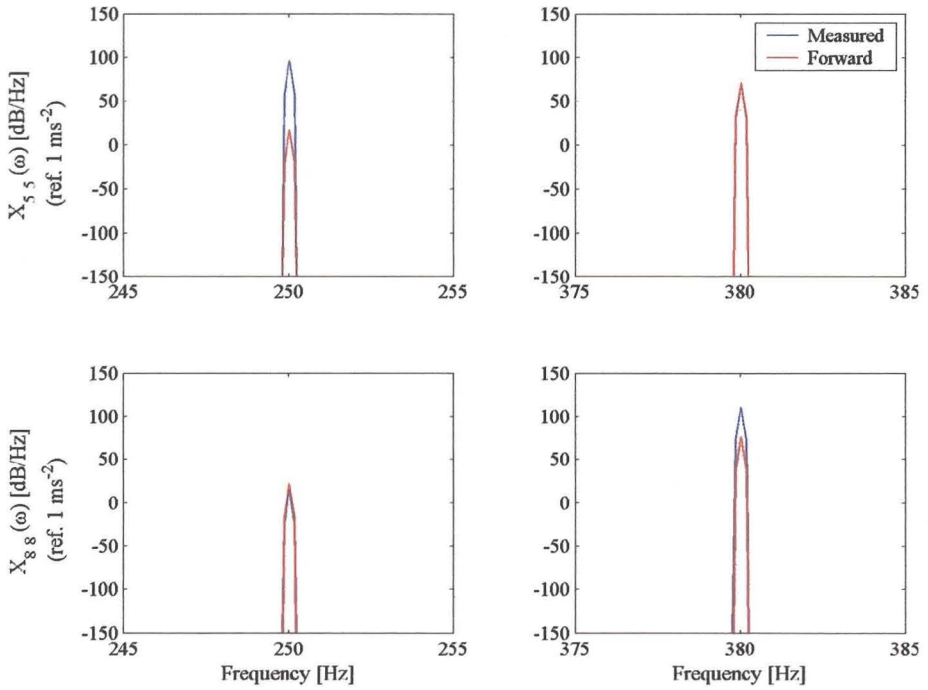

Figure 5.21 – Comparison of the measured and calculated accelerations for the free-free beam

5.4 TWO HARMONIC FORCES: HINGED-HINGED BEAM

This section presents an attempt to apply the force identification process to infer two harmonic forces acting on a hinged-hinged beam. The effect of constraints on both frequency domain methods was investigated.

5.4.1 Details of the Experimental Set-up

The hinged-hinged beam was invoked once again to determine two harmonic forces applied at positions 5 and 8 on the beam.

5.4.2 The Measurements

The measurement procedure described in Section 5.3.2 was repeated, i.e. the inertance frequency response functions were measured first through the use of MIMO excitation. The beam was then subjected to two simultaneous harmonic forces applied at positions 5 and 8 with a frequency content of 380 Hz and 250 Hz, respectively. The point inertance corresponding to reference position 5 is depicted in Figure 5.22, while

the point inertance of reference position 8 in shown in Figure 5.23 (the entire set being represented in Appendix D).

Figure 5.24 shows the ASD of the actual input forces as measured directly with the force transducers. In the figure, F_a denotes the force measured at position 8, while F_b is the force measured at position 5. In contrast to the previous case, the correlation components were orders in magnitude smaller than the actual force components and were considered as negligible. Nine acceleration signals were measured corresponding to position 2 to 10.

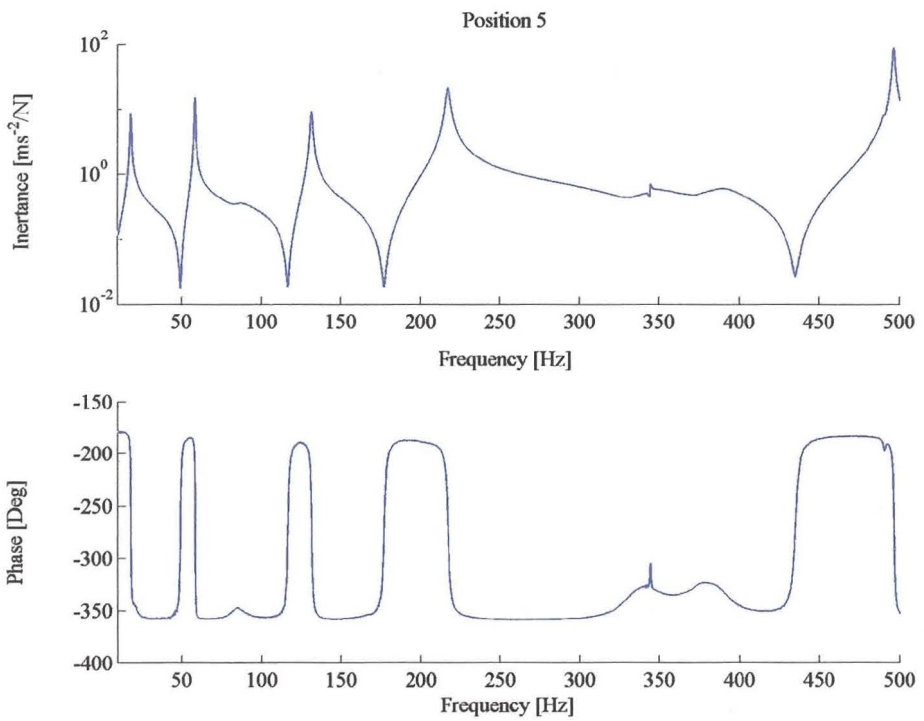

Figure 5.22 – Measured point inertance for the hinged-hinged beam corresponding to reference position 5

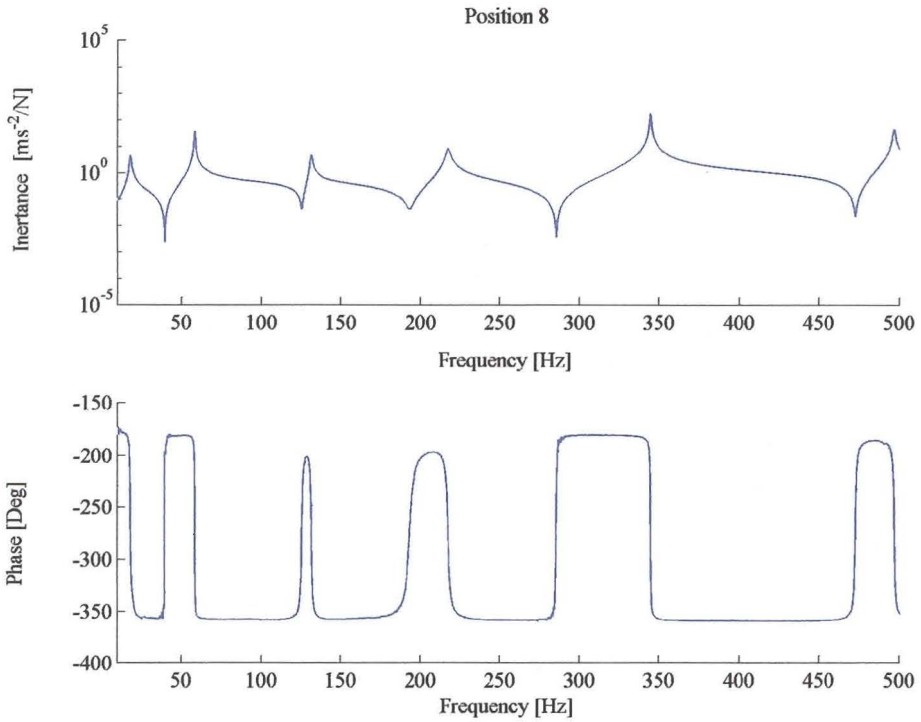

Figure 5.23 – Measured point inertance for the hinged-hinged beam corresponding to reference position 8

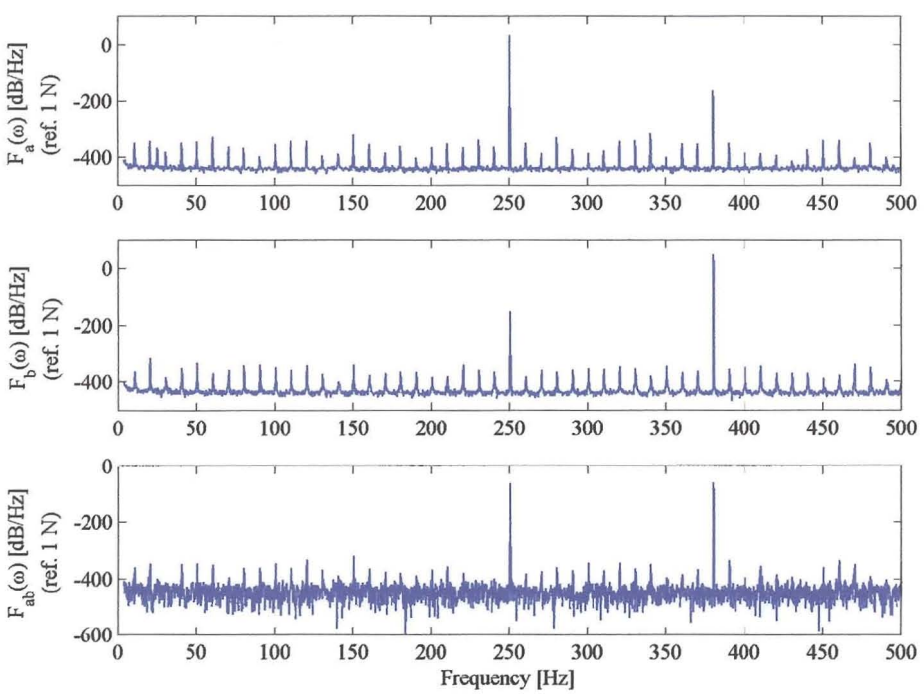

Figure 5.24 – ASD (F_a and F_b) and CSD (F_{ab}) of the two harmonic forces applied to the hinged-hinged beam

5.4.3 Force Determination Results

a) Frequency Response Function Method

Once again the 'raw' frequency response functions were used in the analysis. The coherence function, $\gamma^2(\omega)$, associated with each frequency response function can be used to determine the random error in that measurement. The absolute error, $E(\omega)$, with a confidence limit of 99.7 per cent of the frequency response function magnitude is given by (Powell and Seering, 1984)

$$E(\omega) = 3\left|H(\omega)\right|\left[\frac{1-\gamma^2(\omega)}{2\,n_d\,\gamma^2(\omega)}\right]^{1/2} \tag{5.6}$$

where

n_d is the number of averages used in the measurements.

Calculating the absolute error for each frequency response function results in a matrix $[E(\omega)]$, with dimensions equal to that of the frequency response function matrix. The norm, $\varepsilon(\omega)$ of the $n \times m$ absolute error matrix can serve as a threshold value whereby any singular value smaller than this value will be set to zero. This will improve the condition of the problem, as the inverse of a small number is very large and would, falsely, dominate the pseudo-inverse. The singular values of the frequency response function matrix and the error norm are shown in a logarithmic plot versus frequency in the upper part of Figure 5.25. The lower part of the figure shows the anticipated trend of the condition number of $[H(\omega)]$.

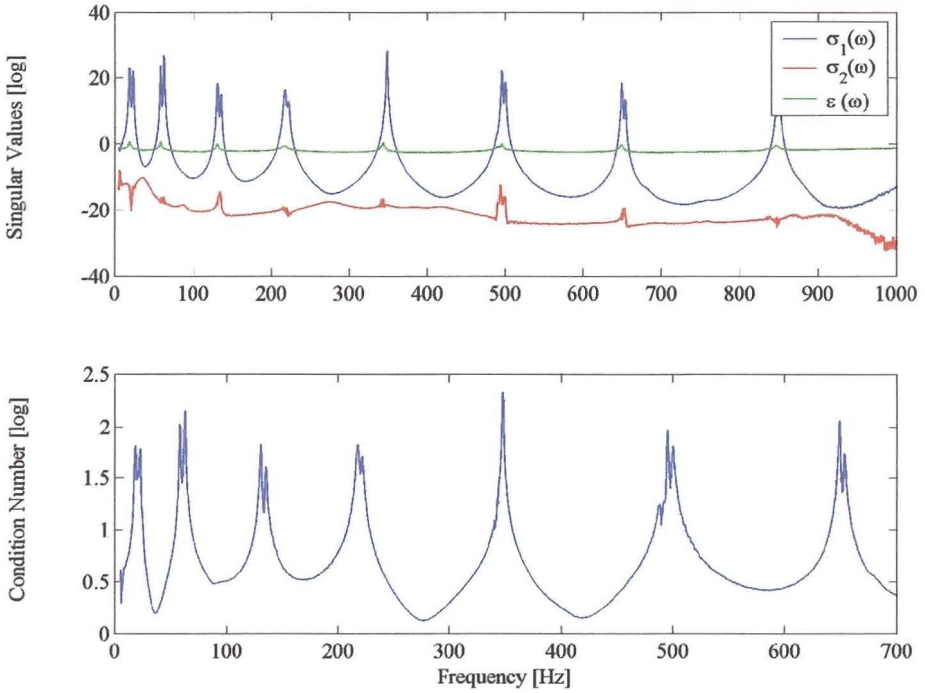

Figure 5.25– Singular values, error norm and condition number of the frequency response matrix for the hinged-hinged beam

The forces may be reconstituted from all nine sensor locations from:

$$\{\hat{F}(\omega)\} = [A(\omega)]^{+}\{\ddot{X}(\omega)\} \tag{5.7}$$

It is obvious from the results (Figure 5.26 and 527) that the frequency response function method accurately identified the two harmonic forces acting on the hinged-hinged beam.

Improving the number of response measurements will likely improve the quality of the force estimates.

The FEN for each force estimate is listed in Table 5.2

Table 5.2 - Force Error Norm of the estimated forces

$\lvert F_a(\omega)\rvert$ [%]	$\lvert F_b(\omega)\rvert$ [%]
5.291	4.724

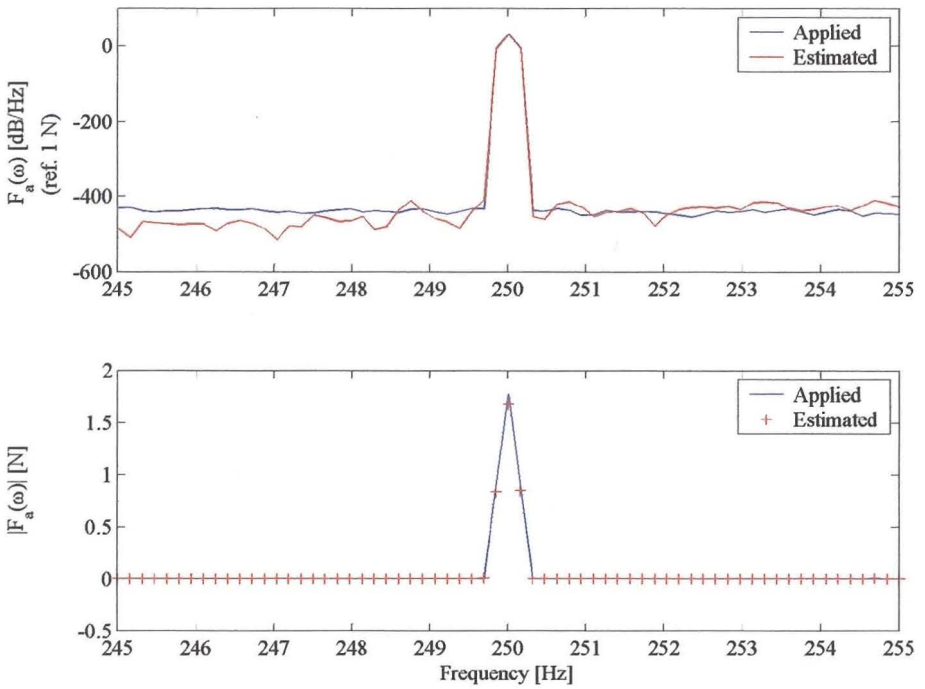

Figure 5.26 – Comparison of the measured and estimated forces applied at position 8 for the hinged-hinged beam

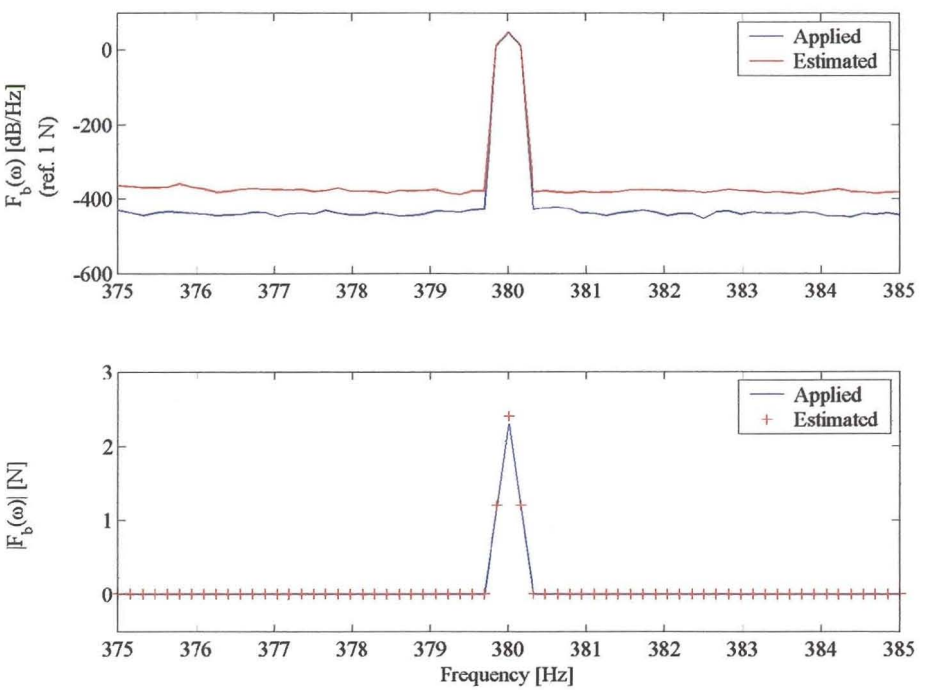

Figure 5.27 – Comparison of the measured and estimated forces applied at position 5 for the hinged-hinged beam

b) Modal Coordinate Transformation Method

The modal coordinate transformation method failed to determine the force estimates correctly.

As mentioned previously, the boundary conditions imposed on the beam were assumed to be representative of a system under operating conditions. An experimental modal analysis was performed on the measured frequency response function data in the chosen frequency range of 0-450 Hz, to extract the natural frequencies and modal damping factors corresponding to the first five bending modes. The reconstructed frequency response functions, without the contribution of the residual terms, were compared to the measured frequency response functions, prior to applying equation (4.13), from which one could determine the forces. This revealed that the residual terms had a significant effect on the accuracy of the frequency response functions in the vicinity of the forcing frequencies (250 and 380 Hz). At first, it was believed that extending the chosen frequency range to 1 kHz to include more modes could circumvent the residual contributions. Having repeated the measurements the reconstructed frequency response functions were compared with the originally measured data. The inclusion of additional modes did not improve the quality of the reconstructed frequency response functions around the fifth mode.

It is obvious from the point inertance of reference position 5, shown in Figure 5.22, that the boundary conditions influenced the proper excitation of the fifth mode (± 340 Hz). This may be attributed to a number of reasons:

Even though the mass of the concrete-filled blocks was considerably higher than that of the test piece, the question may arise whether the blocks were sufficiently rigid to provide the necessary grounding to the structure, since they had not been fixed to the floor.

Another factor that influenced the data was the supports used to constrain the beam. Tightening the bolts too much introduced spurious modes in the frequency range. Figure 5.28 illustrates the different construction methods of the supports, while Figure 5.29 demonstrates their influence on a typical frequency response function measurement. Construction method A was found to have the minimum effect on the data and was employed in the force identification process. Method B was considered not rigid enough, while C and D (attachment of G clamp) shows attempts to make the supports more rigid.

From the above, it is evident that the boundary conditions contributed to the frequency response functions of the beam. These frequency response functions were found to be too complex and could not be reconstructed from the modal parameters within the frequency range alone. Especially the frequency response functions corresponding to reference position 5 were most heavily influenced.

From the above discussion, one might suspect that better force determination will result from excluding the sensor locations, for which the reconstructed frequency response functions deviated substantially from the measured values. However, by excluding these sensor locations it was found that the condition number of the modal matrix increased significantly and also rendered inaccurate force estimates.

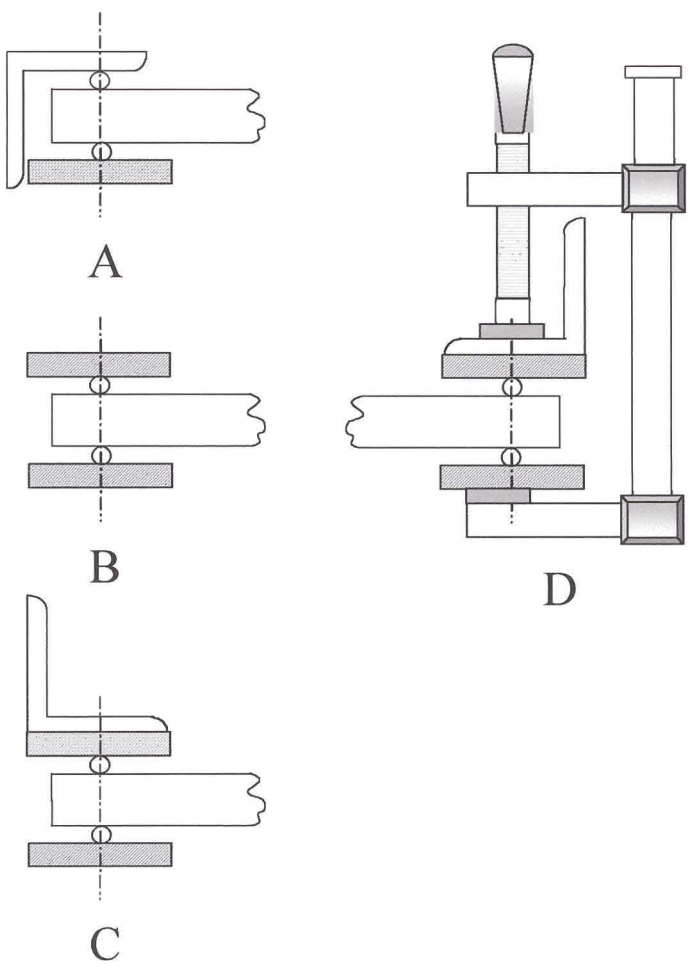

Figure 5.28 – Different constructions methods of the supports used for hinged-hinged beam

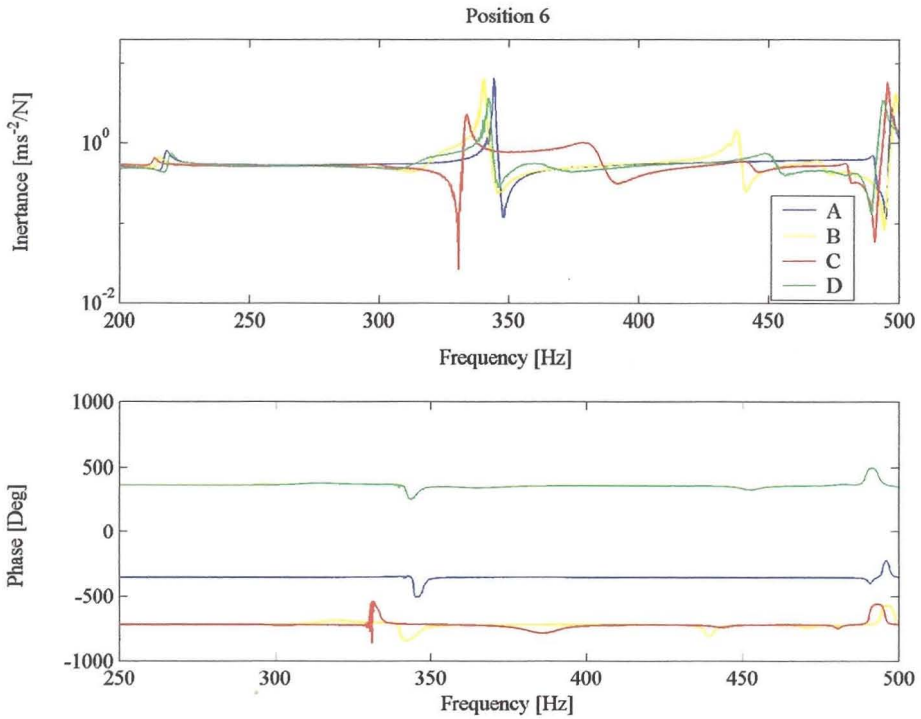

Figure 5.29 – Effect of different supports on FRF measurements corresponding to reference position 8

5.4.4 Strain Measurements

Still using the hinged-hinged beam as test piece, piezoelectric strain gauges were employed to measure frequency response functions for nine different positions along the length of the beam.

Hillary and Ewins, (1984) indicated that the strain responses gave more accurate force estimates than the accelerations. The reason for this behaviour is that the strain responses are more influenced by the higher modes at low frequencies, and therefore the frequency response functions are more complex in shape and hence obtain better force predictions. Han and Wicks (1990) also studied the application of strain measurements.

The piezoelectric strain gauges were calibrated based on the manufacturer's quoted sensitivities and the calibration values are listed in Appendix A. Only two strain gauges could be simultaneously mounted on the beam due to the restriction imposed by the available channels of the measurement system.

The Strain Frequency Response Functions (SFRFs) were measured first by taking 200 averages. Figure 5.30 and 5.31 show the SFRFs associated with each reference

position. The high level of averaging was to reduce the uncorrelated noise between the force and strain response.

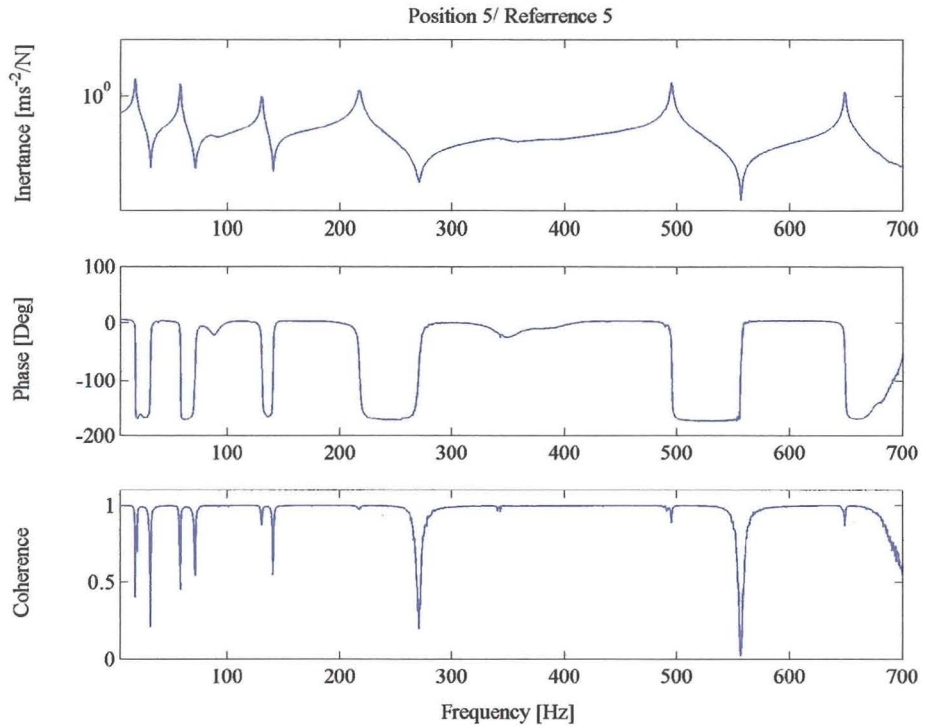

Figure 5.30 – Measured SFRF for the hinged-hinged beam corresponding to reference position 5

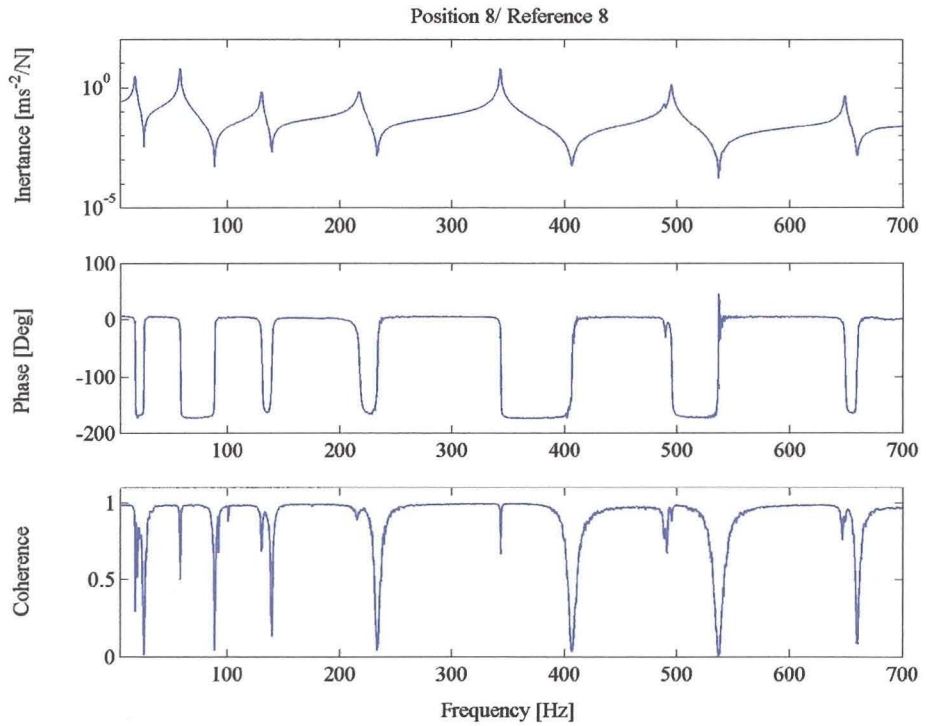

Figure 5.31 – Measured SFRF for the hinged-hinged beam corresponding to reference position 8

Subsequently, the beam was subjected to two simultaneous harmonic forces at positions 5 and 8, and strain responses were measured. An alternative formulation of equation (5.1) was used to determine the two forces.

$$\{\hat{F}(\omega)\} = [Y(\omega)]^{+}\{e(\omega)\} \tag{5.8}$$

where

$\{\hat{F}(\omega)\}$ is the (2×1) estimated force vector,

$[Y(\omega)]$ is the (2×9) SFRF matrix, and

$\{e(\omega)\}$ is the (9×1) strain response vector.

The results can be compared with the directly measured forces in Figures 5.32 and 5.33. Contrary to the expectations, it is apparent in this particular case that the acceleration responses gave better force estimates than the strain responses (Table 5.3).

Table 5.3 - Force Error Norm of the estimated forces

$\lvert F_a(\omega)\rvert$ [%]	$\lvert F_b(\omega)\rvert$ [%]
17.108	12.127

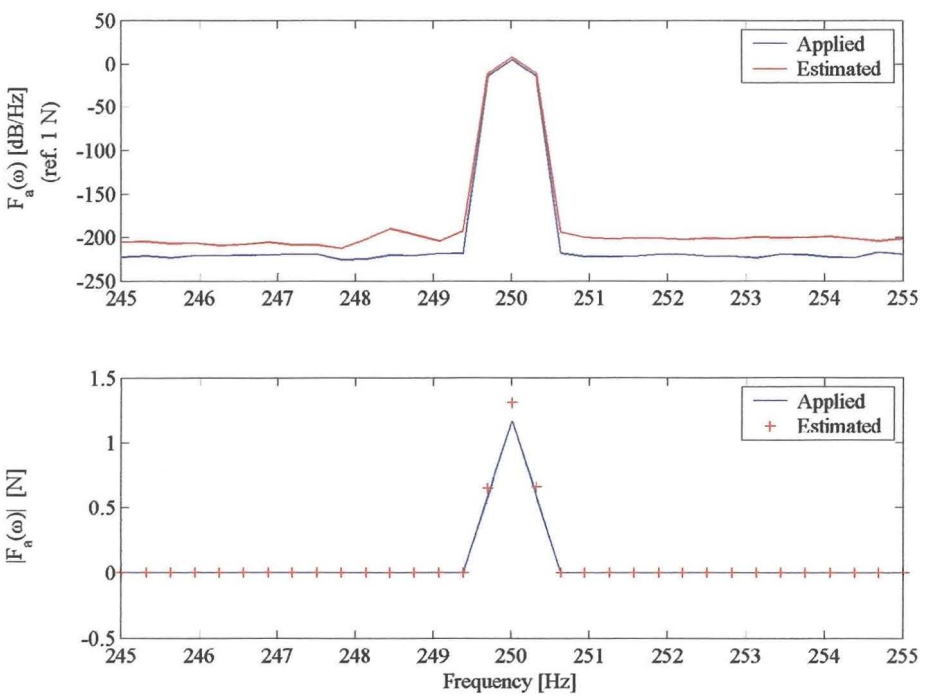

Figure 5.32 – Comparison of the measured and estimated forces applied at position 8 for the hinged-hinged beam

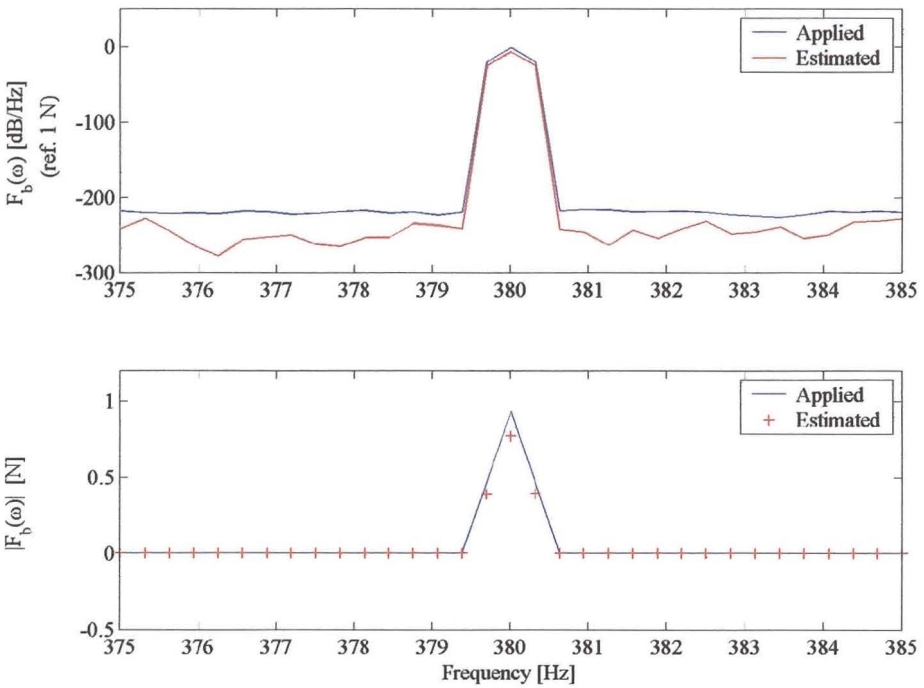

Figure 5.33 – Comparison of the measured and estimated forces applied at position 5 for the hinged-hinged beam.

As mentioned earlier, the strain response is more influenced by the higher modes at low frequencies. Conversely, the strain response is less influenced by the low modes at high frequencies. Thus, the higher the excitation frequencies the fewer modes participate in the strain response of the beam.

Having said that, the main reason for the results noted can be attributed to the sensitivity of the piezoelectric strain gauges as compared to the sensitivity of the accelerometers. Figure 5.34 shows a logarithmic plot of the singular values, the error norm of equation (5.6) and the associated condition number of the SFRF matrix. The results indicated that the values of the error norm of the SFRF matrix were higher than the corresponding values of the inertance frequency response function matrix. This parameter is employed to ascertain the random errors in the SFRF measurements and represent the probable cause for the poorer force estimates obtained. The poor coherence functions in Figure 5.29 and 5.30 confirms this statement.

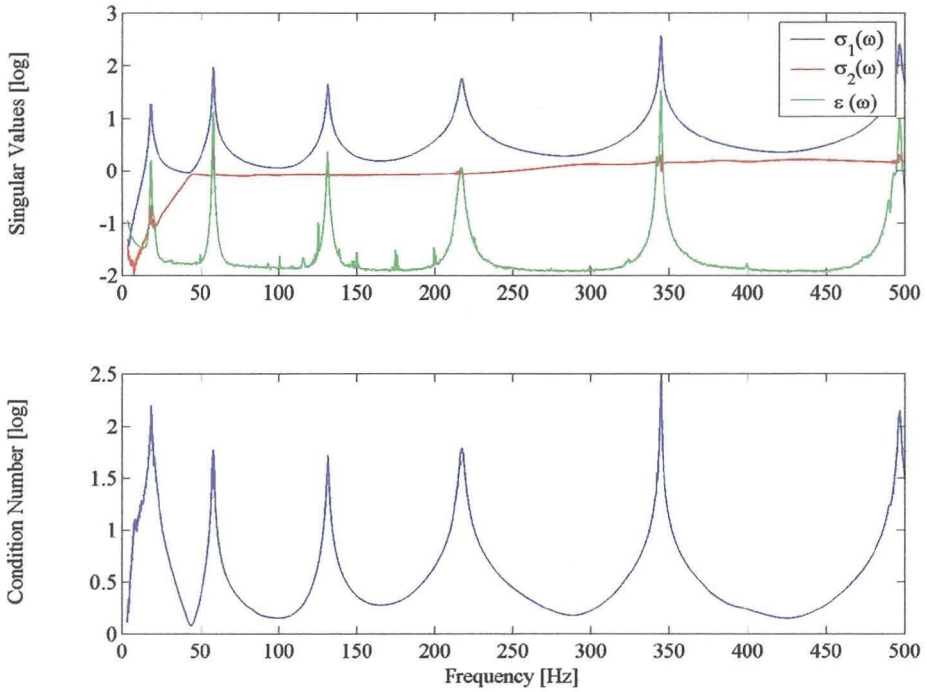

Figure 5.34 – Singular values, error norm and condition number of the SFRF matrix for the hinged-hinged beam

CHAPTER 6

Discussion and Evaluation

6. DISCUSSION AND EVALUATION

6.1 TEST PIECE

An aluminium beam was invoked as the test piece throughout the study. It was deemed advisable to start with a relatively simple structure but unexpectedly gave rise to some difficulties.

The fact that the test piece was a lightly-damped structure required special effort concerning the excitation function used in determining the frequency response functions. In the end a chirp-sine function was used, resulting in much sharper and well-defined peaks of the frequency response functions. The low damping was also mentioned as probable cause for difficulties experienced with the experimental modal analysis.

Another factor that might have influenced the accuracy of the force estimates is that the modes for the beam were very well-separated, and at any given frequency, the response of the beam was dominated by the two nearest modes.

In view of the above-mentioned it may be justifiable to consider a more complex structure with less well-separated modes and with higher damping. In a structure with higher damping the neighboring modes will have a larger contribution to the response of the structure at any given frequency and might not exhibit the same degree of ill-conditioning noted with this test piece.

6.2 APPLIED FORCES

6.2.1 Unknown Forces Locations

Throughout the experimental studies it was assumed that the exact forcing locations were known. In addition, only the columns associated with these input locations were included in the frequency response function matrix. Conversely, for the modal coordinate transformation method only the rows associated with the input locations were included in the reduced modal matrix of equation (4.16). Let's assume that the number of forces and the input locations were unknown.

a) Frequency Response Function Method

The maximum number of forces one can correctly predict will be equal to the rank of the frequency response function matrix, which in turn is equal to the number of significant participating modes (Fabunmi, 1986). For the case of the hinged-hinged beam, the analysis of the 'full' frequency response function

matrix would allow the estimation of maximum six forces, except at frequencies where the frequency response function matrix renders rank deficient. An important prerequisite is that the actual force inputs should be among the locations included in the frequency response function matrix. If not, the estimated forces will be erroneous pseudo-forces. The forces that produce a certain response can then be determined from the pseudo-inversion of the frequency response function matrix. The force amplitudes of the non-forcing locations will be zero (Fregolent and Sestieri, 1990).

b) Modal Coordinate Transformation Method

The same argument can be followed in the case of the modal coordinate transformation method. The modal matrix is generally rectangular with the number of responses exceeding the number of modes within the analysis frequency band. In this case the number of force estimates should be smaller than or equal to the rank of the modal matrix (refer to Section 4.1.2). Proper choice of the set of response locations and orthogonal mode shapes will ensure that the modal matrix is well-conditioned and will not exhibit the ill-conditioning at the resonant frequencies of the structure. Thus the number of force estimates remain constant for the entire frequency range considered. Once again the actual force locations should form part of the set of response locations of the reduced modal matrix, to infer the excitations accurately.

6.2.2 Distributed Forces

Both the frequency response function and modal coordinate transformation methods are discrete representations of continuous functions. The frequency response function, modal matrix and the responses can usually be measured only at a finite number of discrete points and as a result the force identification problem is restricted to the determination of forces at the discrete points. In the case of a distributed loading the responses are used to determine a number of equivalent discrete forces, which are intended to represent the original distributed load. As mentioned before, the number of modes in the frequency response function or modal matrix restrains the number of discrete dynamic forces. Unfortunately, these discrete forces will always be in error, even with a high number of modes and a high matrix dimension (Fregolent and Sestieri, 1990).

6.2.3 Random Forces

Chapter 5 dealt with harmonic force determination only. An attempt to extend the force identification to determine random dual forces was unsuccessful due to shortcomings of the experimental setup. The force spectrums presented in Section 5.3 and 5.4 exhibited some correlation despite the uncorrelated drive signals supplied to the shakers. The correlation was the result of the interaction of the excitation system with the structure and will tend to be greater at the beam's resonant frequencies. Two random forces were applied to the beam and the accelerations were measured. Figure 6.1 presents the decomposition of the directly-measured random force spectral density function matrix obtained from the measurement procedure. The number of distinct non-zero eigenvalues, as well as the ratio between adjacent eigenvalues can be used to ascertain the degree of correlation of the inputs (Maia *et al.*, 1997). It is worth noting that in the vicinity of the resonant frequencies of the beam the ratio between the eigenvalues was high, indicating only a single independent force. In the rest of the frequency range the eigenvalues were of similar magnitude. This shows that there were two independent forces. The reason for the results noted can be explained as follows. Two rather small electromagnetic exciters were used to excite the structurally stiff beam. For the case where a particular exciter was exciting the structure at or near one of the resonant frequencies the other exciter was 'pulled' in phase with the response of the resonant mode. The use of larger electromagnetic shakers, or for that matter even hydraulic shakers, might not exhibit the same behaviour. In addition a more flexible beam might be employed as test piece.

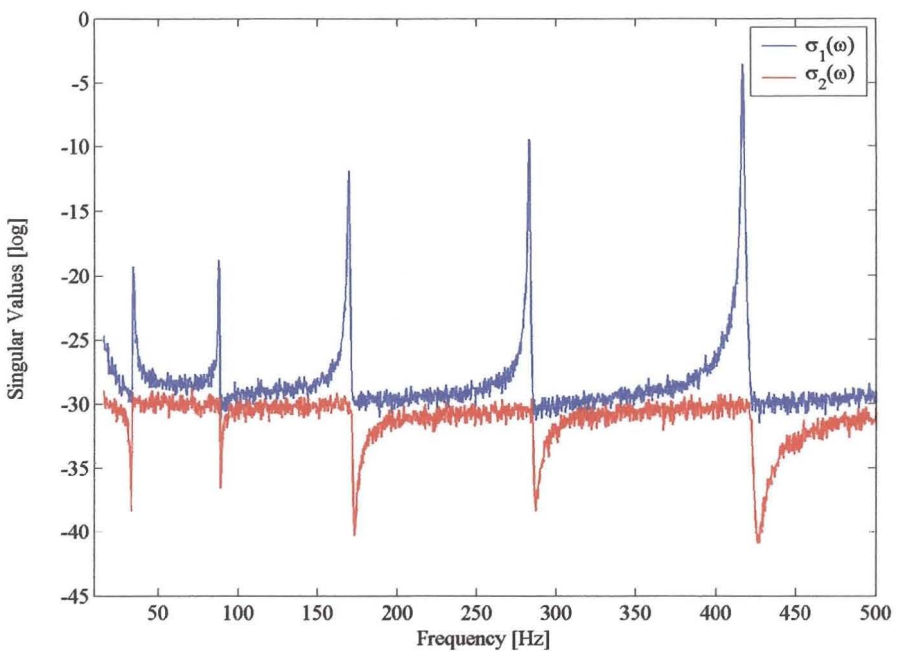

Figure 6.1 – Decomposition of force spectral density function matrix

Instead harmonic forces were applied to the beam, with forcing frequencies more or less in between the structural resonant frequencies.

6.3 THE FREQUENCY RESPONSE FUNCTION METHOD

The formulation of the frequency response function method was described in Chapter 3. No modal parameter estimation is required, although an experimental modal analysis can be performed to 'filter' some of the measurement noise from the frequency response functions.

The number of forces one can attempt to determine is limited by the number of significant participating modes at any given frequency line.

The ill-conditioning of the force predictions at the system's resonant frequencies was illustrated through the use of a numerical simulation. The various modal parameters and responses were perturbated with random errors to resemble experimental measurements. The results indicated that the perturbation of the mode shapes had the most significant affect on the accuracy of the forces. In addition, it was noted that the pseudo-inverse of the frequency response function matrix needs to be computed at each frequency line within the analysis frequency range.

The force predictions might be ameliorated at the structural natural frequencies by truncating very small singular values of the frequency response function matrix from the pseudo-inversion, since the inclusion of these small values might lead to erroneous force estimates.

The condition number of the frequency response function matrix furnishes as a tool to ascertain the expected ill-conditioning of the force predictions. A numerical study highlighted the factors influencing the value of this parameter.

Chapter 5 evaluated the implementation of this method to infer the forces acting on an aluminium beam subjected to different boundary conditions. A single harmonic force was successfully identified on a free-free and hinged-hinged beam. The results of the dual force inputs applied to the free-free beam cannot be completely explained. However, a probable cause was mentioned. In the final experimental study, the frequency response function method was used to determine two harmonic forces on a hinged-hinged beam from both acceleration and strain measurements. Despite the influences of the boundary conditions on the frequency response functions noted, the method was sufficiently successful in determining the applied forces. One of the important issues resulting from the experimental studies was the contribution of the residual terms corresponding to the truncated modes, which affected the accuracy of the frequency response functions and consequently the force predictions. It was

shown that the method has the ability to incorporate the influence of the residual terms in the force identification process. The residual terms corresponding to a particular reference position cannot be synthesised from the modal parameters extracted from the measurement of a single column or row of the frequency response function matrix. As a result the frequency response functions must be measured at all the expected force input locations.

6.4 THE MODAL COORDINATE TRANSFORMATION METHOD

Chapter 4 was concerned with the modal coordinate transformation method. An experimental modal analysis was a prerequisite for implementation of this method. In order to utilise a least-squares estimation of the forces the method requires the number of response locations to exceed the number of linear independent modes in the analysis frequency range, which in turn should preferably be greater than the number of forces one attempts to reconstruct. The results of a numerical study showed that the modal coordinate transformation method did not suffer from the ill-conditioning of the force estimates at the structural natural frequencies due to the inversion of the modal matrix. The successive integration of the acceleration to displacement signals was shown to amplify the errors in the low frequencies and might affect the force results.

This method was computationally much faster than the frequency response function method, since the pseudo-inverse of the modal matrix needed to be calculated only twice, regardless of the frequency resolution considered in the analysis.

A separate numerical study on a free-free beam indicated that the condition number of the modal matrix is a function of the set of response locations chosen and the modes included in the modal matrix.

The modal transformation is based on the assumption that the modal vectors are orthogonal and linearly independent functions. This assumption might be violated during the experimental modal analysis and a reciprocal modal vector was described as an alternative method of performing the modal transformation.

This method has the advantage of being able to identify forces at locations which may be inaccessible for frequency response function measurements. Based on the reciprocal theorem, another point on the structure can be artificially excited from which one can extract the modal parameters. Having measured only the response at the inaccessible force input location, the force estimate corresponding to this point can then be determined (Kim and Kim, 1997). The results of the experimental studies in Chapter 5 pointed out that this procedure is only valid when the values of the residual terms of the truncated modes outside the analysis frequency range are

negligible. Although the residual terms corresponding to the low and high modes can be obtained from the experimental modal analysis, these terms have to be omitted when executing the modal coordinate transformation method. The findings of Section 5.1, where a free-free beam was used to predict a single harmonic force, indicated that the low frequency contribution, i.e. the RBM, had the most adverse affect on the accuracy of the reconstructed frequency response functions at the excitation frequency.

The frequency response function method for determining a single force resulted in a condition number of unity (the ratio of a single singular value by itself). However, the modal coordinate transformation method required the inversion of the modal matrix, and since more than one mode was included in the modal matrix, the value of the condition number was greater than unity.

In the second experimental study a hinged-hinged beam was investigated to exclude the effect of the RBM to the response of the beam. At first not enough modes were included in the analysis to infer the force estimate correctly at the excitation frequency. It was noted that more modes were required in the force identification process than the number of modes required in modeling of the response of the structure. This method also displays the truncation problem generally encountered in experimental modal analysis and are caused by the limited number of modes, limited number of measurement points and the lack of rotational degrees-of-freedom (Shih *et al.*, 1989). As jet, it is uncertain as to the number of modes, or the analysis frequency range required to guarantee success with the modal coordinate transformation method. This might prevent the method from becoming popular in cases where the vibration measurements are very expensive and/or labour intensive to perform and a second round of measurements are just not viable.

The final experimental evaluation was a hinged-hinged beam subjected to two simultaneous harmonic forces. Constraints imposed on the beam influenced the frequency response functions around the fifth mode. As a consequence, the frequency response functions were difficult to recreate from the modal parameters alone and spoiled the force identification.

This method was applied under the assumption of proportional damping and would require a more elaborate calculation procedure if this assumption was not fulfilled (Desanghere and Snoeys, 1985).

6.5 CONCLUSION

Two frequency domain force identification procedures were proposed in this work. In view of the above-mentioned advantages and disadvantages associated with each method it can be concluded that the frequency response function method is superior to the modal coordinate transformation method for the applications considered in this study.

CHAPTER 7

Conclusion

7.1 CONCLUSION

Two frequency domain force identification procedures were considered in this work, i.e. the frequency response function method and modal coordinate transformation method. Both numerical and experimental examples were used to assess the performance of each technique.

The objective of this research was to implement these methods in an experimental investigation on a simple, well-behaved structure, given the lack of experimental work pertaining to especially the modal coordinate transformation method. A single harmonic force was determined on an aluminium beam subjected to different boundary conditions. The work was then extended to predict two sinusoidal forces from measured acceleration and strain signals.

The frequency response function was sufficiently successful in identifying the forces for the majority of experimental studies, with the exception of the dual force inputs on the free-free beam, which certainly requires further attention. Some of the most important issues concerned with this method are:

- Force predictions at the structural resonant frequencies are likely to behave ill-conditioned due to errors in the measured response and frequency response functions.
- The method has the ability to account for the residual terms, which might have a significant effect on the accuracy of the frequency response function and consequently the force estimates.
- Frequency response functions must be measured at all the expected force input locations.

In the modal coordinate transformation method the pseudo-inverse is generally well-conditioned and the analysis is computationally much faster than the former method. The method also has the advantage of identifying forces at locations that are not included in the initial frequency response function measurements. Despite the advantages associated with the modal coordinate transformation method this method has shown rather limited success. The difficulties encountered were not as much due to the numerical formulation of the method as they were to the prerequisites required:

- This method requires a good set of modal parameters from which one should be able to reconstruct the originally measured frequency response functions.
- More modes are needed in the force identification process than the number of modes required in the modeling of the response of a structure.
- The contribution of residual terms of the truncated modes should be small in the analysis frequency range.

Based on the results presented it was concluded that the frequency response function method was superior to the modal coordinate transformation method for the experimental examples considered.

7.2 FUTURE WORK

Further experimental studies on more complex structures should be investigated to make the force identification methods more applicable to real engineering structures.

The determination of distributed forces needs to be further developed. In particular, the number of equivalent discrete force estimates that one would require to approximate a particular continuous forcing function.

The issue concerning the truncation problem, i.e. the number of modes required to successfully apply the modal coordinate transformation method also requires further research.

It would also be interesting to examine the effect of measurement positions with respect to the excitation locations on the condition number and accuracy of the force estimates, considering three particular situations: a) fully collocated inputs and outputs; b) partially collocated inputs and outputs; and c) fully non-collocated inputs and outputs. This suggestion follows from the fact that for some time domain identification methods the relative position of the inputs and outputs has been found to have a significant influence on the stability of the inverse problem.

REFERENCES

AVITABILE, P., Modal Space: Back to Basics, *Experimental Techniques*, January/February, 1999.

BALMèS, E. (1), *Experimental and Analytical Structural Dynamics Toolbox*, User's Guide, Version 3, 1997.

BALMèS, E. (2), 1997, New results on the identification of normal modes from experimental complex modes, *Mechanical Systems and Signal Processing*, Vol. 11, no. 2, pg. 229-243.

BARTLETT, F. D. Jr. & FLANNELLY, W. G., 1979, Model Verification of Force Determination for Measuring Vibratory Loads, *Journal of American Helicopter Society*, Vol. 24, pp. 10-18.

BATEMAN, V. I., CARNE, T. G., GREGORY, D. L., ATTAWAY, S. W. & YOSHIMURA, H. R., 1991, Force Reconstruction for Impact Tests, *ASME Journal of Vibration and Acoustics*, Vol. 113, No. 2, pp. 192-200.

BATEMAN, V. I., CARNE, T. G. & McCALL, D. M., 1992, Force Reconstruction for Impact Tests of an Energy-Absorbing Nose, *The International Journal of Analytical and Experimental Modal Analysis*, Vol. 7, No. 1, pp. 41-50.

BRANDON, J. A., 1988, On the Robustness of algorithms for the computation of the Pseudo Inverse for Modal Analysis, *The 6th International Modal Analysis Conference*, Orlando, Florida, February, pp. 397-400.

BROCH, J. T., *Principles of Experimental Frequency Analysis*, London: Elsevier, 1990.

CARNE, T. G., BATEMAN, V. I. & MAYES, R. L., 1992, Force Reconstruction Using a Sum of Weighted Accelerations Technique, *Proceedings of the 10th IMAC*, pp. 291-298.

CARNE, T. G., BATEMAN, V. I. & MAYES, R. L., 1998, Force Reconstruction Using the Sum of Weighted Accelerations Technique – Max-Flat Procedure, *Proceedings of the 16th IMAC*, Santa Barbara, California, pp. 1054-1062.

CLARK, W. W., KIM, J. H. & MARAGONI, R. D., 1998, Using Residual Flexibility for Improved Observation of reaction Forces in Flexible Structures, *Journal of Vibration and Acoustics*, Vol. 120, pp. 401-408.

DA SILVA, L. A. & RADE, D. A., 1999, Time Domain-Based Identification of Mechanical Characteristics of Supporting Elements, *Proceedings of the 17th IMAC*, pp. 1616-1621.

DESANGHERE, G., 1983, Identification of External Forces based on Transferfunction Measurements: Frequency Response Method, *Proceedings of the 8th Int. Seminar on Modal Analysis*, Kath. Univ., Leuven, Belgium, pp. 1-28.

DESANGHERE, G. & SNOEYS, R., 1985, Indirect Identification of Excitation Forces, *Proceedings of the 10th Int. Seminar on Modal Analysis*, pp.1-25.

DESANGHERE, G. & SNOEYS, R., 1985, Indirect Identification of Excitation Forces by Modal Coordinate Transformation, *Proceedings of the 3rd IMAC*, Orlando, Florida, pp.685-690.

DOBSON, B.J. & RIDER, E., 1990, A review of the indirect calculation of excitation forces from measured structural response data, *Proceedings of the Institution of Mechanical Engineers Part C: Journal of Mechanical Engineering Science*, Vol. 204, pp. 69-75.

DONGARRA, J. J., BUNCH, J. R., MOLER, C. B. & STEWART, G. W., *LINPACK Users' Guide*, SIAM, Philadelphia, 1979.

DUBOWSKI, D.G. & DOBSON, B. J., 1985, Computation of Excitation Forces Using Structural Response Data, *The 56th Symposium on Shock and Vibration*, Monterey, California, pp. 101-105.

ELLIOTT, K. B., JUANG, J. N. & ROBINSON, J., 1988, Force Prediction Using Singular-Value Decomposition, *Proceedings of the 6th IMAC*, Kissimmee, pp.1582-1588.

FABUNMI, J. A., 1986, Effect of Structural Modes on Vibratory Force Determination by Pseudoinverse Technique, *AIAA Journal*, Vol. 24, No.3, pp. 504-509.

FASANA, A. & PIOMBO, B. A. D., 1996, Identification of Linear Mechanical Systems by Deconvolution Techniques, *Mechanical Systems and Signal Processing*, Vol. 11, No. 3, pp. 305-373.

FLANNELLY, W. G. & BARTLETT, F. D., JR., 1979, Model Verification of Force Determination for Measuring Vibratory Loads, *Journal of the American Helicopter Society*, Vol. 24, pp. 10-18.

FREGOLENT, A. & SESTIERI, A., 1990, Assessment of Procedures for Force Identification from Experimental Response, *Proceedings of the 15th Int. Seminar on Modal Analysis*, Leuven, Belgium, pp. 825-839.

GENARO, G. & RADE, D. A., 1998, Input Force identification in the Time Domain, *Proceedings of the 16th IMAC*, Santa Barbara, California, pp.124-129.

GOLUB G. H. & VAN LOAN, C. F., *Matrix computations*, Second Edition, The Johns Hopkins University Press, Baltimore and London, 1989.

GREGORY, D. L., PRIDDY, T. G. & SMALLWOOD, D. O., 1986, Experimental Determination of the Dynamic Forces Acting on Non-Rigid Bodies, *SAE Technical Paper Series*, Paper No. 861791, Aerospace Technology Conference and Exposition, Long Beach, CA.

HAN, S., 1998, Analysis on Natural Frequency Distortion due to the Attachment of Shakers, *Proceedings of the 16th IMAC*, Santa Barbara, California, pp.1656-1661.

HAN, M-C & WICKS, A. L., 1990, Force Determination with Slope and Strain Response Measurement, *Proceedings of the 8th IMAC*, Kissimmee, pp.365-372.

HANSEN, M. & STARKEY, J. M., 1990, On Predicting and Improving the Condition of Modal-Model-Based Indirect Force Measurement Algorithms, *Proceedings of the 8th IMAC*, pp. 115-120.

HANSEN, P. C. & O'LEARY, D. P., 1991, The Use of the L-Curve in Regularization of Discrete Ill-Posed Problems, *Report UMIACSTR-91-142*, Dept. of Computer Science, Univ. of Maryland.

HASHEMI, I. W. & HAMMOND, J. K., 1996, Recognition and Inversion of Non-Minimum Phase Systems Using L_1 and L_2 Norms, *Proceedings of the Conference held at Swansea*, UK, pp. 194-204.

HE, J. & IMREGUN, M., 1995, Different Forms of Orthogonality for MDOF Systems, *Modal Analysis*, Vol. 10, No. 3, pp. 131-141.

HENDRICX, I. W., 1994, Accurate Vehicle FRF Measurements for Indirect Force Determination Based upon Matrix Inversion, *Tools for Noise and Vibration Analysis – ISMA19*, pp. 1037-1048.

HILLARY, B., 1983, Indirect Measurement of Vibration Excitation Forces, Ph.D. Thesis, Department of Mechanical Engineering, Imperial Collage, London.

HILLARY, B. & EWINS, D. J., 1984, The Use of Strain Gauges in Force determination and Frequency Response Function Measurements, *Proceedings of the 2nd IMAC*, Orlando, FL, pp. 627-634.

JORDAN, R. W. & WHITSON, G. S., 1984, Remote Impact Analysis by Use of Propagated Acceleration Signals, II: Comparison Between Theory and Experiment, *Journal of Sound and Vibration*, Vol. 97, No. 1, pp. 53-63.

KAMMER, D. C., 1990, Sensor Placement for On-Orbit Modal Identification and Correlation of Large Space Structures, *Proceedings of the 1990 American Control Conference*, San Diego, Ca, May 23-25, pp.2984-2990.

KAMMER, D. C., 1996, Input Force Reconstruction Using a Time Domain Technique, *American Institute of Aeronautics and Astronautics Meetings Papers*, pp. 21-30.

KARLSSON, S. E. S., 1996, Identification of External Structural Loads from Measured Harmonic Responses, *Journal of Sound and Vibration*, Vol. 196, No. 1, pp. 59-74.

KIM, Y. R. & KIM, K. J., 1997, Indirect Input Identification by Modal Model Technique, *Proceedings of the 15th IMAC*, pp.1263-1269.

KREITINGER, T. L. & WANG, M. L., 1988, Force Identification from Non-linear Structural Response, *Proceedings of the 6th IMAC*, pp.1655-1661.

LEWIT, M., 1993, Reciprocal Measurement of Mechanical Input Power with the Equivalent Force Approach, *The 4th International Congress on Intensity Techniques*, pp. 145-152.

MAIA, N. M. M., 1991, Fundamentals of Singular Value Decomposition, *Proceedings of the 9th IMAC*, Florence, Italy, pp. 1515-1521.

MAIA, N. M. M. & SILVA, J. M. M., *Theoretical and Experimental Modal Analysis*, Research Studies Press, 1997.

MAS, P., SAS, P. & WYCKAERT, K., 1994, Indirect Force Identification Based upon Impedance Matrix Inversion: A Study on Statistical and Deterministical Accuracy, *ISMA 19 – Tools of Noise and Vibration Analysis*, pp. 1049-1065.

McCONNELL, K. G., *Notes on Vibration Frequency Analysis*, Society of Experimental Mechanics, Inc., 1992.

MEIROVITCH, L. & BARUH, H., 1983, On the Problem of Observation Spillover in Self-Adjoint Distributed-Parameter Systems, *Journal of Optimization Theory and Application*, Vol. 39, No.2, February, pp.269-291.

MEIROVITCH, L. & BARUH, H., 1985, The Implementation of Modal Filters for Control of Structures, *Journal of Guidance, Control and Dynamics*, Vol. 8, No.6, November-December, pp. 707-716.

MENKE, W., *Geophysical Data Analysis: Discrete inverse theory*, Academic Press, Inc., 1984.

O'CALLAHAN, J. & PIERGENTILI, F., 1996, Force Estimation Using Operational Data, *Proceedings of the 14th IMAC*, pp.1586-1592.

OJALVO, I. U. & ZHANG, L. –M., 1993, Tutorial: Fundamentals of Ill-Conditioning, *Modal Analysis*, Vol.8, No. 2, pp. 165-176.

OKUBO, N., TANABE, S. & TATSUNO, T., 1985, Identification of Forces Generated by a Machine Under Operating Conditions, *Proceedings of the 3rd IMAC*, Orlando, Florida, pp. 920-927.

OLSEN, N., 1984, Excitation Functions for Structural Frequency Response Measurements, *Proceedings of 2nd IMAC*, Orlando, Florida, pp. 894-902.

ORY, H., GLASER, H. & HOLZDEPPE, D., 1985, Reconstruction of Forcing Functions Based on Measured Structural Responses, *2nd International Symposium on Aeroelasticity and Structural Dynamics*, RWTH, Aachen, FRG, pp. 656-668.

ORY, H., GLASER, H. & HOLZDEPPE, D., 1986, Quality of Modal Analysis and Reconstruction of Forcing Functions Based on Measured Output Data, *Proceedings of the 4th International Conference on Modal Analysis*, Los Angeles, pp. 850-857.

PARK, H. & PARK, Y., 1994, Transient Response of an Impacted Beam and Indirect Impact Force Identification Using Strain Measurements, *Shock and Vibration*, Vol. 1, No. 3, pp. 267-278.

POWELL R. E. & SEERING, W., 1984, Multichannel Structural Inverse Filtering, Transactions of the American Society of Mechanical Engineers, *Journal of Vibration, Acoustics, Stress and Reliability in Design*, Vol. 106, pp. 22-28.

RANDALL, R. B., *Application of B&K Equipment to Frequency Analysis*, Brüel & Kjær, Second Edition, 1977.

SARKAR, T. K., WEINER, D. D. & JAIN, V. K., 1981, Some Mathematical considerations in Dealing with the Inverse Problem, *IEEE Transactions on Antennas and Propagation*, Vol. AP-29, No.2, March 1981, pp. 373-379.

SHELLEY, S., FREUDINGER, L., ALLEMANG R. J. & ZHANG Q., 1991, Implementation of a Modal Filter on a Five Meter Truss Structure, *Proceedings of the 9th IMAC*, pp. 1036-1044.

SHELLEY, S. J., FREUDINGER, L. C. & ALLEMANG R. J., 1992, Development of an On-line Parameter Estimation System Using the Discrete Modal Filter, *Proceedings of the10th IMAC*, pp. 173-183.

SHELLEY, S. J. & ALLEMANG R. J., 1992, Calculation of Discrete Modal Filters Using the Modified Reciprocal Modal Vector Method, *Proceedings of the 10th IMAC*, pp. 37-45.

SHIH, C. Y., ZHANG, Q. & ALLEMANG R. J., 1989, Force Identification by Using Principle and Modal Coordinate Transformation Method, *Vibration Analysis – Technique and Application*, ASME Publications DE-Vol. 18-4, pp. 303-309.

STARKEY, J. M. & MERRILL, G. L., 1989, On the Ill-Conditioned Nature of Indirect Force Measurement Techniques, *Int. Journal of Analytical and Experimental Modal Analysis*, Vol. 4, No. 3, pp. 103-108.

STEVENS, K. K., 1987, Force Identification Problem – An Overview, *Proceedings of the 1987 SEM Conference on Experimental Mechanics*, pp. 838-844.

The Student Edition of Matlab - Users Guide, The Math Works, Inc., Version 4, 1995.

VAROTO, P. S. & McCONNELL, K. G., 1997, Predicting Random Excitation Forces from Acceleration Response Measurements, *Proceedings of the 15th IMAC*, pp.1-6.

WARWICK, D. C. & GILHEANY, J. J., 1993, Dynamic Force Estimation Via Modal Decomposition of Operational Response Measurements in a Multi-Source Environment, *Proceedings of the 11th IMAC*, pp. 278-285.

WHITSON, G. S., 1984, Remote Impact Analysis by Use of Propagated Acceleration Signals, I: Theoretical Methods, *Journal of Sound and Vibration*, Vol. 97, No. 1, pp. 35-51.

ZAVERI, K., *Modal Analysis of Large Structures – Multiple Exciter Systems*, Brüel & Kjær, 1984.

ZIAEI-RAD, S. & IMREGUN M., 1995, On the Accuracy Required of Experimental Data for Finite Element Model Updating, *Journal Sound and Vibration.*

ZHANG, Q., ALLEMANG R. J. & BROWN, D. L., 1990, Modal Filters: Concept and Applications, *Proceedings of the 8th IMAC*, pp. 487-496.

ZHANG, Q., SHIH, C. Y. & ALLEMANG R. J., 1989, Orthogonality Criterion for Experimental Modal Vectors, *American Society of Mechanical Engineers*, Publication DE, Vol. 18-4, New York, pp. 251-258.

APPENDICES

APPENDIX A – MEASUREMENT SYSTEM AND CALIBRATION

1. MEASUREMENT SYSTEM

Table A.1 – Measurement system for the identification of a single harmonic force

Equipment	Description	Serial Number
Signal generator & analyser	DSPT Siglab Model 20-42	SN 11251
Signal amplifiers	Rotel stereo integrated amplifiers RA-970 BX	SN 522 45811 SN 434 75550
Shakers	Vibro Pet Model Pet-01 IMV Corp.	SN 40-381-2 SN 40-376-2
Condition amplifiers	Model 480E09 ICP Power Unit	SN 17185 SN 3657 SN 3435 SN 17187
Force transducers	PCB208 B02	SN 12980 SN 12742
Shear accelerometers	PCB U353 B65 PCB U353 B66 PCB B15	SN 20520 SN 44564 SN 50276
Piezoelectric strain gauges	PCB 740 B02 PCB 740 B02	SN 823 SN 857
PC	Pentium 100 MHz "Apollo"	SN 0467570

2. CALIBRATION FACTORS

2.1 Accelerometer/Force Transducer Pair

Alternating voltage signals were measured from both the accelerometer and force transducers. These signals had to be multiplied by a calibration factor to obtain the correct magnitude of the frequency response functions. Since the frequency response function is simply the ratio of the response to the force, a straightforward technique can be applied to determine the calibration factor for each pair of accelerometer/force transducer. The force transducer and accelerometer are attached to the rigid body of known mass (m = 4.02 kg), as depicted in Figure A.1.

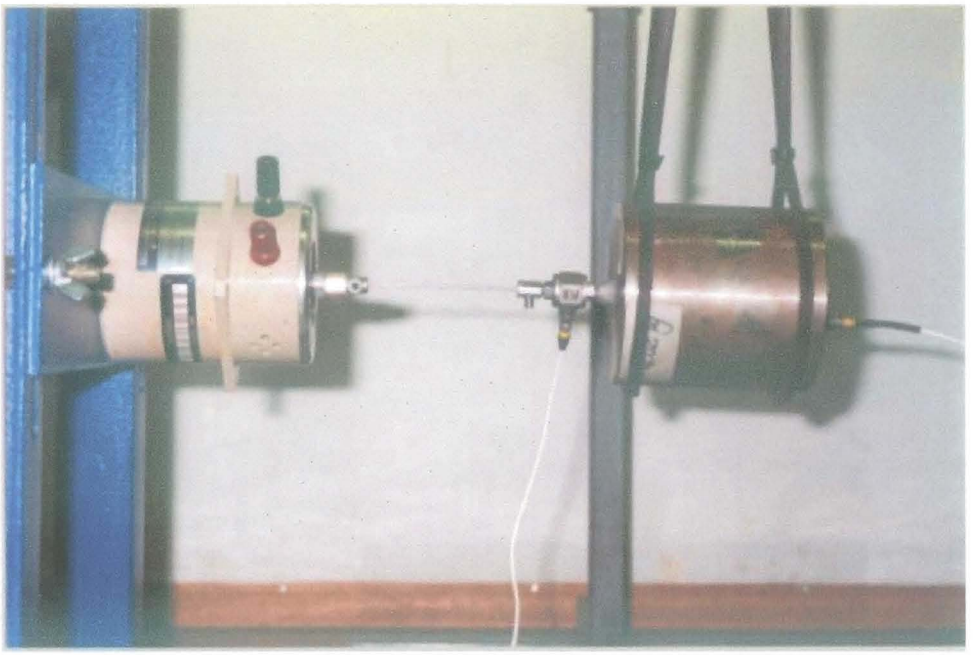

Figure A.1 – Calibration measurement setup

A time-varying force is applied to a rigid body for which the inertance is measured for the specified frequency range. The measured quantity has units of volt/volt and corresponds to:

$$A(\omega) = \frac{\ddot{x}(t)}{f(t)} = \frac{1}{m} \tag{A.1}$$

from which the overall sensitivity for each pair of accelerometer/transducer can be calculated. Figure A.2 illustrates a typical inertance and coherence measurement for one of the pairs of accelerometer/force transducer used in the experimental measurements. The overall sensitivities are listed in Table A.1.

Table A.1 – Calibration of accelerometer/force transducer pair

Accelerometer/ force transducer pair	Overall Sensitivity $\left[\frac{V/V}{m.s^{-2}/N}\right]$
SN 44564 & SN 12742	1.1610
SN 20520 & SN 12742	1.2746
SN 44564 & SN 12980	1.1584
SN 20520 & SN 12980	1.2933
SN 50276 & SN 12980	9.9367

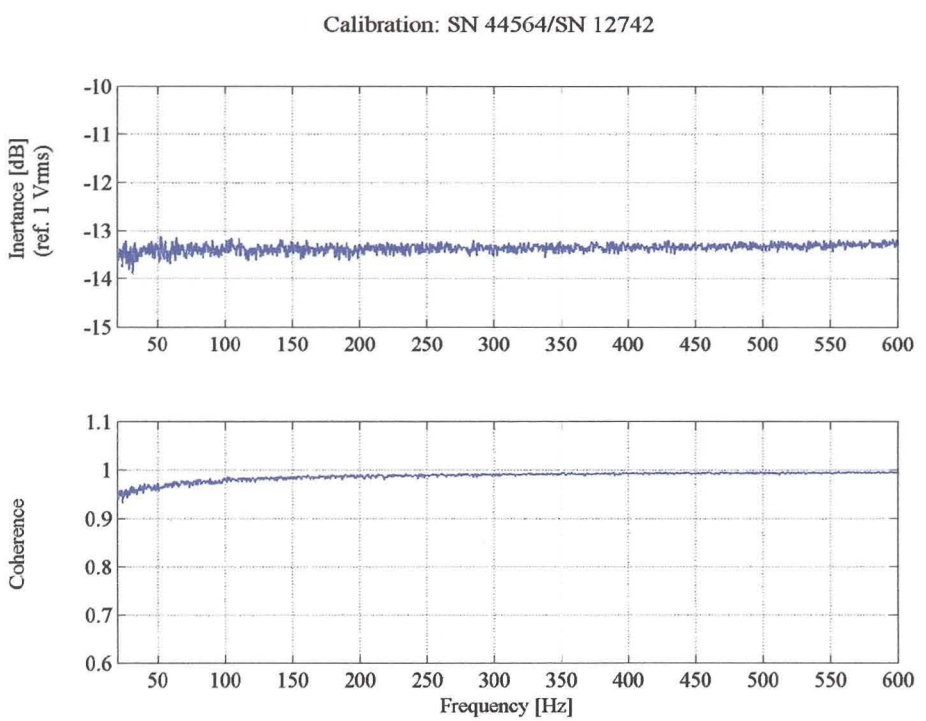

Figure A.2 – Inertance and coherence plots for the calibration of an accelerometer/force transducer pair

2.2 Accelerometers

The accelerometers were calibrated separately with a hand-held calibrator. This calibration was done with the accelerometers still connected to the rest of the measurements system as used in experimental setup. The calibration factors for each of the accelerometers are listed in Table A.2.

Table A.2 – Calibration of accelerometers

Accelerometer	Calibration factor $\left[\frac{m.s^{-2}}{Vrms}\right]$
SN 44564	154.841
SN 20520	172.358
SN 50276	1261.221

2.3 Force Transducers

Having determined the calibration factors for the accelerometers, the calibration factor for each of the force transducers was deduced from the overall sensitivity ratios given in Section 2.1 of this appendix. Two values were obtained for each force transducer, of which the average was used in the force identification process. These calibration values are given in Table A.3.

Table A.3 – Calibration of force transducers

Force transducer	Calibration factor $\left[\frac{N}{Vrms}\right]$
SN 12742	134.297
SN 12980	133.472

2.4 Piezoelectric Strain Gauges

The manufacturer's quoted sensitivities were used to determine the calibration factor for the piezoelectric strain gauges and are given in Table A.4.

Table A.4 – Calibration of piezoelectric strain gauges

Piezoelectric Strain Gauges	Calibration factor $\left[\frac{\mu\varepsilon}{Vrms}\right]$
SN 823	24.595
SN 857	28.3409

APPENDIX B - MODAL ANALYSIS OF FREE-FREE BEAM

Number of averaged Procedures: 100

The identified natural frequencies, modal damping factors and normal modes are listed in Tables B.1 and B.2.

Table B.1 - Natural frequencies and modal damping factors for the free-free beam

Natural frequencies [Hz]	Modal damping factors x $[10^{-4}]$
32.538	29.313
88.471	7.6010
172.76	17.404
286.01	6.8997
426.03	4.7836

Table B.2 – Identified normal modes for the free-free beam

Position	Mode 1 x $[10^{-1}]$	Mode 2 x $[10^{-1}]$	Mode 3 x $[10^{-1}]$	Mode 4 x $[10^{-1}]$	Mode 5 x $[10^{-1}]$
1	7.1528	-7.1878	7.2027	-5.7285	4.7910
2	4.0191	-1.5927	-0.4212	2.1804	-3.6031
3	0.7958	2.7162	-5.0597	4.4827	-2.1790
4	-1.8826	4.9710	-2.9900	-1.6166	4.8615
5	-3.7555	3.4185	2.4462	-5.0856	0.8848
6	-4.3651	0.0434	5.2002	-0.0889	-5.1665
7	-3.7685	-3.1402	2.5276	4.9914	0.6129
8	-1.9486	-4.8481	-2.8685	1.7411	5.1903
9	0.6817	-2.6716	-4.6202	-4.4145	-2.0095
10	3.7753	1.3380	-0.5484	-2.2280	-3.6572
11	7.0687	6.8776	6.4475	6.4463	6.1806

The following figures show the measured frequency response function data and the reconstructed normal mode model obtained after optimisation for the reference position 11. The truncated modes are accounted for by the inclusion of the residual terms in the normal mode model. It can be seen that the normal mode model corresponds fairly well to the experimentally measured data. At the high frequencies the normal mode model deviates slightly from the measured data due to the residuals of the truncated modes.

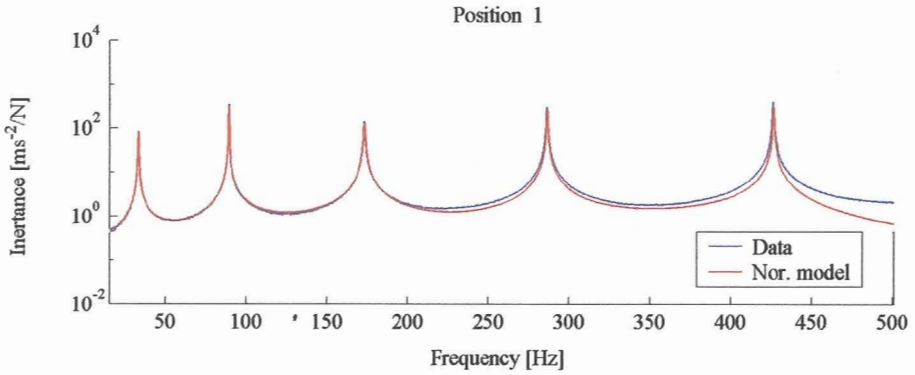
Position 1
Inertance [ms-2/N]
Frequency [Hz]
Data
Nor. model

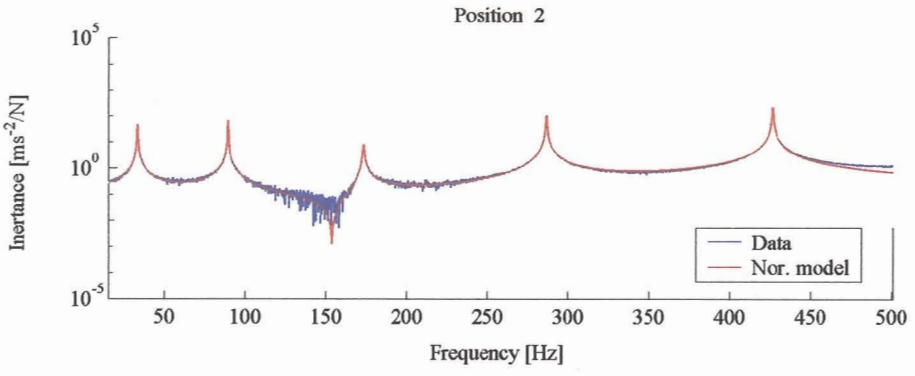
Position 2
Inertance [ms-2/N]
Frequency [Hz]
Data
Nor. model

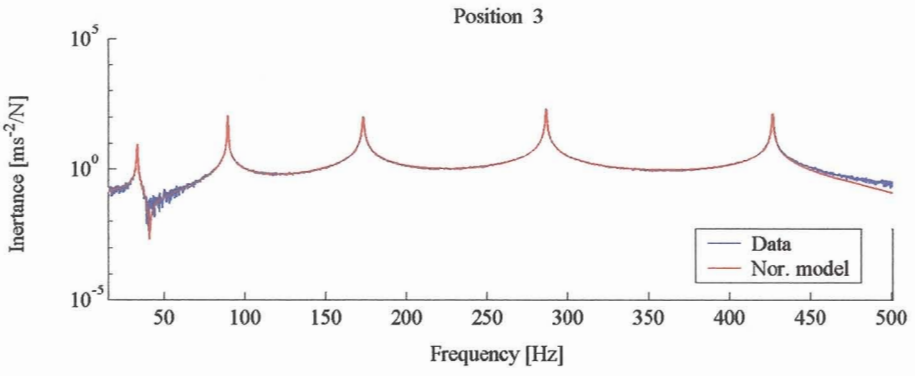
Position 3
Inertance [ms-2/N]
Frequency [Hz]
Data
Nor. model

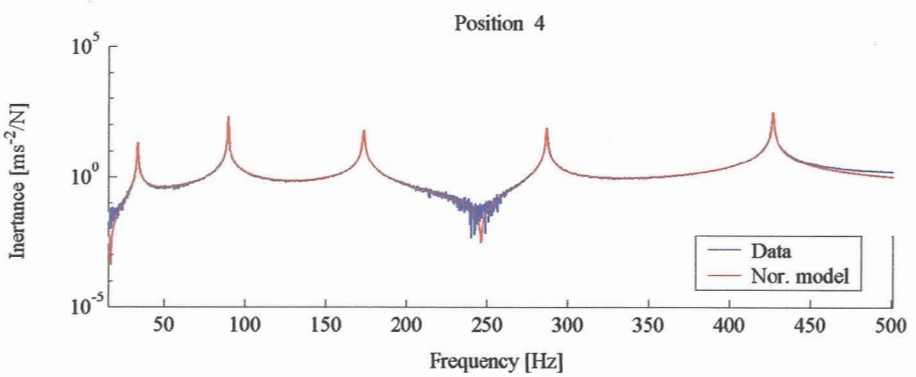
Position 4
Inertance [ms-2/N]
Frequency [Hz]
Data
Nor. model

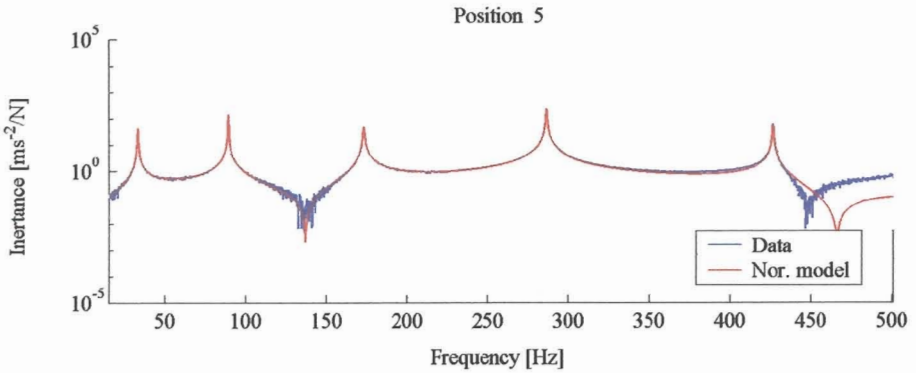
Position 5
Inertance [ms-2/N]
Frequency [Hz]
Data
Nor. model

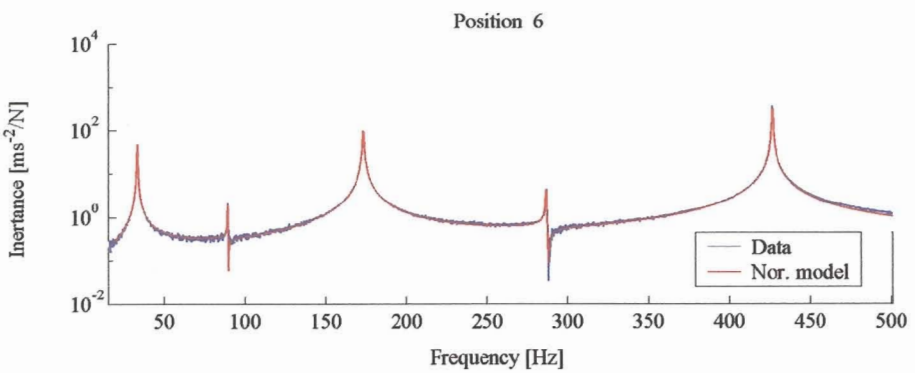
Position 6
Inertance [ms-2/N]
Frequency [Hz]
Data
Nor. model

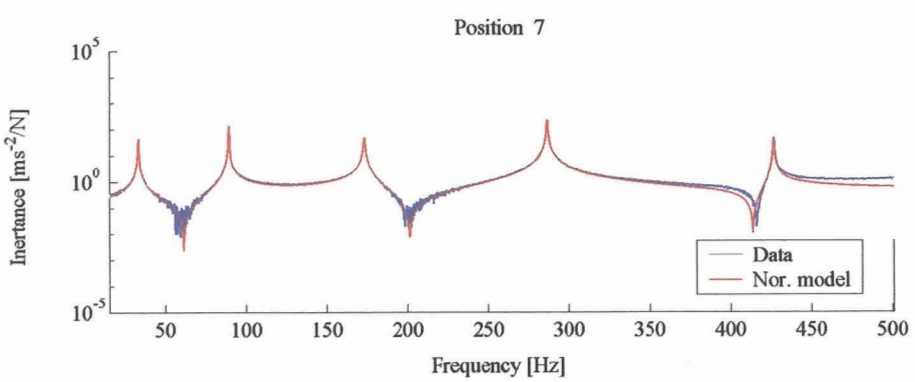
Position 7
Inertance [ms-2/N]
Frequency [Hz]
Data
Nor. model

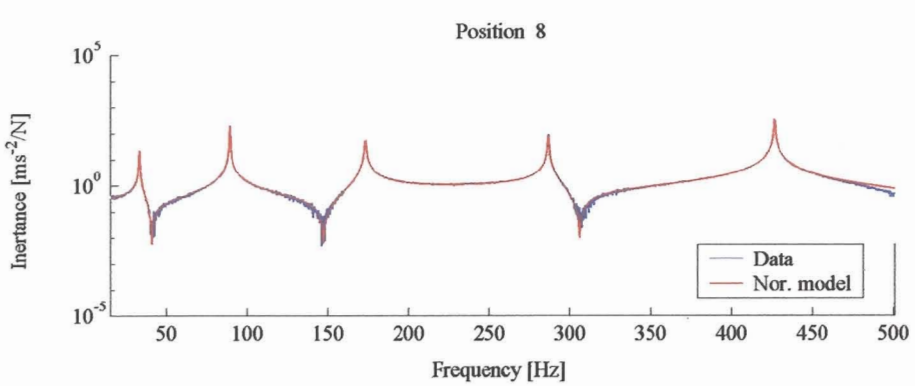
Position 8
Inertance [ms-2/N]
Frequency [Hz]
Data
Nor. model

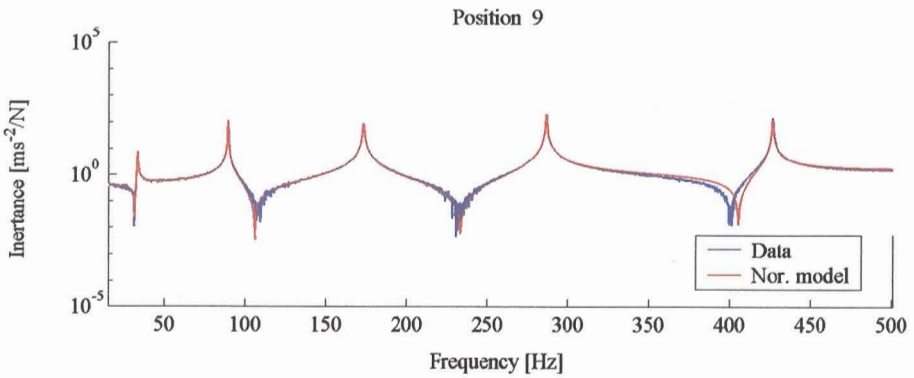
Position 9
Inertance [ms-2/N]
Frequency [Hz]
Data
Nor. model

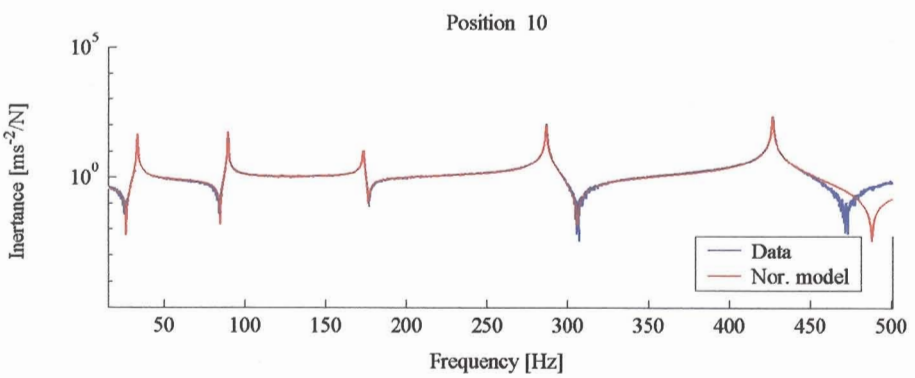
Position 10
Inertance [ms-2/N]
Frequency [Hz]
Data
Nor. model

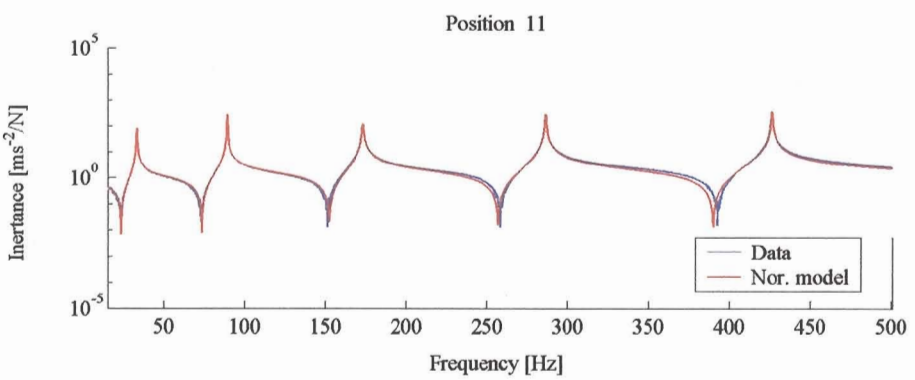
Position 11
Inertance [ms-2/N]
Frequency [Hz]
Data
Nor. model

APPENDIX C - MODAL ANALYSIS OF HINGED-HINGED BEAM

Number of averaged Procedures: 100

The identified natural frequencies, modal damping factors and normal modes are listed in Tables C.1 and C.2.

Table C.1 - Natural Frequencies and modal damping factors for the hinged-hinged beam

Natural frequencies	Modal damping factors x $[10^{-4}]$
17.130	81.206
57.222	22.496
129.81	41.237
216.48	36.900
342.64	7.6922

Table C.2 – Identified normal modes for the hinged-hinged beam

Position	Mode 1 x $[10^{-1}]$	Mode 2 x $[10^{-1}]$	Mode 3 x $[10^{-1}]$	Mode 4 x $[10^{-1}]$	Mode 5 x $[10^{-1}]$
2	1.1956	-2.7045	3.9763	4.7034	-5.4634
3	2.6710	-4.8463	5.1423	3.0304	-0.4111
4	4.1645	-5.0361	1.9649	-2.8866	5.2821
5	5.3259	-3.0588	-2.7845	-4.7733	0.1926
6	5.1190	-0.0773	-5.1073	-0.1078	-5.1595
7	4.7935	2.8529	-2.9713	4.7192	0.0530
8	4.0780	4.8785	1.8480	2.9380	5.1217
9	3.0438	4.8799	4.9294	-2.9332	-0.2507
10	1.6110	2.8048	4.0255	-4.6629	-5.2576

The following figures show the measured frequency response function data corresponding to reference position 8 and the reconstructed normal mode model without the contributions of the residual terms.

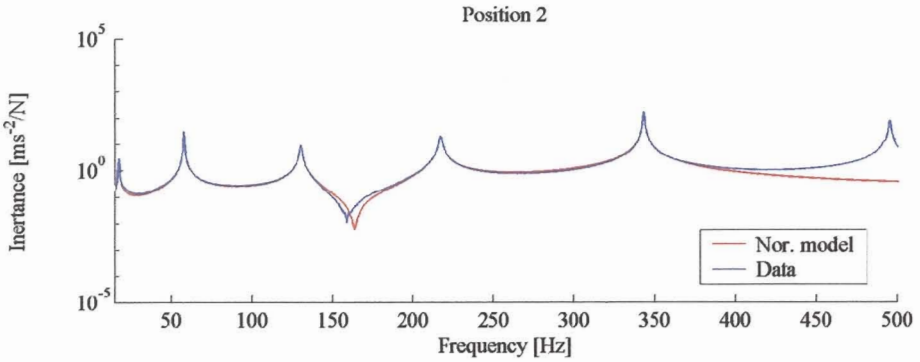
Position 2
Inertance [ms-2/N]
Frequency [Hz]
Nor. model
Data

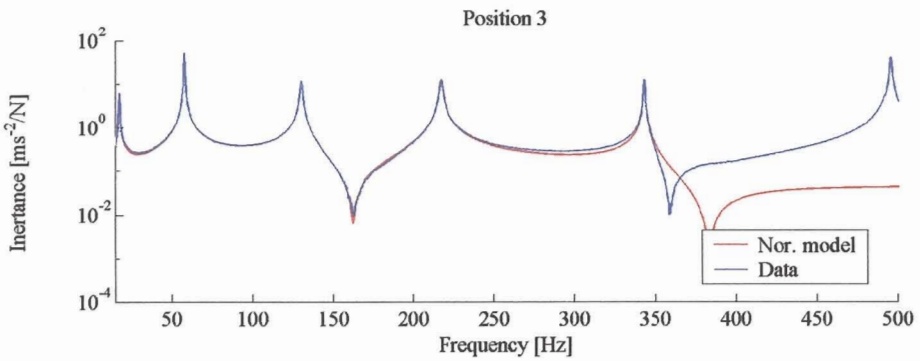
Position 3
Inertance [ms-2/N]
Frequency [Hz]
Nor. model
Data

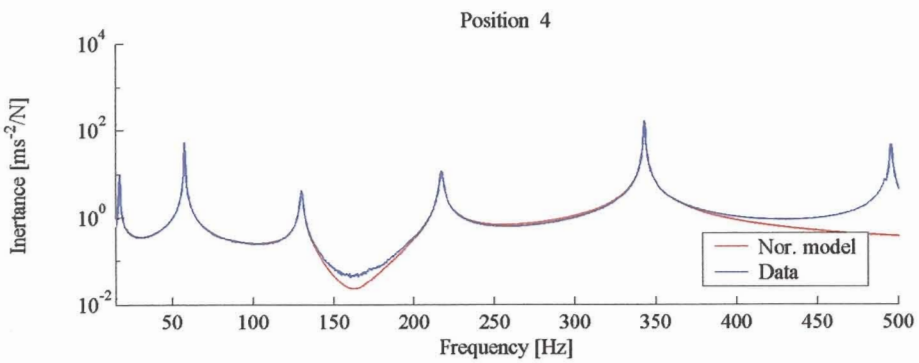
Position 4
Inertance [ms-2/N]
Frequency [Hz]
Nor. model
Data

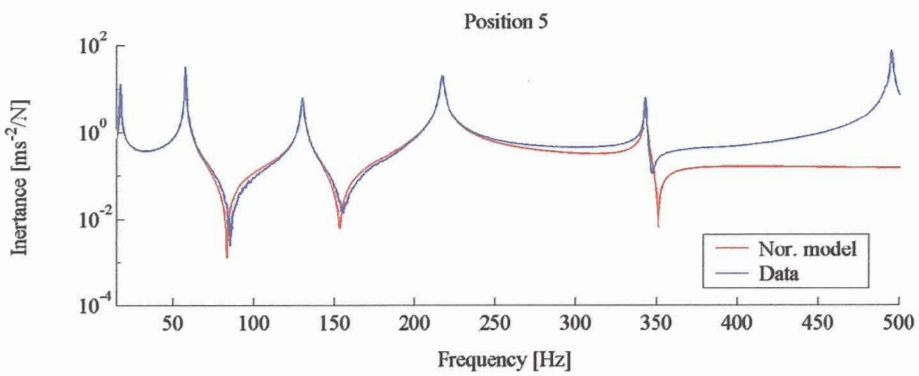
Position 5
Inertance [ms-2/N]
Frequency [Hz]
Nor. model
Data

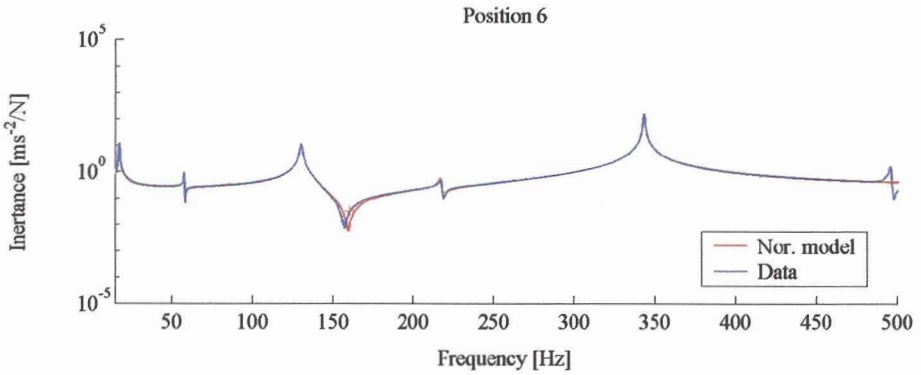
Position 6
Inertance [ms-2/N]
Frequency [Hz]
Nor. model
Data

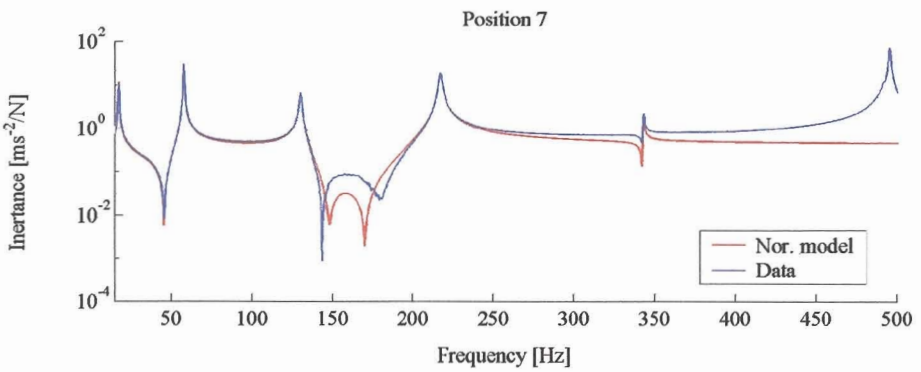
Position 7
Inertance [ms-2/N]
Frequency [Hz]
Nor. model
Data

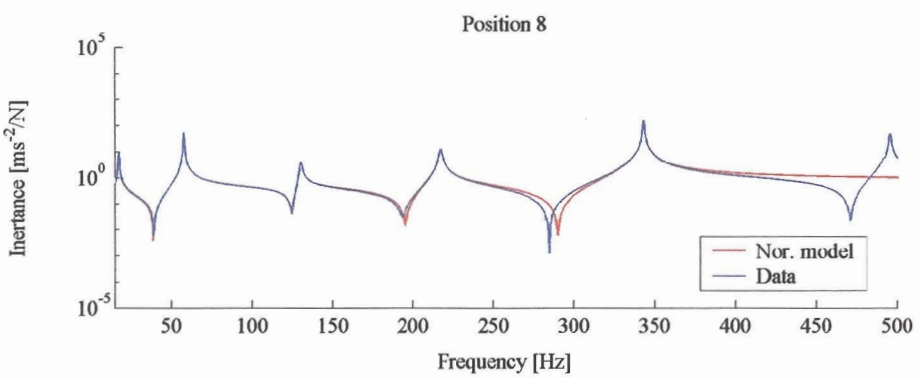
Position 8
Inertance [ms-2/N]
Frequency [Hz]
Nor. model
Data

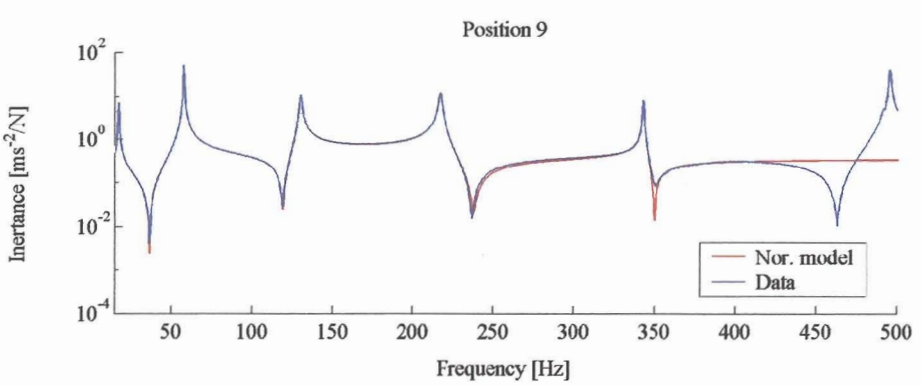
Position 9
Inertance [ms-2/N]
Frequency [Hz]
Nor. model
Data

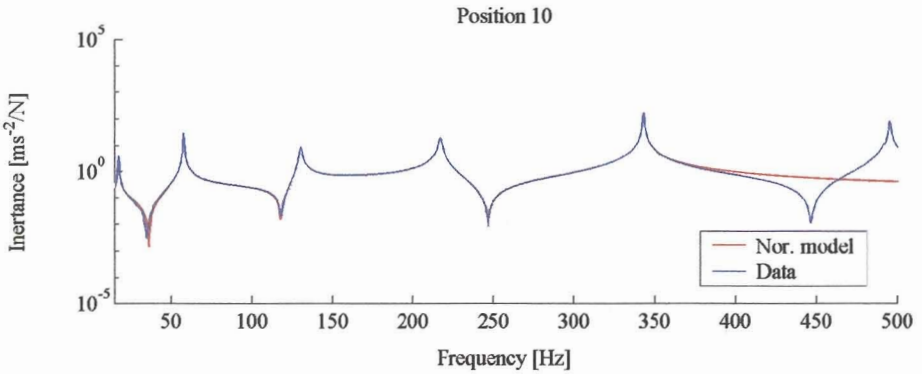
Position 10
Inertance [ms-2/N]
10^5
10^0
10^-5
50
100
150
200
250
300
350
400
450
500
Frequency [Hz]
Nor. model
Data

APPENDIX D - MODAL ANALYSIS OF HINGED-HINGED BEAM

Number of averaged Procedures: 200

The identified natural frequencies, modal damping factors and normal modes are listed in Tables D.1 and D.2.

Table D.1 - Natural frequencies and modal damping factors for the hinged-hinged beam with two harmonic force inputs

Natural frequencies [Hz]	Modal damping factors x [10^{-4}]
17.228	148.44
57.303	42.140
129.79	44.154
216.31	56.103
342.66	8.410
494.19	11.672
648.33	10.021

Table D.2 – Identified normal modes for the hinged-hinged beam with two harmonic force inputs

Position	Mode 1 x [10^{-1}]	Mode 2 x [10^{-1}]	Mode 3 x [10^{-1}]	Mode 4 x [10^{-1}]	Mode 5 x [10^{-1}]
2	-1.0774	-2.7529	4.0682	4.7618	-4.9274
3	-2.4214	-4.7255	5.1187	3.1239	-0.4099
4	-3.6565	-4.9741	2.0027	-2.8965	4.6762
5	-4.3895	-3.2095	-2.7771	-4.8207	0.1359
6	-4.6137	-0.1007	-4.8680	-0.0438	-4.7837
7	-4.2844	2.9175	-2.8460	4.7831	0.0314
8	-3.6914	4.7672	1.9263	3.0309	4.7526
9	-2.6569	4.7833	5.0503	-2.9069	-0.2191
10	-1.3283	2.9776	3.9585	-4.6472	-4.8786

Position	Mode 6 x [10^{-1}]	Mode 7 x [10^{-1}]
2	-4.8896	3.7760
3	2.4546	4.2764
4	3.0719	1.4962
5	-4.5333	2.9315
6	-0.0551	4.4332
7	4.6077	2.7099
8	-2.9897	1.6478
9	-2.4897	4.2718
10	4.8393	3.5324

The following figures show the measured frequency response function data and the reconstructed normal mode model without the contributions of the residual terms.

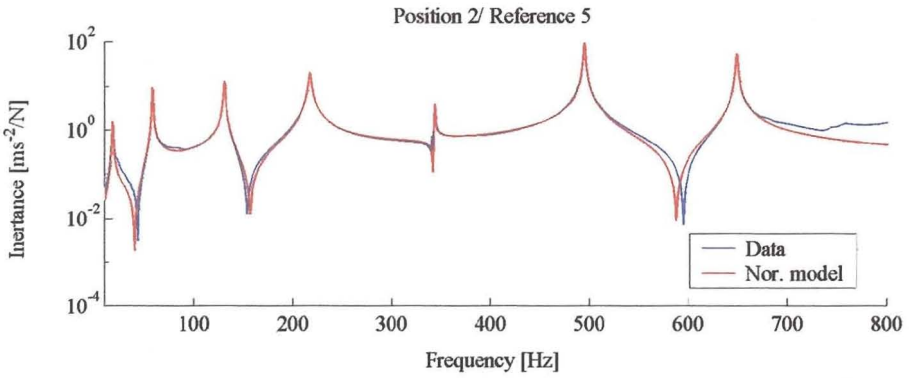
Position 2/ Reference 5
Inertance [ms-2/N]
Frequency [Hz]
Data
Nor. model

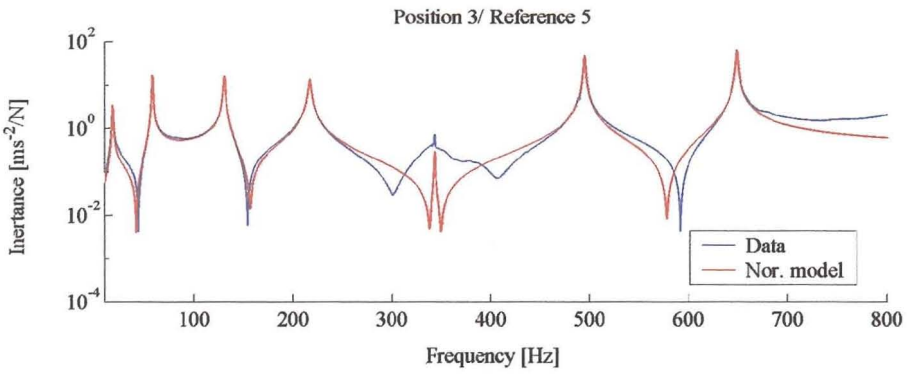
Position 3/ Reference 5
Inertance [ms-2/N]
Frequency [Hz]
Data
Nor. model

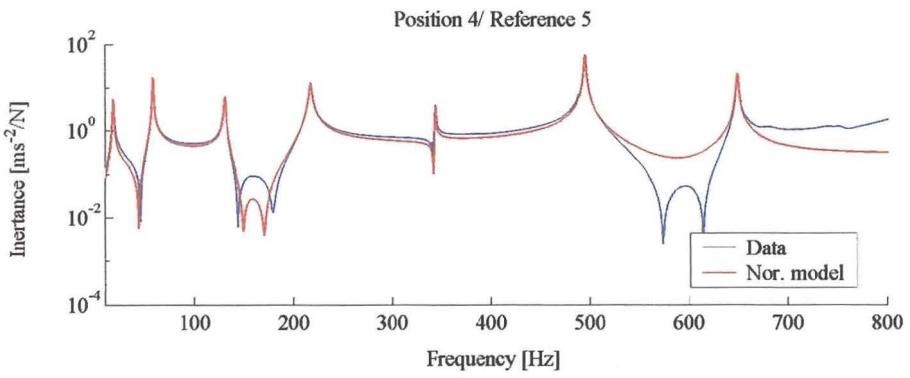
Position 4/ Reference 5
Inertance [ms-2/N]
Frequency [Hz]
Data
Nor. model

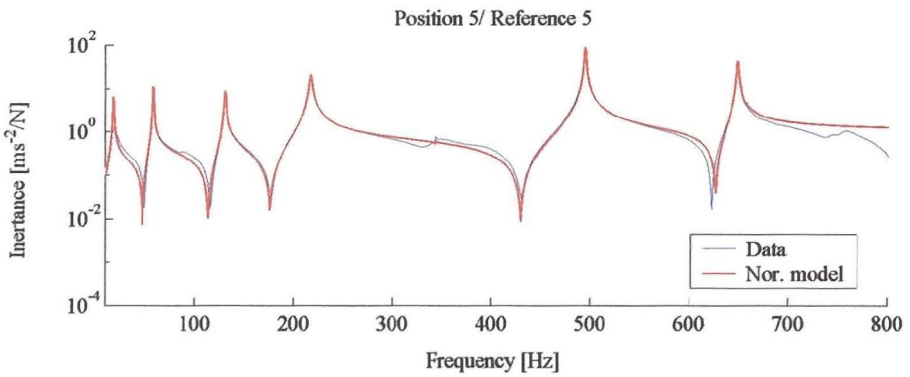
Position 5/ Reference 5
Inertance [ms-2/N]
Frequency [Hz]
Data
Nor. model

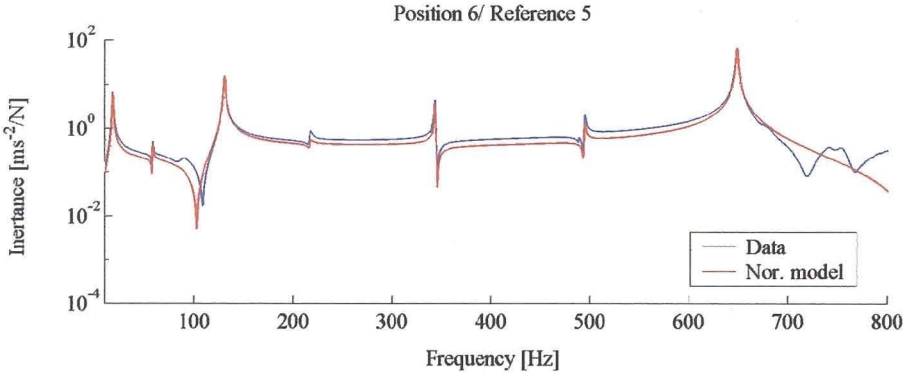
Position 6/ Reference 5
Inertance [ms-2/N]
Frequency [Hz]
Data
Nor. model

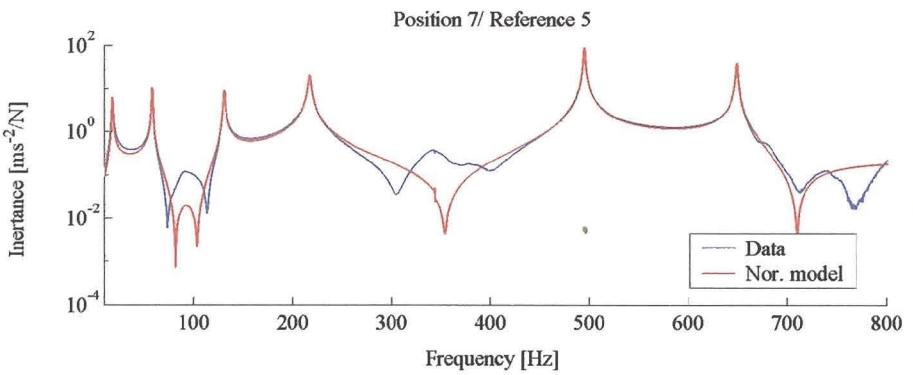
Position 7/ Reference 5
Inertance [ms-2/N]
Frequency [Hz]
Data
Nor. model

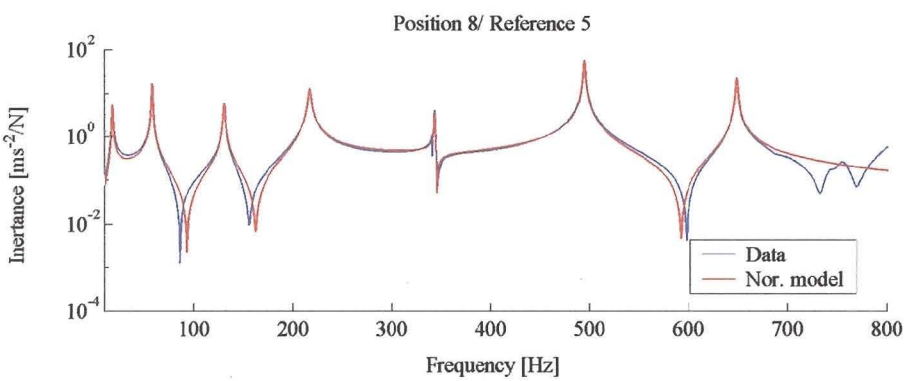
Position 8/ Reference 5
Inertance [ms-2/N]
Frequency [Hz]
Data
Nor. model

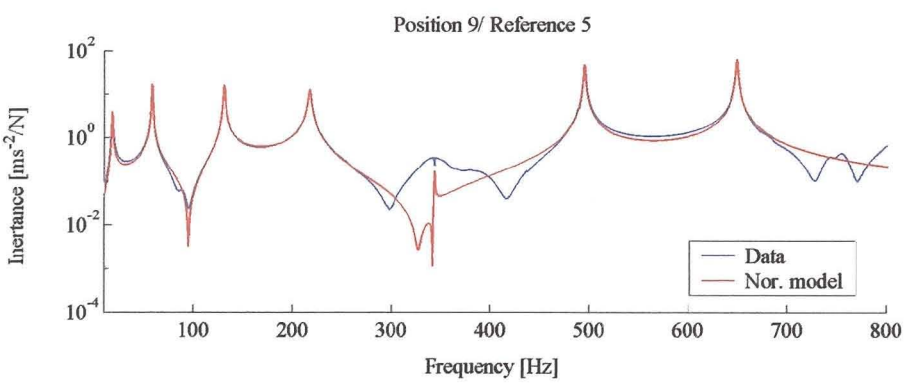
Position 9/ Reference 5
Inertance [ms-2/N]
Frequency [Hz]
Data
Nor. model

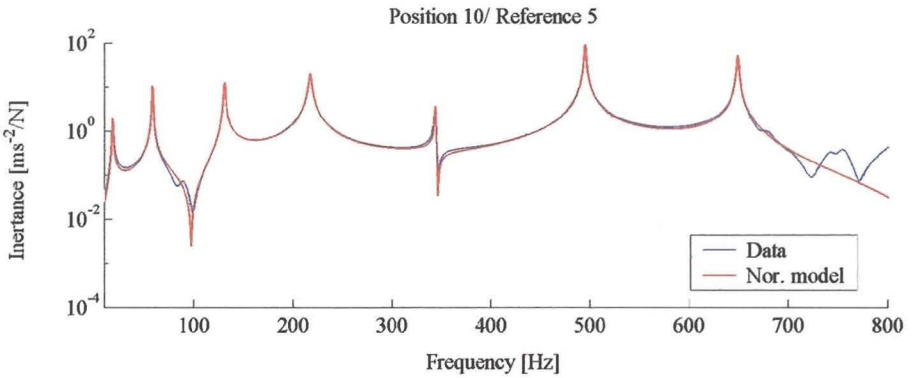
Position 10/ Reference 5
Inertance [ms-2/N]
Frequency [Hz]
Data
Nor. model

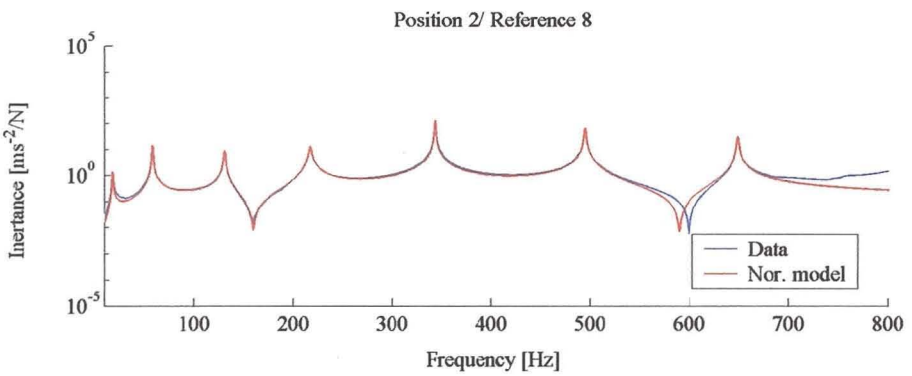
Position 2/ Reference 8
Inertance [ms-2/N]
Frequency [Hz]
Data
Nor. model

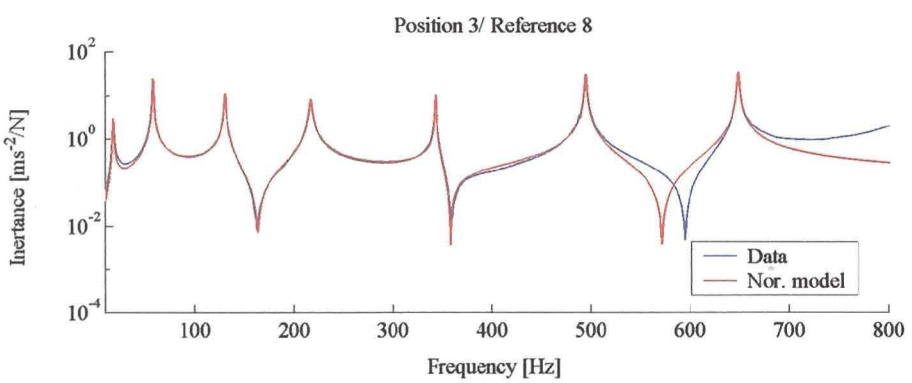
Position 3/ Reference 8
Inertance [ms-2/N]
Frequency [Hz]
Data
Nor. model

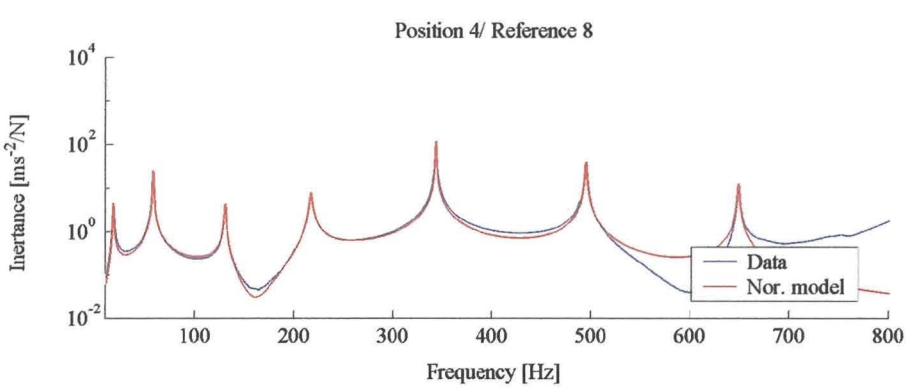
Position 4/ Reference 8
Inertance [ms-2/N]
Frequency [Hz]
Data
Nor. model

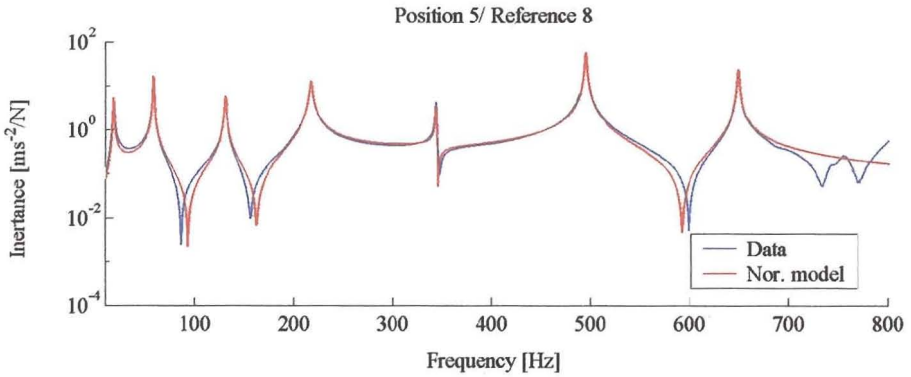
Position 5/ Reference 8
Inertance [ms^{-2}/N]
10^{2}
10^{0}
10^{-2}
10^{-4}
100
200
300
400
500
600
700
800
Frequency [Hz]
Data
Nor. model

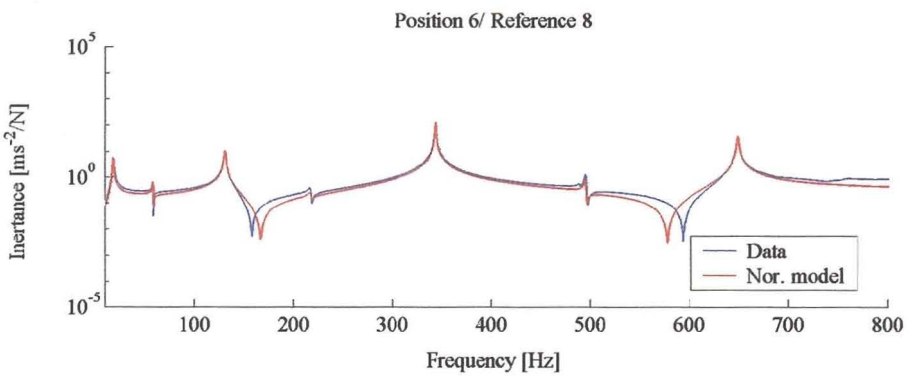
Position 6/ Reference 8
Inertance [ms^{-2}/N]
10^{5}
10^{0}
10^{-5}
100
200
300
400
500
600
700
800
Frequency [Hz]
Data
Nor. model

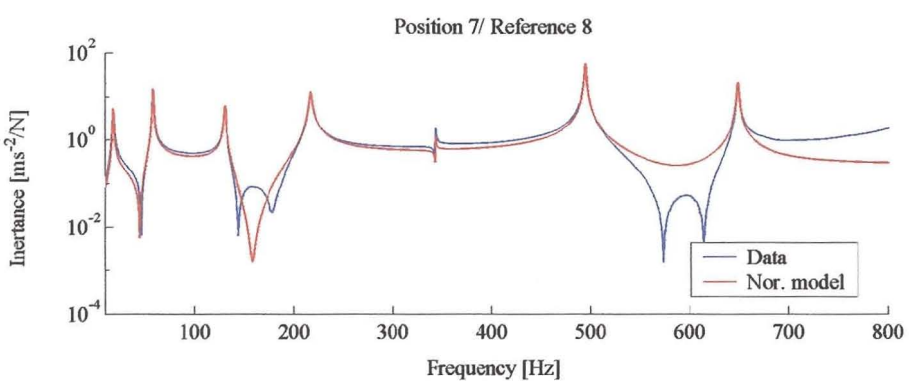
Position 7/ Reference 8
Inertance [ms^{-2}/N]
10^{2}
10^{0}
10^{-2}
10^{-4}
100
200
300
400
500
600
700
800
Frequency [Hz]
Data
Nor. model

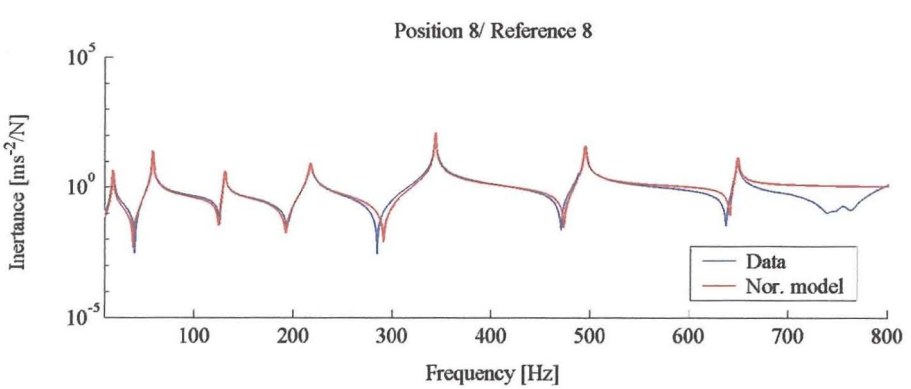
Position 8/ Reference 8
Inertance [ms^{-2}/N]
10^{5}
10^{0}
10^{-5}
100
200
300
400
500
600
700
800
Frequency [Hz]
Data
Nor. model

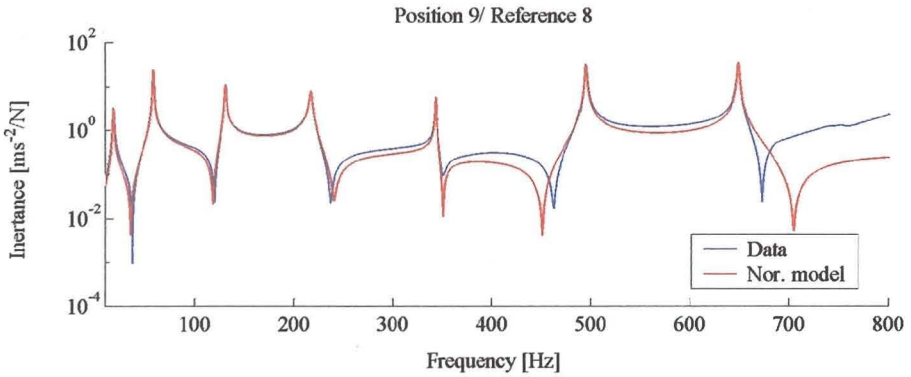
Position 9/ Reference 8
Inertance [ms-2/N]
10^2
10^0
10^-2
10^-4
100
200
300
400
500
600
700
800
Frequency [Hz]
Data
Nor. model

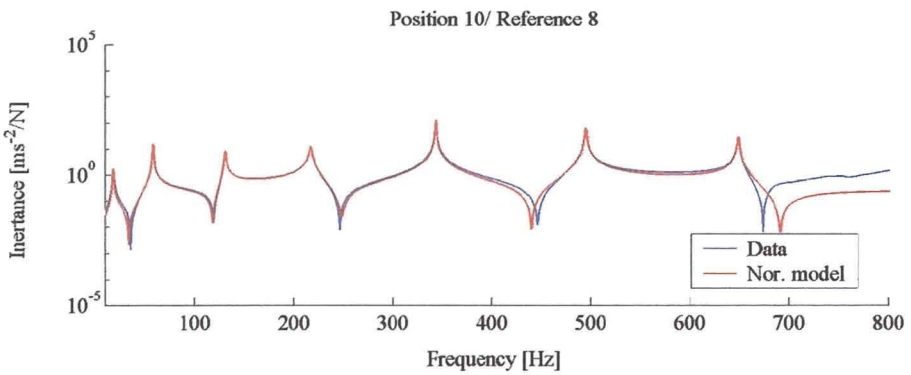
Position 10/ Reference 8
Inertance [ms-2/N]
10^5
10^0
10^-5
100
200
300
400
500
600
700
800
Frequency [Hz]
Data
Nor. model

APPENDIX E – PHOTOS

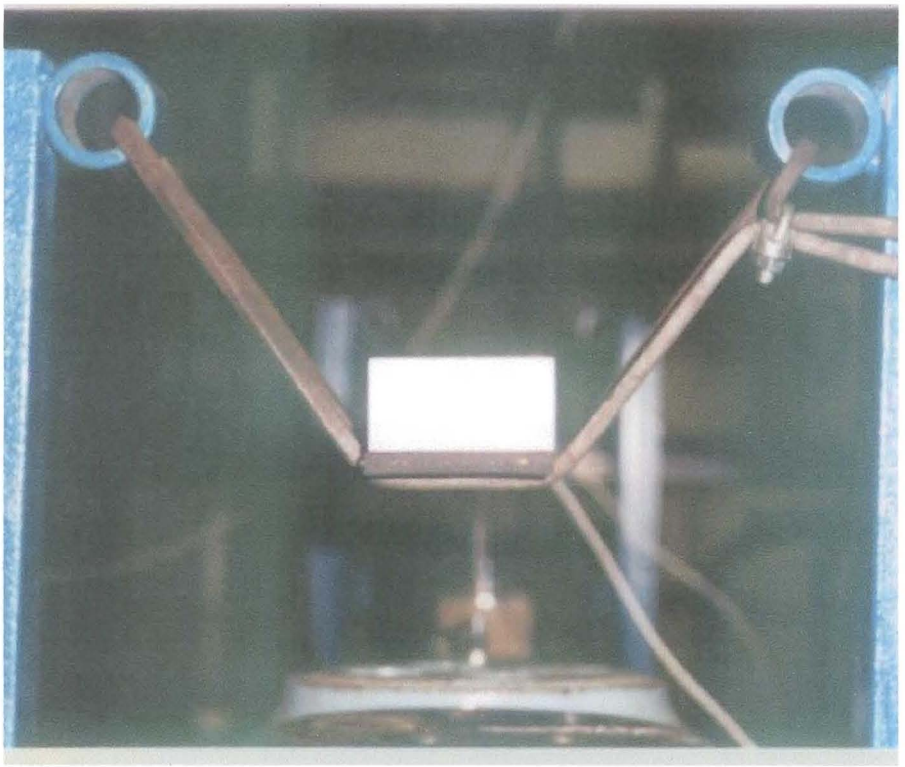

Figure E.1 – Suspension of free-free aliminium beam with rubber strip attached.

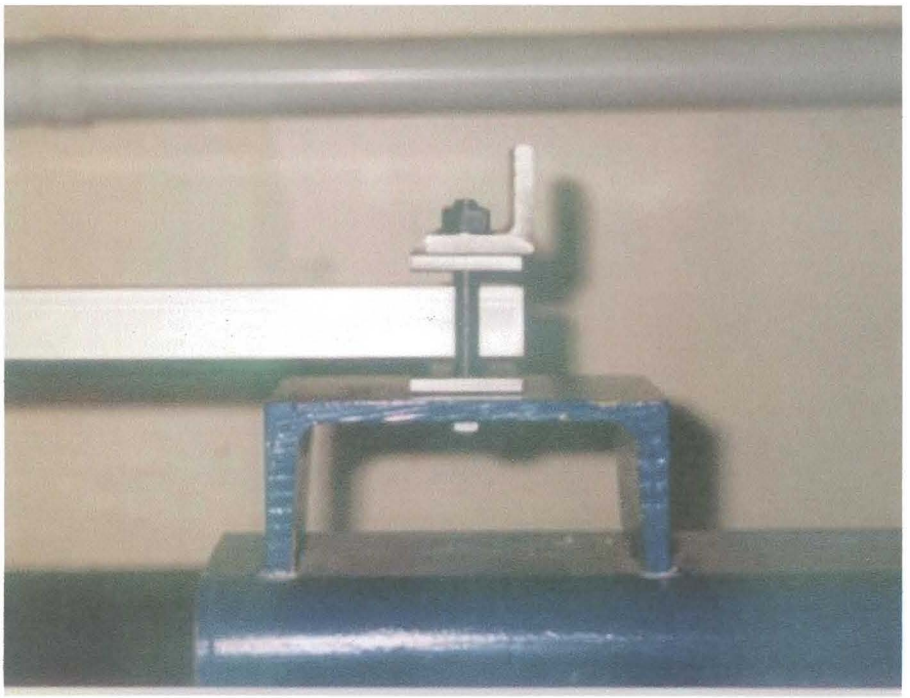

Figure E.2 – Construction of the support for the hinged-hinged aliminium beam.

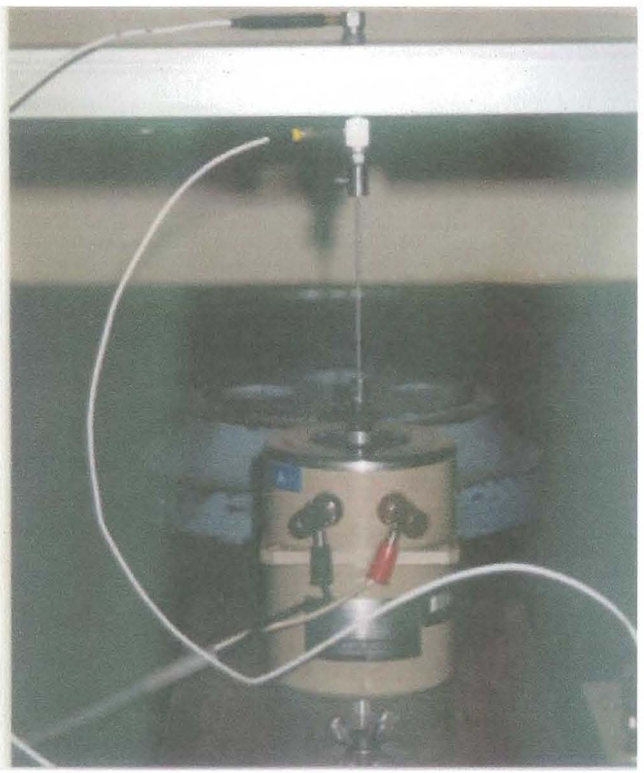

Figure E.3 – Structure-exciter attachment with force transducer and accelerometer.

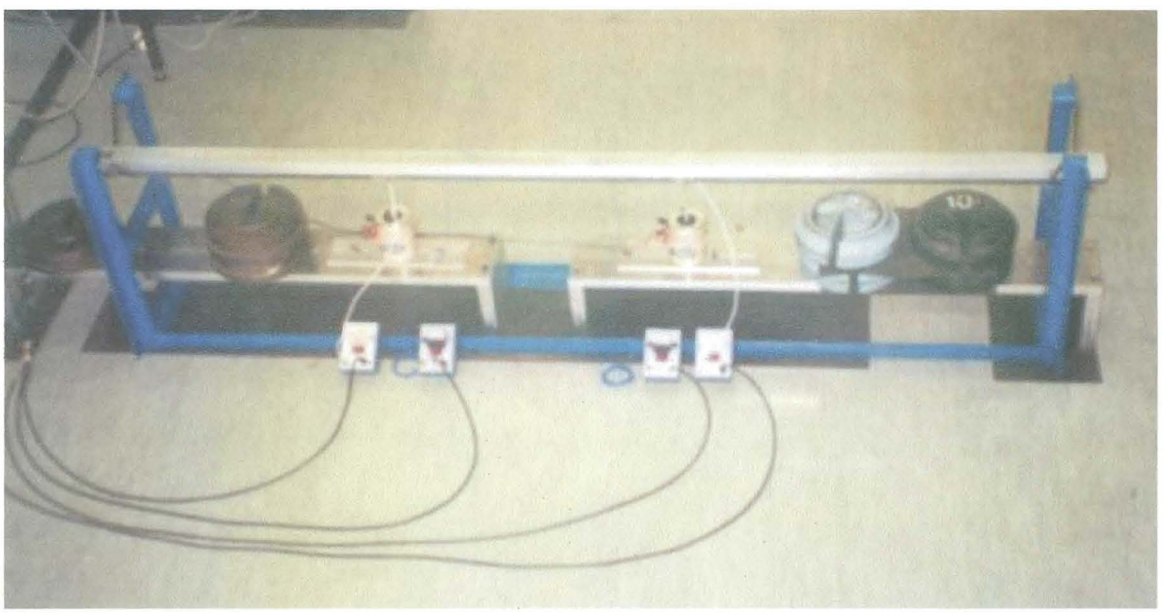

Figure E.4 – Structure-exciter attachment for free-free beam.

Figure E.5 – Structure-exciter attachment for hinged-hinged beam.

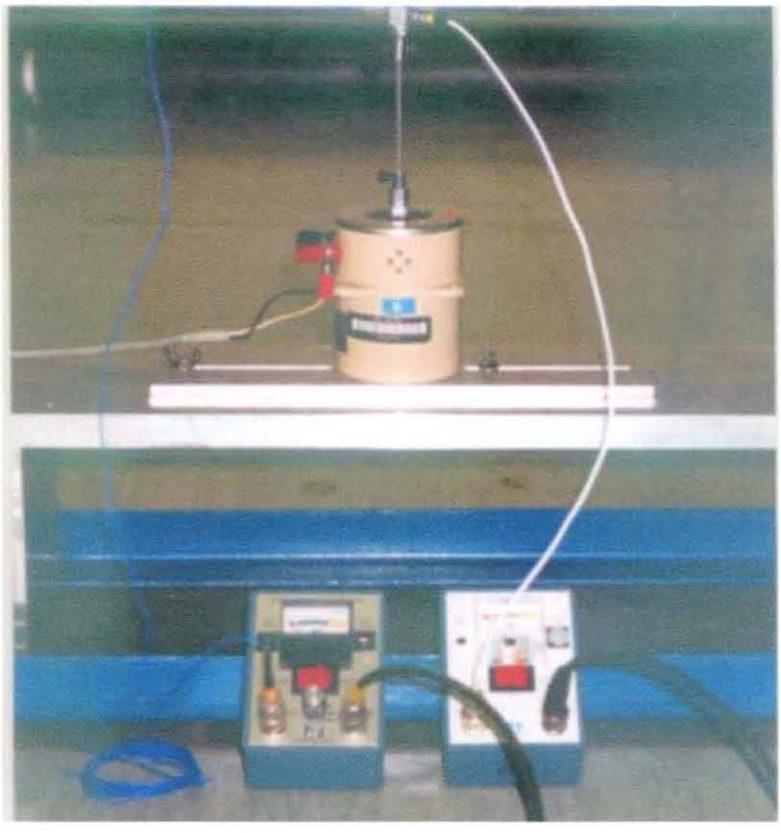

Figure E.6 – Structure-exciter attachment with force transducer and piezoelectric strain gauge